

FINAL REPORT

Managing the Integrity

of Early Pipelines –

Crack Growth Analysis

and Revalidation Intervals

To

U.S. Department of Transportation

Research and Special

Projects Agency

Contract DTRS56-03-T-0003

February 2005

Final Report

on

**Managing the Integrity of Early Pipelines –
Crack Growth Analysis and Revalidation Intervals**

Prepared for

U. S Department of Transportation

Research and Special Projects Agency

Contract DTRS56-03-T-0003

by

B. N. Leis and T. P. Forte

February 2005

BATTELLE

505 King Avenue

Columbus, Ohio, 43201-2693

Acknowledgements

This work was prepared under contract to the Research and Special Projects Agency U. S Department of Transportation, under DTRS56-03-T-0003, with Mr. James Merritt serving as the contracting officer's technical representative. Cost-share for this project came under funding from the Interstate Natural Gas Association of America, associated with their project on Integrity Characteristics of Vintage Pipelines. This INGAA project was under the management of their working group on Integrity Management, chaired on behalf of INGAA by Mr. Andrew Drake of Duke Energy Gas Transmission.

Neither Battelle nor the Government, nor INGAA through its cost-share involvement, nor any person acting on their behalf:

Makes any warranty or representation, expressed or implied, with respect to the accuracy, completeness or usefulness of any information contained in this report or that the use of any information, apparatus, method, or process disclosed in this report may not infringe privately owned rights.

Assumes any liabilities with the respect to the use of, or for damages resulting from the use of any information, apparatus, method or process disclosed in this report.

Government Reporting Page Goes Here

Table of Contents

	Page
Introduction.....	1
Background.....	1
Objectives and Scope.....	3
Definitions.....	4
Approach – Quantitative Threat Assessment.....	5
High-Level View of Threat Assessment.....	6
Threat Assessment Process for Crack-Like Defects.....	7
Key Tasks and Report Organization.....	8
The Vintage Pipeline System and Representative Scenarios.....	9
Vintage Pipeline System: Mileage.....	9
Vintage Pipeline System: Diameter and Wall Thickness.....	10
Interplay between Diameter, Wall Thickness, Grade, and Design Factor.....	13
Vintage Pipeline System: Grade and Design Factor.....	14
Design Parameters that Characterize the Vintage Pipeline System.....	15
Fracture Properties for the Vintage Pipeline System.....	16
Failing Defect Sizes for the Vintage Pipeline System.....	18
Prediction Methods.....	18
Selection of Failure Criteria Used Herein.....	21
Reference Stress for Defect-Free Pipelines.....	22
Validity of Collapse and Fracture Based Formulations.....	23
Predicted Failing Defect Sizes.....	25
Critical and Failing Defect Sizes for Vintage Pipelines.....	34
Summary for Failing Defect Sizes.....	39
Growth Mechanisms, Thresholds, and Kinetics.....	40
Possible Approaches to Assess Thresholds and Kinetics.....	40
Corrosion Threshold and Kinetics.....	41
Fatigue Thresholds and Kinetics.....	44
Stress-Corrosion Cracking Kinetics and Thresholds.....	49
Hydrogen Stress Cracking Kinetics and Thresholds.....	54
Service Loadings and Operating Environment.....	57

Table of Contents (continued)

	Page
.....	Page
Pressure and Temperature Histories	58
Axial Poisson-Induced Stresses	59
MTBF and Revalidation Intervals	59
Model Formulation	60
Presentation Format	64
Calculated Crack-Growth Intervals and Trends	64
Discussion	81
Validation.....	85
Flow Chart for Integrity Assessment.....	85
Summary and Conclusions	86
Recommendations.....	87
References.....	89
Appendix A: Experience with Historic Line Pipe	A-1

List of Figures

Figure 1. Reportable natural gas transmission incidents 1984-2000.....	2
Figure 2. Flowcharts of the integrity assessment and management process	7
Figure 3. Cumulative mileage by decade (OPS ⁽²⁾).....	10
Figure 4. Cumulative mileage by diameter (OPS ⁽²⁾).....	10
Figure 5. Incident frequency for OPS data as a function of design factor (after Reference 23)	11
Figure 6. Trends in vintage diameter and wall thickness.....	12
Figure 7. Evolution of line-pipe yield stress	13
Figure 8. Distribution of gas-transmission class locations in the U.S. by geographic region ⁽⁷⁾	15
Figure 9. Historical evolution of USE for line pipe	16
Figure 10. Decreasing ductility with Y/T for C-M steels.....	17
Figure 11. Underestimated crack size as a consequence of a conservative pressure prediction.....	21
Figure 12. Failure in defect-free pipe.....	22

List of Figures (continued)

	Page
Figure 13. Failure pressure for axial defects	24
Figure 14. Predicted failure pressure for axial defects	25
Figure 15. Failing defect sizes vs. toughness	27
Figure 16. Trends in plastic collapse versus toughness controlled failure	29
Figure 17 Consolidated collapse-controlled failure	30
Figure 18 Leak versus rupture boundary	32
Figure 19. Toughness for brittle fracture arrest	33
Figure 20. Failing sizes for blunt defects	35
Figure 21. Failing sizes for sharp defects at 15 ft-lb toughness	36
Figure 22. Corrosion rate trends for buried steel coupons and pipelines	43
Figure 23. Fatigue resistance of several grades of line pipe steel	47
Figure 24. Trends in SSRT and TTT used to characterize SCC resistance	51
Figure 25. SCC resistance of several grades of line pipe steel	52
Figure 26. Aspects of hydrogen-related cracking behavior of line-pipe steel	55
Figure 27. Typical pressure and temperature gradients between compressor stations	58
Figure 28. MTBF in years for axial corrosion	69
Figure 29. MTBF in cycles for axial fatigue cracking	72
Figure 30. MTBF in years for axial cracking with typical high pH SCC kinetics	75
Figure 31. Circumferential MTBF in cycles for Poisson-induced axial stress corresponding to pressure at 72-percent of SMYS	78
Figure 32 Failure probability for pipelines where SCC is controlled by after-coolers	81
Figure 33. Trends in pipeline resistance to SCC involving the temperature and pressure service history	82
Figure 34. Illustrating the nonlinear dependence of MTBF on pressure cycling and the value of R_{σ}	84
Figure 35. Flow chart to guide integrity management of corrosion, fatigue, and SCC	85

List of Tables

Table 1. Categories of threats to integrity of natural-gas transmission pipelines	3
Table 2. Summary of property combinations by decade for US gas transmission system.....	14
Table 3. Wall thickness calculated per 49CFR Part 192	15
Table 4. Summary of property combinations by decade for the pipe body	18

Executive Summary

Recent changes in the U. S. Department of Transportation Office of Pipeline Safety regulatory requirements mandate transmission pipeline operators develop formal integrity management plans that address threats to their system. The objective of this work was to develop a quantitative assessment of time-dependent threats, with a focus on vintage onshore gas transmission pipelines. Characteristics of the vintage pipeline system were established in terms of diameters, wall thickness, service conditions, grade and toughness and pipeline designs typical of this system identified. Analyses to quantify mean-time-between-failure and related re-inspection intervals were performed for these typical vintage pipelines addressing time-dependent degradation and possible failure due to corrosion, fatigue, and stress corrosion cracking. Hydrogen embrittlement also was considered, although not in regard to mean-time-between-failure (MTBF). Results developed were used to quantify pipeline life as a function of the sizes of defects that have caused incidents in vintage pipeline systems.

Tools and technology were developed and used to generate results and trends useful in assessing the severity of threats due to anomalies introduced by historic steel-making, pipe-making, construction, and fabrication. Such information was used to develop guidance in implementing integrity management plans.

Important conclusions regarding re-inspection intervals that can be derived from this work and the MTBF results generated include:

- Re-inspection intervals for corrosion targeted at the order of seven to ten years appear to be viable based on the present results.
- Re-inspection intervals involving fatigue will depend on the pipeline's operating pressure history. For the high-stress ratio (minimum stress/maximum stress) infrequent cycling that is typical of most gas-transmission pipeline service fatigue is an unlikely cause of failure, such that fatigue is not a viable threat for such gas-transmission pipelines. However, where the stress ratio falls below about 0.7 fatigue does become a concern. Re-inspection intervals for such pipelines should be evaluated as a function of the current condition of the pipeline and its operating pressure history.
- Re-inspection intervals involving high pH SCC will depend on the pipeline's current condition, past experience with SCC, the pipelines right-of-way, and its operating pressure history in reference to pressure as it affects temperature and pressure cycles. For Class 1 scenarios the wall stress at MAOP is above typical high pH SCC thresholds such that this threat should be evaluated, whereas where the pressure or right-of-way-induced stresses are well below apparent thresholds this threat is diminished. Typical laboratory test conditions used to study high pH SCC under accelerated conditions produce growth rates orders of magnitude faster than often observed in the field. While acceleration is useful and essential to evaluate factors controlling SCC, care must be used where such data guide integrity management decisions. Right-of-way and operational factors have a first-order effect on SCC kinetics and must be addressed when making integrity management decisions. Where growth rates are high, in-line inspection will have diminished value, while hydrotesting remains effective with the added benefit of blunting deeper cracks and diminishing the microplastic strain essential for SCC nucleation.

This page intentionally blank.

Introduction

Background

Recently the U. S. Department of Transportation (DoT) through the Office of Pipeline Safety (OPS) issued guidance for transmission pipeline operators that require formal integrity management plans (IMPs)¹ be developed for portions of systems that run through so-called high consequence areas (HCAs). These “protocols” were issued for the gas transmission industry operating under Title 49 of the Code of Federal Regulations Part 192 (49 CFR Part 192)^{(2)*} in 2004. This was preceded by definition of HCAs. Corresponding protocols were issued a few years earlier for hazardous liquid pipelines operating under Title 49 of the Code of Federal Regulations Part 195 (49 CFR Part 195)⁽²⁾. Such protocols require that pipeline operators establish and demonstrate the safe condition of their pipeline system passing through HCAs, with the requirement to periodically revalidate that safe condition.

One aspect of demonstrating the safe condition of a pipeline is evaluation of potential threats to pipeline safety. Causes of pipeline failure and their consequences can change along a pipeline within an HCA, as well as change over time along the right-of-way (RoW). Consequences involve factors often independent of the pipeline, as for example the public exposure along the RoW within an HCA, but also depend on pipeline in regard to operating pressure and the product transported. Threats to safety reflect pipeline design and operation, as well as the current condition of the pipeline and contributory conditions along the RoW.

Threats to pipeline safety when considered in light of historical causes of transmission pipeline incidents provide perspective for their significance in terms of pipeline integrity. Figure 1 presents results for US gas transmission pipelines⁽³⁾ for the period from 1984 through 2000. Results are shown therein as a bar graph that partitions each threat into a portion that reflects “pipe” incidents versus “non-pipe” incidents. This indicates that integrity management embraces more than the pipeline. For most HCAs, the focus is on pipe-related events, but as time passes more than the line pipe could become a factor. Currently, as evident from Figure 1, most threats involve pipe much more so than non-pipe concerns, which perhaps reflects the extent to which pipeline systems comprise mostly line pipe.

Consider next the left side of the chart in Figure 1, which addresses the nature of the incident and its cause. Causes shown in Figure 1 reflect potential threats to pipeline integrity as identified in work by Kiefner et al⁽⁴⁾. These threats were subsequently grouped into the nine broad categories shown in Table 1, which evolved as part of the consensus development of ASME B31.8S⁽⁵⁾. With some modification and additions, the threat categories identified by Kiefner et al have since been incorporated into the formal incident reporting⁽⁶⁾ required by DoT OPS, which started in 2002. “Reportable” incidents are now characterized for the formal reporting in terms of 25 causes grouped by the Government into seven categories. In contrast, ASME B31.8S introduces nine categories, as indicated in Table 1. These nine categories encompass those of the OPS, but

¹ For the requirements, definitions, and related guidance, see Reference 1.

* Numbers in superscript parenthesis refer to the list of references compiled at the end of this report.

subdivide some categories in reference to cause. The categories used in Figure 1 make reference to those adopted in B31.8S.

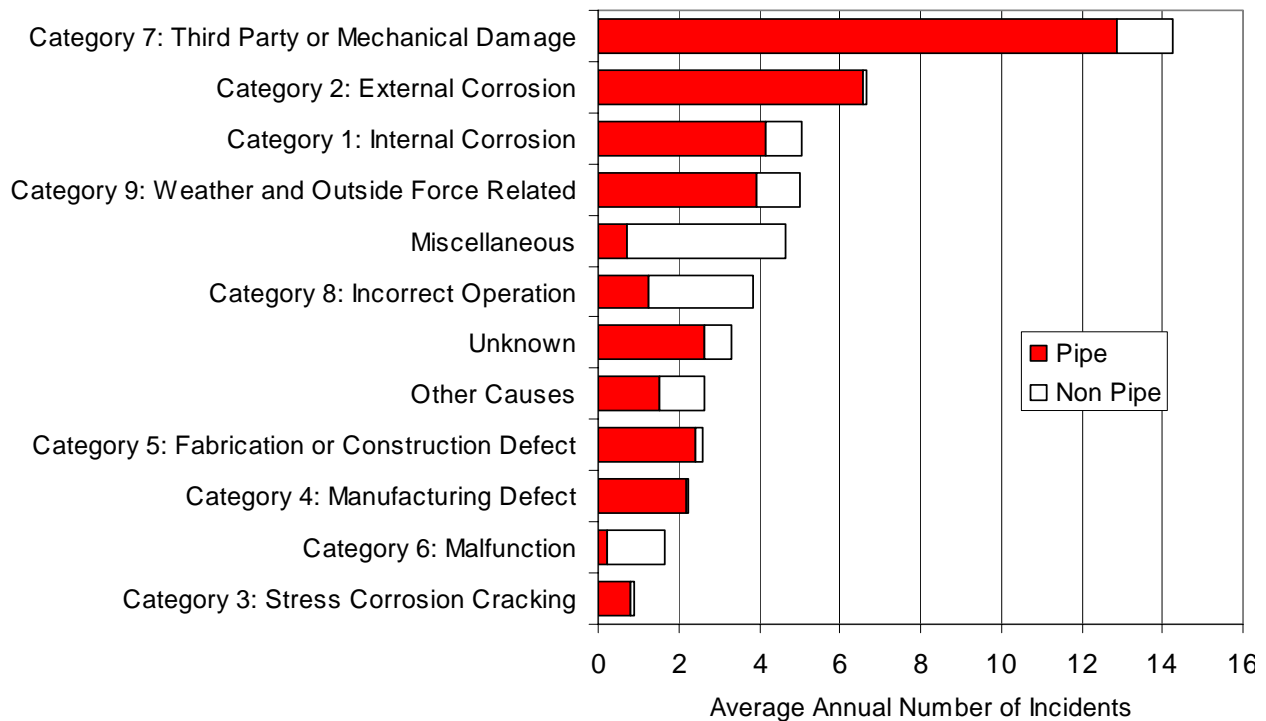


Figure 1. Reportable natural gas transmission incidents 1984-2000

The threat categories in Table 1 can be differentiated by their time-based behavior, as indicated in the fourth column. “Time Dependent” behavior indicates such threats can increase or decrease over time. Time-based inspection and maintenance practices can be effective in managing such threats. “Stable” behavior indicates such threats do not change over time, unless a change in the service conditions occur, such as a pressure increase, which activates the threat. Once activated, the otherwise stable threat can become time dependent. One-time inspection and/or maintenance practices can be effective in managing stable threats. The final grouping is “Time Independent” or threats whose occurrence is random in time. Because they lack a time dependence, such threats are managed best by protecting against their occurring or by limiting their consequences^(e.g., see 7,8).

The threat categories in Table 1, whether from the OPS reporting form or in B31.8S, apply to all pipelines regardless of age. However, as much change has occurred over time in both line pipe and its construction into pipelines⁽⁹⁻¹¹⁾, incidents and their causes in Categories 4 and 5 reflect the era the line pipe was made and the pipeline was constructed. As such, consideration of these threat categories is unique when assessing vintage pipeline integrity. For purposes of this report, pipe making and construction practices that are no longer used, including some early variations of current practices, are herein considered “historic.” “Vintage” pipelines are taken as those lines built using historic steel and pipe making pipe technology and related construction practices. Analysis of steel and pipe making practices and construction methods used to characterize the US gas-transmission pipeline infrastructure in Reference 11 indicates the vintage pipeline system involves construction prior to about 1970.

This report presents tools, technology, and related results useful in assessing the severity of threats due to anomalies introduced by historic steel-making, pipe-making, construction, and fabrication. Such information serves as guidance in developing and implementing an IMP, as an aid to managing the integrity of the vintage pipeline system.

Table 1. Categories of threats to integrity of natural-gas transmission pipelines

Category		Threat	Time Based Behavior
OPS	B31.8S		
F1	1	External corrosion	Time Dependent
F1	2	Internal corrosion	
F1	3	Stress corrosion cracking	
F5	4	Manufacturing defects	Stable unless activated by a change in service conditions
F5	5	Fabrication and construction defects	
F6	6	Equipment related defects	
F3	7	Third party or mechanical damage	Time Independent or Random
F6	8	Incorrect operations	
F2	9	Weather and outside force related	

This report complements other work done under the auspices of the Interstate Natural Gas Association of America (INGAA) in cooperation with the Gas Technology Institute, which was the cost-share project for this effort. One objective of that project was to identify which vintage line pipe and construction practices were more likely to involve historic defects in reference to B31.8S Categories Four and Five⁽¹¹⁾. In turn, that project complements parallel efforts of the Pipeline Research Council International (PRCI), and others, to help formalize the IMP efforts of their member companies. Central to this work was the consensus development of ASME B31.8S, whose provisions play an integral role in Title 49 of the Code of Federal Regulations Part 192 (49 CFR Part 192), Subpart O, Pipeline Integrity Management. ASME B31.8S recommends that gas pipeline operators identify and evaluate potential threats to the integrity of each pipeline segment within HCAs. This report uses the tools and technology discussed to trend the time-dependent growth of defects to help operators develop rational integrity management plans in reference to the potential for defect growth and the revalidation of lines that might involve such defects.

Objectives and Scope

The objective of this project was to develop a quantitative basis for evaluating the significance of specific time-dependent threats on steel pipelines, which can be used to assist in evaluating the viability of mitigative measures used in integrity management. This report is specific to the threats covered by the shading in Table 1, and so addresses categories one through five. This report does not address the remaining threat categories (i.e., equipment related defects, third party or mechanical damage, incorrect operations, and weather/outside-force).

As proposed, the scope embraced time-dependent material and construction threats including defects in pipe seams, pipe bodies, pipe-to-pipe girth welds and other fabrication welds, and

defects that result from pipe making or pipeline construction. Time-dependent threats to be covered include: external corrosion, internal corrosion, and stress-corrosion cracking. Defects as defined above embraced those present in the pipe steel and/or coating, but not with respect to problems with corrosion protection and/or avoidance systems.

By virtue of its INGAA cost-share, the focus here is transmission pipelines, which for present purposes are defined in reference to 49CFR Part 192. Issues unique to larger-diameter trunk-lines operating at low-wall-stress pipelines can be found in Reference 12. While the planned focus was transmission pipelines operating at higher pressures, the results developed could be used in situations involving lower pressures for otherwise identical circumstances, although the results adapted to other applications like lower-pressure pipelines could be quite conservative. Finally, because the cost-share project for this work involves gas-transmission applications, the focus here is operational scenarios considered representative of the typical operation of such pipelines.

The report does not address offshore pipelines or service lines, nor does it address pipelines not made of typical historic line-pipe steel or constructed with other than usual historic practices. The cost-share companion study for this project done under the auspices of the INGAA Foundation⁽¹¹⁾ provides guidance on determining whether a given type of flaw is likely to be present on a given historic pipeline, and if so, indicates whether the flaw may grow or otherwise presents a current threat to integrity.

Definitions

Terms are introduced in pipe-related codes and specifications to discriminate operating and related design circumstances and to describe abnormalities that may exist. Terms involving features introduced in manufacturing and construction are defined consistent with the definitions adopted in ASME B31.8S, whereas terms involving operation and design reflect 49CFR Part192, which regulates these aspects.

For the present the design factor (DF) and the specified minimum yield stress² (SMYS) are as defined by 49CFR Part 192, which regulates these parameters (e.g., see §105, §107, and §111). The American Petroleum Institute (API) Specification 5L⁽¹³⁾ also includes definitions for SMYS and ultimate tensile stress (UTS), denoted specified minimum tensile stress (SMTS), the latter being adopted for present purposes. To ensure consistent understanding of terms beyond those defined in 49CFR Part192 and API Specification 5L, the following definitions are introduced:

- Anomaly – Any deviation in the properties of the engineered product, typically found by nondestructive inspection. (The term indication is sometimes used in place of anomaly.)
- Flaw – A deviation in the properties or function of the engineered product that is outside of the engineering specifications for the type of service anticipated in design.
- Imperfection – A flaw that an analysis shows does not lower the failure pressure below the specified minimum yield pressure or limit functionality of the engineered product.

² Regulations, codes, and specifications tend to use strength, which has units of force, in this usage, whereas this term defines a value with units of force per unit area, which is stress. To be consistent with its use and units, the term stress is used herein. Such is also done for UTS.

- Defect – A flaw that an analysis shows could reduce the failure pressure to below the minimum specified yield pressure or limit functionality of the engineered product.
- Critical Defect³ – A flaw that an analysis predicts could fail below the pipeline’s maximum allowable operating pressure (MAOP), or precludes in-service function.
- Transmission Pipeline – By 49 CFR 192.3, these are pipelines operating at over 20-percent of the yield pressure. Typically, transmission pipelines are larger diameter steel lines operating at higher pressures transporting gas from a gathering line or storage facility to a distribution center, storage facility, or large volume customer.

In regard to these definitions, Reference 11 elaborates 1) the types of anomalies produced by historic manufacturing, fabrication, and construction practices, 2) the qualitative conditions necessary to “activate” the anomalies whereby otherwise dormant anomalies become active threats, and 3) mitigation practices used to control the growth of the anomalies in reference to buried vintage pipelines. Reference 11 should be consulted for guidance in these aspects, which are not considered – except that qualitative conditions that “activate” defects noted in that work are herein translated into quantitative measures that can be used by pipeline engineers.

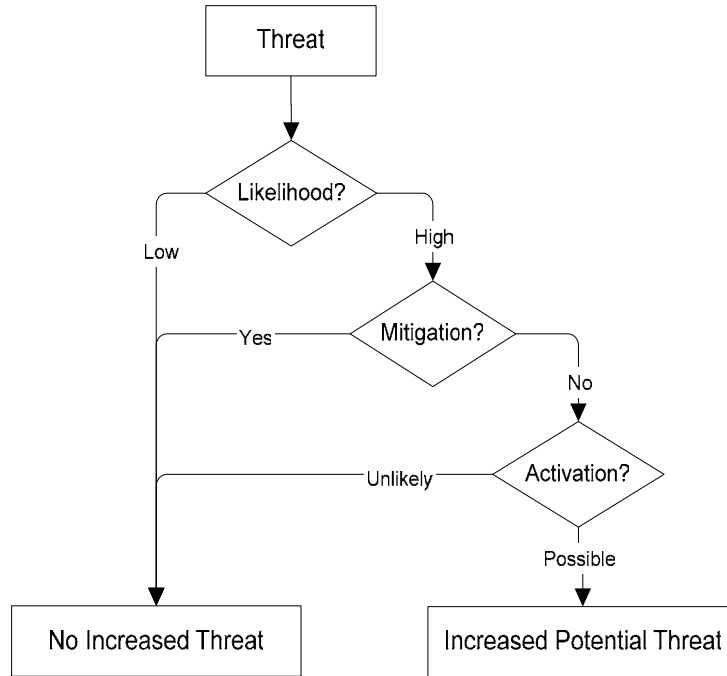
Approach – Quantitative Threat Assessment

Technology for assessing defect severity and the interval for revalidation for any structure has been presented and discussed in textbooks since the early 1970s, when the necessary technology reached widespread practical utility. Its utility and popularity are evident in textbooks focused on its use that include specific structural applications^(e.g., 15-17). The ensuing decade gave rise to handbooks to facilitate broader use of such technologies, which further illustrate their utility and application^(e.g., 18,19). As the aerospace, nuclear, ground vehicle, and offshore industries were among the first to capitalize on this technology, the early manuals and advanced-technology conference proceedings focused on related problems^(e.g., 19-22).

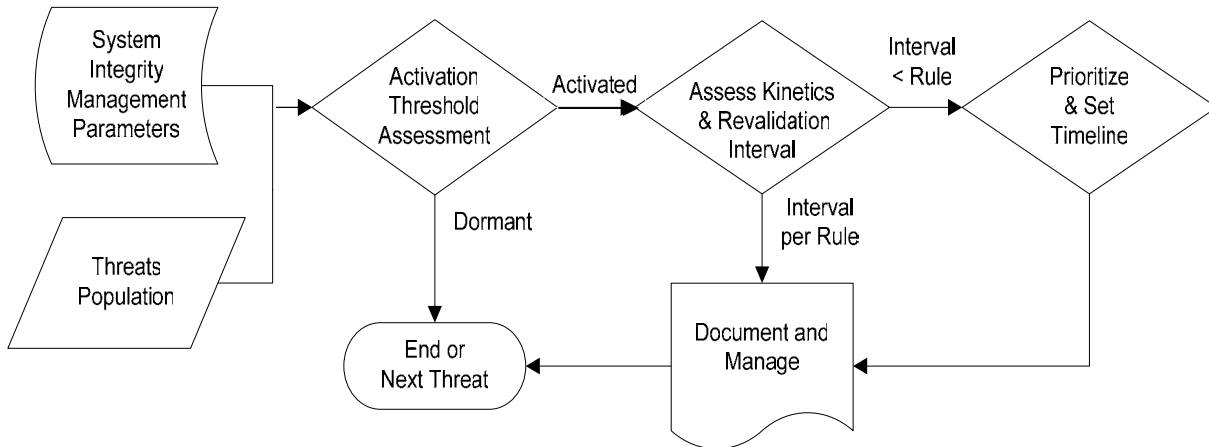
The utility of such technology was likewise adapted for pipeline applications. The initial work was largely empirical^(e.g., 23), apparently because transmission pipelines neither behaved linearly as was the case for the aluminum alloys popular in the aerospace industry, nor did they show the large-scale plasticity evident in nuclear piping operating at higher temperatures. More formal adaptation that recognized the moderate plasticity shown by the line pipe predominant in the industry through the 1970s began for axial cracking in 1984⁽²⁴⁾. This work culminated in a time-marching adaptation of technology developed for nuclear piping that targeted the response typical of then available line-pipe steels⁽²⁵⁾, which since has been extended to include a plastic-collapse formulation^(e.g., see 26). The time-dependence of this fracture formulation, when coupled with appropriate analysis for cycle dependent processes like fatigue^(e.g., 27), or other time and/or stress dependent mechanisms like stress-corrosion cracking^(e.g., 28) (SCC) provides the basis to assess the response of defects in transmission pipeline systems.

This report makes use of available technology to develop pipeline-specific results to help in integrity management of vintage pipeline systems. The approach taken to implement this technology is presented in the flowcharts in Figure 2.

³ The term critical defect is often used to identify a defect that will rupture⁽¹⁴⁾. Such use is not implied here.



a) threat assessment



b) activation and revalidation intervals

Figure 2. Flowcharts of the integrity assessment and management process

High-Level View of Threat Assessment

Figure 2a outlines the threat assessment approach and so presents its implementation from a high level. Figure 2a indicates threat assessment involves three major activities sequenced in the order noted, which are associated with:

1. the likelihood the flaw is present,
2. the effect of mitigation and/or control, and

3. the presence of other conditions that increase or decrease the likelihood a flaw will grow or become “active.”

The chosen sequence reflects the level of complexity involved in addressing threats, with the first focused on its existence, and the second whether actions have been taken to mitigate or otherwise offset concern for the threat. Each of the first two steps can be evaluated based on company records, with consideration of both steps possible during that evaluation, as follows.

As guidance for the first step, Appendix A tabulates information in reference to pipe supplier, seam type if any, year of production, grade, and construction practices. This first step requires evaluation of company files and the experience of operators with similar vintage pipelines. For well developed IMPs, such information should be readily available in the IMP database. This consideration of whether defects could be present or a threat exists is done without reference to the technology issues dealt with herein.

The second step is taken only when the first step indicates it is necessary. As needed, the files or database are evaluated to assess the effects of actions taken to mitigate the threat or defect, or to control its future development or consequences. For example, where the likelihood of weld-seam defects is indicated in step one, where the files indicate a high-pressure hydrotest has been done and the historical operation is unchanged, long dormant defects are unlikely to become active. Alternatively, where vintage construction practices introduced features like couplings or oxyacetylene welds that have since been rehabilitated or otherwise shown to be stable, these long stable features are unlikely to become an integrity issue. However, when threats of defects cannot be concluded inactive, then step three is implemented.

While Steps One and Two can be implemented without resort to technology, Step Three typically requires quantitative rather than qualitative evaluation. Exceptions to this include scenarios addressed directly in the literature, for which available data or published integrity assessments facilitate simple and direct evaluation. Examples of construction features for which analysis exist include wrinklebends⁽²⁹⁾. Likewise, where mechanisms like SCC or hydrogen-stress cracking (HSC) are involved but can be shown inactive by reference to a published threshold stress or other characteristics of the line pipe^(e.g., 30,31), Step Three can be straightforward. However, all other scenarios require detailed consideration of the approach and results presented herein, or to other similar results.

Threat Assessment Process for Crack-Like Defects

Prior work⁽⁷⁾ has considered material and construction threats as well as the in-service growth of defects associated with such threats, and developed a plan to implement such results in an IMP⁽⁸⁾. Reference 8 deals with blunt corrosion defects quite simply, but presents only a high-level approach for crack-like defects, as their analysis and the related kinetics is much more complex. As is evident later, issues related to blunt corrosion defects are rather directly evaluated. For this reason, this report addresses crack-like defects in more detail, dealing with them in the manner outlined by textbooks and conference papers beginning in the 1970s. Such references indicate the evaluation of crack-like defects, in reference to activation and the related kinetics concerns identified in Figure 2a, tracks the process presented in the flowchart presented in Figure 2b.

Figure 2b indicates the generic analysis process for crack-like defects requires information that characterizes the population of defects (type, size, shape, and orientation) as well as information

that characterizes the line pipe wherein the defects are found and the pipelines operational and RoW factors that can promote growth of such features.

The approach to address the scope of crack-like defect type, size, shape, and orientation involves first considering all such features as sharp, and thereafter assessing what is found in the field as either predominantly circumferential or axial. In this context, results will be developed specific to these two orientations. Finally, a range of defect sizes and shapes will be considered, with depth evaluated relative to the wall thickness and length evaluated over a range from one inch up to a length equal to the pipe diameter, with results presented for combinations of depth and length over that range of values.

Ideally, the flowchart in Figure 2b would evaluate all plausible combinations of pipe geometry and properties of practical interest, and all possible service/operational loadings and RoW scenarios of concern. Quantifying the response of defects in pipe seams, pipe bodies, pipe-to-pipe girth welds and other fabrication welds, and defects that result from pipe making or pipeline construction to service loadings is practically impossible given the endless possible combinations of defect type, size, shape, and orientation for every plausible combination of pipe geometry and properties, over all possible service loading and RoW scenarios.

The approach taken to address the breadth of vintage pipeline scenarios involves identifying and evaluating cases that represent the extremes of the vintage pipeline system, and an intermediate scenario. This will be done for corrosion and the cracking mechanisms that pose a first-order threat to pipelines: specifically fatigue, SCC, and HSC. Thresholds and kinetics will be developed that characterize typical response. Axial crack-like defects respond to pressure, which herein will be generalized in reference to pressure-induced stress. Pipeline service will be considered in a generic fashion in terms of maximum pressure coupled with pressure cycles, where as noted in the introduction the focus is operational histories common to gas-transmission service. In contrast, circumferential defects respond to axial loads that for the present will be assessed in reference to the axial wall stress. As the behavior of pipelines is elastic and the stresses are simply related to pressure and axial or bending loads, results presented in terms of stress reflect broad coverage of possible field scenarios.

Key Tasks and Report Organization

Tasks to meet the objectives can be directly identified in reference to Figure 2b. Six tasks can be so identified to establish the technical basis to assess effect severity and revalidation intervals for pipelines that involve such defects:

1. characterize the vintage pipeline system and identify representative scenarios,
2. identify factors controlling degradation at time-dependent fabrication and construction defects.
3. determine the condition of the subject pipeline and establish the likely presence of defects that are likely active and so can fail in a time-dependent manner, and determine their terminal sizes,
4. mathematically characterize defects as a function of size and shape as the basis to assess material and construction defects, and develop an algorithm that embeds these factors and thereafter develop results to assess their significance,

5. extend the flow-chart of Figure 2b to lead users on a go – no-go path to determine if their crack-like defect is a concern, and over what timeline, and
6. use full-scale tests and incident trends and/or experience to validate the results.

The report develops in the sequence indicated above, beginning by identifying scenarios that represent the vintage pipeline system in terms of the parameters essential to integrity analysis of crack-like defects. Thereafter, factors controlling degradation at time-dependent defects are developed, along with screening to determine whether the subject pipeline is likely to involve crack-like defects that are active and so can fail in a time-dependent manner. Next, previously developed software is used to mathematically characterize crack-like defects and develop results to evaluate their significance. Finally, a flowchart is presented to determine if a defect is a concern, and over what timeline, and thereafter the results are validated.

The Vintage Pipeline System and Representative Scenarios

As indicated above it is impractical to consider all plausible service/operational loadings and RoW scenarios, but it is practical to evaluate representative scenarios characterized in reference to line pipe properties that control pipeline integrity. Such can be done via parametric analyses of defect size and shape for the range of line pipe diameter and wall thickness that define typical vintage line pipe geometric properties, over the range of line pipe steel grades and toughness considered typical of the vintage pipeline system.

The vintage pipeline system might be defined in reference to line pipe properties (pipe geometry and steel properties) that have caused recurrent problems for vintage pipelines by trending the OPS incident database^(e.g., 2). However, this database reflects incidents from the period from 1984, and so reflects scenarios other than that typical of the vintage pipeline system. For this reason, resources other than the OPS incident database have been used to scope line pipe properties that dominate the vintage pipeline system, beginning in reference to pipeline mileage and then progressing through diameter, wall thickness, grade, design factor, and toughness.

Vintage Pipeline System: Mileage

Figure 3 shows the cumulative distribution of gas-transmission pipeline mileage for construction over the interval from before 1940 through 2002. This information was compiled from data on the OPS website based on data submitted by the operating companies concerning their transmission-pipeline network. This annual data has been downloaded from the same website that addresses the incident data⁽²⁾.

Figure 3 indicates that in 2002 the natural-gas pipeline infrastructure in the US comprised ~300,000 miles of transmission pipelines. Of this, ~13,000 miles (~4-percent of the total) was built before 1940, ~29,000 miles (~10-percent of the total) was in service through 1950, ~53,000 miles (~18-percent of the total) through 1960, ~125,000 miles (~43-percent of the total) through 1970, and ~200,000 miles (~69-percent of the total) through 1980, which can be determined from Figure 3. Consequently, the vintage pipeline system as defined herein comprises about 68-percent of the gas-transmission infrastructure.

Vintage Pipeline System: Diameter and Wall Thickness

Insight into line pipe geometry (diameter and wall thickness) that comprises the vintage pipeline system can be developed from several sources. For example, Figure 4 derived from the same OPS infrastructure database used to generate Figure 3 shows the cumulative distribution of line-pipe diameter for the pipeline infrastructure completed prior to 2002. It is evident from this figure that as the mileage increased the diameter of line pipe used also increased. Unfortunately, diameter is not so

characterized in reference to construction period nor is such information available to quantify the distribution of wall thickness as such data have not been compiled.

Fortunately, other sources are available to characterize the line pipe geometries that comprise the vintage pipeline system. A web-crawl of steels suppliers directed at the evolution in the width of steel strip and plate, which are dictated by mill rolling capacity, could be used to establish the maximum diameter of seamed pipe as a function of time. But, this is impractical as many mills have closed, with this data otherwise lost save for the history compiled by Keifner and Clark⁽⁹⁾. Subsequent comments by Kiefner⁽¹⁰⁾ and Clark et al⁽¹¹⁾ serve to distill the extensive detail of Reference 9. For example, Kiefner⁽¹⁰⁾ indicates that larger diameter line pipe – the order of 24 inches – was available in the 1920s, produced with an electric-resistance-weld (ERW) long seam, with diameters from 24 to 30 inches available beginning in the 1940s produced with a double-

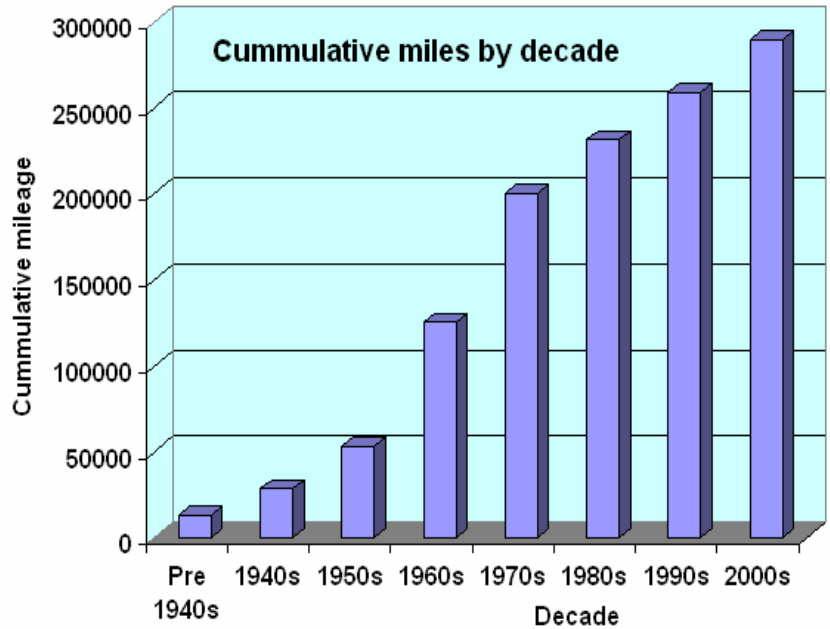


Figure 3. Cumulative mileage by decade (OPS⁽²⁾)

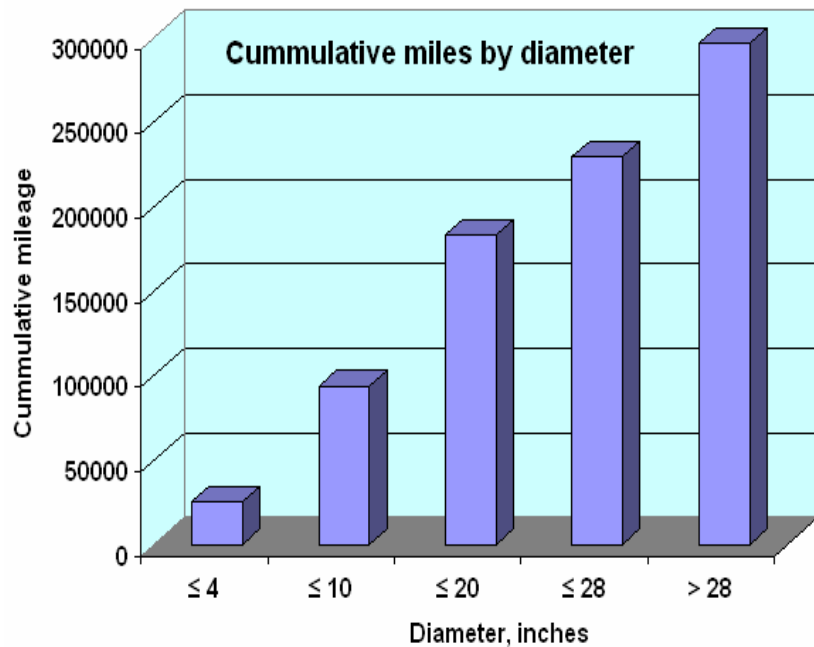


Figure 4. Cumulative mileage by diameter (OPS⁽²⁾)

submerged-arc-weld (DSAW) long seam, as well as by other processes. Kiefner further notes that 36-inch diameter line pipe becomes available in the 1950s, citing its availability in grades X42 and X52. Clark et al⁽¹¹⁾ indicate the timeline for various steel-making and pipe production practices. Still larger diameters and higher strength grades became available in the 1960s, with the trend to larger diameter and higher strength continuing today, driven by economics and related concerns⁽³⁴⁾. The data available imply the distribution of mileage shown in Figure 4 reflects use of increased diameter as it became available, with construction continuing to use smaller diameters as economics dictated.

Finally, because the comments by Kiefner⁽¹⁰⁾ and Clark et al⁽¹¹⁾ provide little quantitative data, the distribution of line pipe sizes in use in vintage pipeline systems has been characterized by use of the assumption that on average incidents on cross-country (remote) pipelines do not correlate directly with design factor of the pipeline or the properties of the line pipe. The viability of this assumption and the resulting data can be demonstrated in regard to Figure 5, reproduced from Reference 35. This figure presents results for the then current OPS incident database (circa 1984 to 2000) sorted by Class Location, which defines the design factor (except for unusual circumstances)⁽³⁾. Thereafter, the data were normalized by pipeline mileage as a function of Class Location to offset the significant differences in mileage distribution between these locations. Because the mileage for the design factors representing Class 3 and 4 Locations was relatively small, this mileage was combined to reduce inaccuracy that could otherwise be introduced in this normalization⁴.

Figure 5 indicates that normalized incident frequency does not increase with increasing design factor, but rather suggests the reverse trend. As can be seen in the figure, such was observed for each of the OPS incident categories in use when this data was assembled, which were corrosion,

outside forces, material/construction defects, and other causes. That increased design factor did not correlate well with the likelihood of failure was rationalized in Reference 35 for two reasons. First, the design factor immediately adjacent to area where failure originates is identical to the design factor just inches away from the origin, which proves design factor is not a first-order factor controlling incident likelihood. Second, considerations other than the design factor were noted to control the likelihood of an incident, whereas line pressure was noted as a possible influence

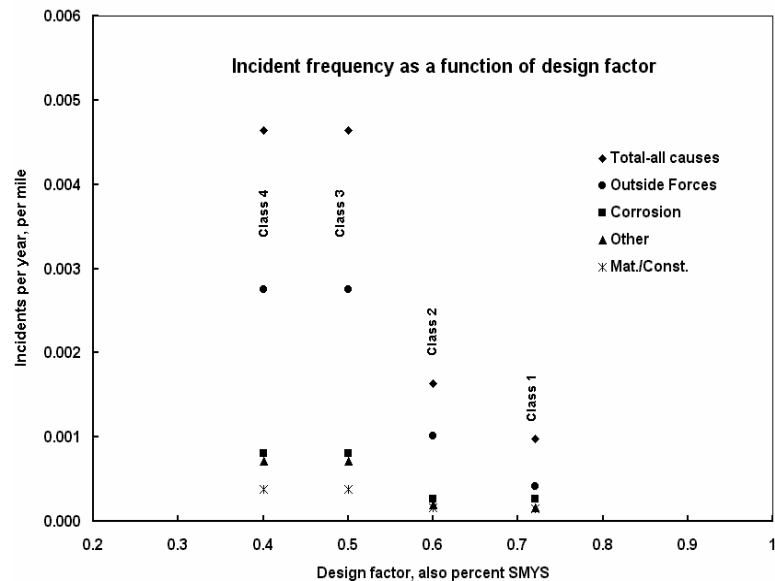


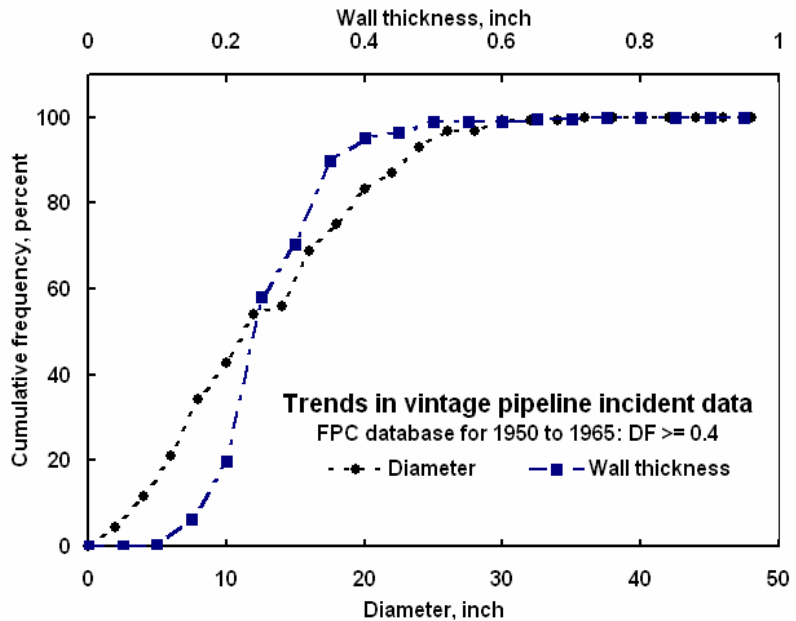
Figure 5. Incident frequency for OPS data as a function of design factor (after Reference 23)

⁴ For further details, see Reference 35 where these results are compiled and analyzed.

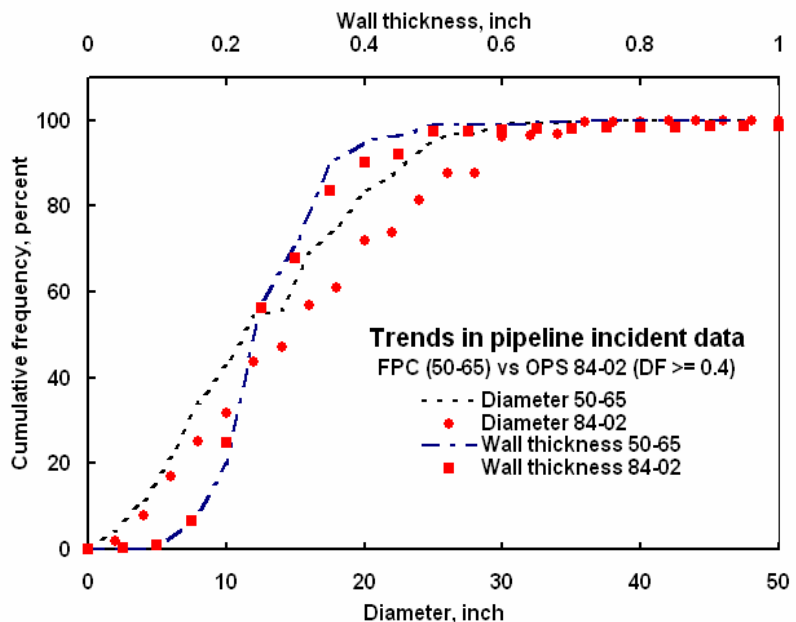
on consequences. For example, stray currents or other RoW aspects drive corrosion and related processes, which are independent of design factor. Material and construction incidents reflect the location of defects introduced by an upset in pipe steel or making, or in pipeline construction, which are random with reference to design factor. Outside force incidents equally reflect otherwise uncontrolled events, which are random in regard to design factor. As a similar rationale applies to pipeline properties, they too are uncorrelated with design factor. On this basis, the assumption that incidents on cross-country (remote) pipelines do not correlate with design factor or line pipe properties is viable as are data developed through its use.

Figure 6 presents trends derived based on the just-noted assumption. Figure 6a represents the vintage system based on the Federal Power Commission (FPC) database⁽³²⁾ in terms of incidents occurring over the interval from 1950 to 1965. Consequently, this distribution reflects pipeline construction and line pipe produced through 1965. Figure 6b presents the results from Figure 6a as dashed lines and contrasts these to results from the OPS database representing incidents that occurred from 1984 through 2002, which reflects construction and line pipe through 2002. While not shown for the sake of clarity, similar trends develop for the incident database covering the period from 1970 through 1983⁽⁴⁷⁾.

It is apparent from Figures 6a and 6b that the vintage system can be represented by extremes in diameter chosen at 4-inches and 24-inches, with 12-inches being a reasonable mean diameter. Similarly chosen extremes on wall thickness are 0.187-inch and 0.375-inch, with 0.225-inch being a reasonable mean. In reference to Figure 4, the indicated range of diameters and wall thicknesses represent



a) vintage pipeline trends derived from the FPC database⁽³²⁾



b) pipeline trends derived from the OPS database⁽²⁾

Figure 6. Trends in vintage diameter and wall thickness

about two-thirds of the gas-transmission pipeline infrastructure. This outcome is consistent with the independent indication of the vintage system based on mileage evident in Figure 3.

Interplay between Diameter, Wall Thickness, Grade, and Design Factor

While Figure 6 indicates the vintage gas-transmission pipeline system can be represented by a set of diameter and wall thickness combinations chosen independently by inspection of this figure, this approach to identify these parameters is in conflict with 49CFR Part 192 (§105, §107, and §111). The equation in Part 192 §105 shows these parameters are not independent, and also indicates they are coupled to grade and design factor, the latter being elaborated on in Part 192 §107 and §111.

The relationship between wall thickness and diameter conditioned by design factor and grade is evident in the trends presented in Figure 6b. As indicated above, this figure contrasts the vintage system characterized by dashed trends with the more modern system represented by data trends. It is evident there that there is little difference in the wall thickness distributions for incidents reported beginning in 1950 and those beginning in the mid-1980s. This outcome reflects the effects of steel grade, which has increased continually and significantly over this period as is evident in Figure 7. This outcome also reflects the overarching economic push to limit the cost of steel and construction costs, both being driven by wall thickness⁽³⁴⁾. Finally, it reflects the interplay between pipe diameter, wall thickness, and grade according to working stress (elastic) design (WSD) as detailed in textbooks on the theory of elasticity^(e.g., 36).

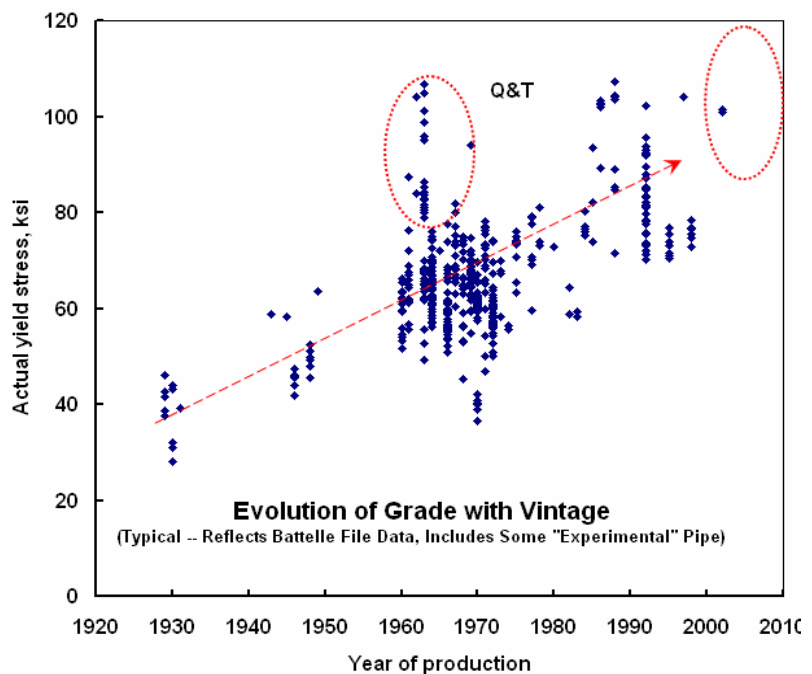


Figure 7. Evolution of line-pipe yield stress

The regulations (49CFR Part 192) in sections 105, 107, and 111 outline this relationship, wherein maximum allowable stress (MAS) can be written as:

$$\text{MAS} = \text{DF} \cdot \text{SMYS} , \tag{1}$$

where DF = design factor whose value is less than one to provide a margin of safety to ensure the response remains elastic in service, with:

$$\text{MAOP} = \text{DF} \cdot \text{SMYS} \cdot (t / R) \tag{2}$$

where t = wall thickness and 2R = pipeline outside diameter (OD). Early pipeline designs used a single design factor = 0.72⁽³⁷⁾, while design under 49CFR192 involves three design factors. One

is a class-location factor that accounts for population density near the pipeline, which ranges from 0.4 for pipelines in heavily populated areas to 0.72 for lines in less populated or rural areas. The second is a longitudinal joint factor that accounts for seam welds that had a higher flaw frequency, which ranges from 0.6 for early welding processes up to 1.0. The third is a temperature de-rating factor, which applies at operating temperatures above 250°F (uncommon because gas transmission pipelines typically operate at 140°F and less). Of these, the first is relevant across the vintage pipeline system, while the second two would be evaluated on a case specific basis.

Vintage Pipeline System: Grade and Design Factor

It remains to quantify the time variation of SMYS and DF in order to use Equation 2 to identify wall thickness trends consistent with Figures 3 through 6. Unfortunately, no known database has been developed that tabulates line pipe grade, diameter, wall thickness, or design factor by vintage, mileage, or any other useful metric. However, other publications and related analyses can be used to quantify these parameters.

The range of grades that can be considered typical of the vintage system can be inferred from Figure 7. These archival Battelle data reflect actual yield stress for more than 700 joints of line pipe produced over the interval from the 1930s to the present. These results indicate that SMYS in the vintage system can be represented by Gr A or Gr B at the lower end, with X52 or X60 representing the upper end, and X42 being a reasonable mean level. These grades remain viable when considered in reference to publications that explore the historic availability of certain classes of steel and the introduction of new grades^(e.g., 9-11,35), but suggest Gr B be adopted as the lower limit, with X52 taken as the upper limit. Such considerations lead to Table 2, which summarizes line pipe grades that typify transmission pipeline construction in the US. Given these results, Gr B, X42, and X52 are adopted to represent the majority of the line pipe in the vintage US transmission pipeline system.

Table 2. Summary of property combinations by decade for US gas transmission system

Decade	≤ 1930s	1940s	1950s	1960s	1970s	1980s	1990s
Grade	GrA/GrB	GrB/X46	X42/X52	X52/X60	X60/X65	X65/X70	X75

It is noteworthy that technology is evolving to better characterize the mechanical properties of line pipe in-situ, which could be useful in managing some unique vintage scenarios. Field hardware and techniques exist to measure the hardness of the pipe in-situ^(e.g., 38), and correlations exist between hardness and the mechanical properties by which to infer the yield stress^(e.g., 39). Commercial equipment has been developed to both make the field measurement and infer the mechanical properties^(i.e., 38). Databases also are being developed to supplement operating company files^(e.g., 40-42). As the IMP process continues to be implemented, further information will become available in complement to that recently published^(e.g., 43,44), broadening these databases even further.

It remains to establish the likely variation in the design factor for the vintage system in order to identify values of wall thickness that couple with diameter, to fully characterize the vintage pipeline system for subsequent analyses of crack-growth thresholds and inspection intervals.

The distribution of the design factor can be bracketed for the vintage pipeline system in reference to Figure 8, which is reproduced here from Reference 7. Figure 8 presents the distribution of gas-transmission pipeline mileage grouped by geographic region, and then subdivided by class location for about 50,000 miles of the ~30,000 miles that comprise the US system. While only about 17-percent of the system was characterized when these data were gathered in 2001, the trends in these data are clear. Figure 8 indicates that in 2001 even highly urbanized areas were 65 to 70-percent Class 1, whereas much of the rest of the system was at 90 to 95-percent Class 1. Given this dominance and the observation that much of this encroachment to the transmission pipeline system has been recent⁽⁴⁵⁾, the vintage pipeline system can be reasonably represented by DF = 0.72.

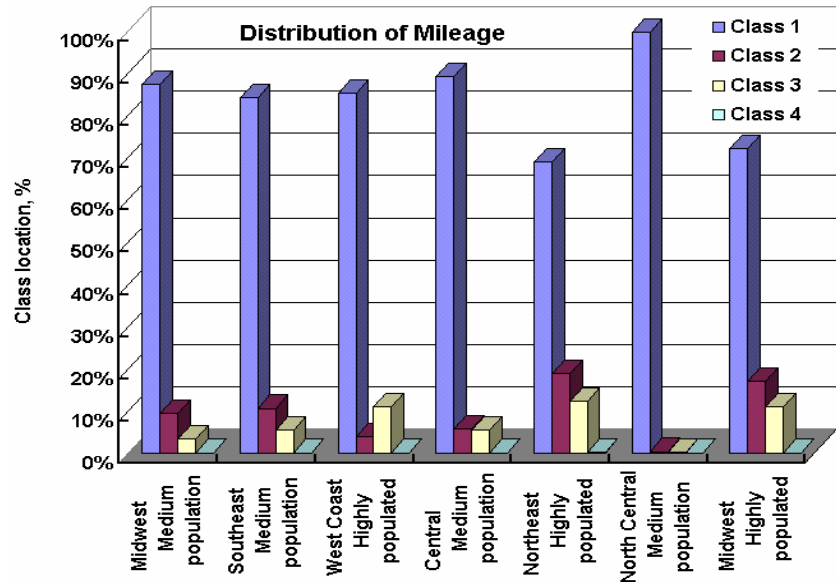


Figure 8. Distribution of gas-transmission class locations in the U.S. by geographic region⁽⁷⁾

Design Parameters that Characterize the Vintage Pipeline System

In view of the above discussion, with DF = 0.72 the values of MAS representing Gr B, X42, and X52 are 25.2 ksi, 30.2 ksi, and 37.4 ksi, respectively. On this basis, values of wall thickness for Gr B, X42, and X53 for 4-, 12-, and 24-inch diameter pipelines operating at the same design pressure are as indicated in Table 3. As can be seen from this table, wall thickness ranges from quite thin at 0.040 inch, up through 0.357 inch for pipelines designed for MAOP = 750 psi, a not uncommon design pressure based on the data assembled by the Federal Power Commission (FPC)⁽³²⁾. Such bounds on thickness are consistent with the limits evident in Table 4.

Table 3. Wall thickness calculated per 49CFR Part 192

Grade	Wall thickness (inch)	Pipe diameter		
	@750 psi	4 inch	12 inch	24 inch
Gr B		0.060	0.179	0.357
X42		0.050	0.149	0.298
X52		0.040	0.120	0.240

If viable, these values and the underlying trends in Figures 7 and 8 should be consistent with the historic evolution in diameter and wall thickness evident in Figure 6b. Recall that Figure 6b

contrasts data that begins in 1950 with that beginning in the mid-1980s. Figure 6b indicates that the distribution of wall thickness has remained more or less constant over this period, whereas the ratio of the slopes for the 1950s and mid-1980s diameter trends indicates diameter increased by a factor of 1.5 or 50-percent. If the earlier assumption that incidents are random in reference to design parameters is adopted, and the design factor is taken constant over this period, the increase in diameter must be due to increased grade line pipe available over this period, all else being equal. That is, the increased diameter should occur in proportion to the increase in SMYS over this time period. Figure 7 indicates that SMYS has increased from ~52 ksi to ~80 ksi over the period beginning in 1950 and ending in mid-1980, for an increase of $80/52 = 1.54$ or 54-percent. Thus, the data in Figure 6 indicate a 50-percent increase in diameter whereas the results in Figure 7 point to an increase over this same period of 54-percent. This consistency among these independently determined trends lends credence to the line-pipe properties adopted in terms of SMYS, diameter, and wall thickness, and indicates the parameters are viable metrics for the vintage system.

Fracture Properties for the Vintage Pipeline System

The remaining parameters needed to assess pipeline integrity and revalidation intervals become important when the pipe wall thickness required according to WSD is diminished locally by the presence of an anomaly. The other parameters important in such situations involve fracture initiation. Textbooks address fracture initiation and fracture-initiation resistance or toughness in general terms, while References 14 and 35 focus on line pipe steels and pipeline issues. The toughness of typical vintage line pipe is difficult to determine, as little has been written on this topic. The literature^(e.g., 14-17,35,46-48) addresses the need for toughness or tend to trend it in terms of so-called upper shelf energy (USE) based on Charpy-vee-notch (CVN) test⁽⁴⁹⁾ data. However, little is available in reference to the ductile-to-brittle transition temperature (DBTT), a potentially important parameter in specifying steel⁽⁵⁰⁾, whose behavior has been shown to vary significantly depending on the steel involved^(e.g., 51). The exceptions to this involving vintage line-pipe steel covering both toughness and DBTT include References 40-44 and 52. References 40 and 52 include data for vintage longitudinal weld seams.

Figure 9 presents one assessment of the evolution of toughness available over the time interval of interest, beginning in the 1930s and

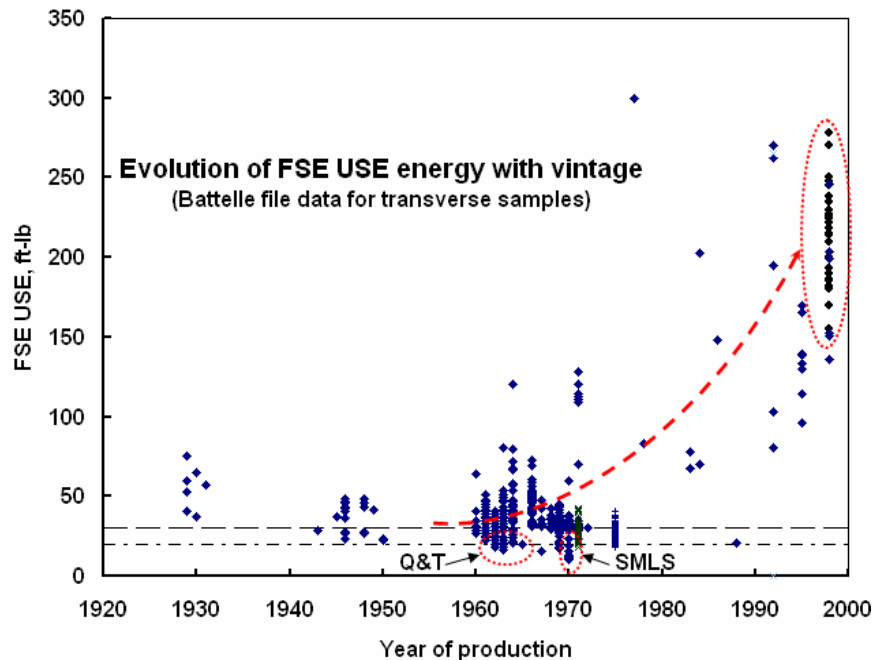


Figure 9. Historical evolution of USE for line pipe

continuing to recent time. These archival Battelle data reflect toughness characterized by the full-size equivalent (FSE) USE for in excess of 600 joints of line pipe. Carbon-Manganese (C-M) steels, which typify steels available through the 1960s, show a trade-off between strength and ductility. Thus, the trend to increasing SMYS in these steels evident in Figure 7 indicates a decrease can be anticipated in ductility over this interval. In turn, this limits the strain over which strain hardening develops, which implies the UTS will lie closer to SMYS. Accordingly, the ratio of yield stress, Y, to ultimate stress, T, that is Y/T, will tend toward unity as SMYS increases. Figure 10 confirms this expectation in reference to C-M steels, indicating that a 30-percent reduction in ductility can be expected by increasing SMYS from Gr B to X52.

While not directly related, a decrease in ductility can signal a related decrease in fracture toughness such that the strength increase evident in Figure 7 for C-M steels could promote a decrease in USE. While the data are sparse, the results in Figure 9 show this tendency. Therein the toughness data for early-vintage steels is found to be slightly superior to that of the 1940s through the 1960s. Fortunately, the push for higher strength in trade for ductility and toughness ended in the late 1950s with the appearance of running brittle fracture⁽¹⁴⁾. Control of this

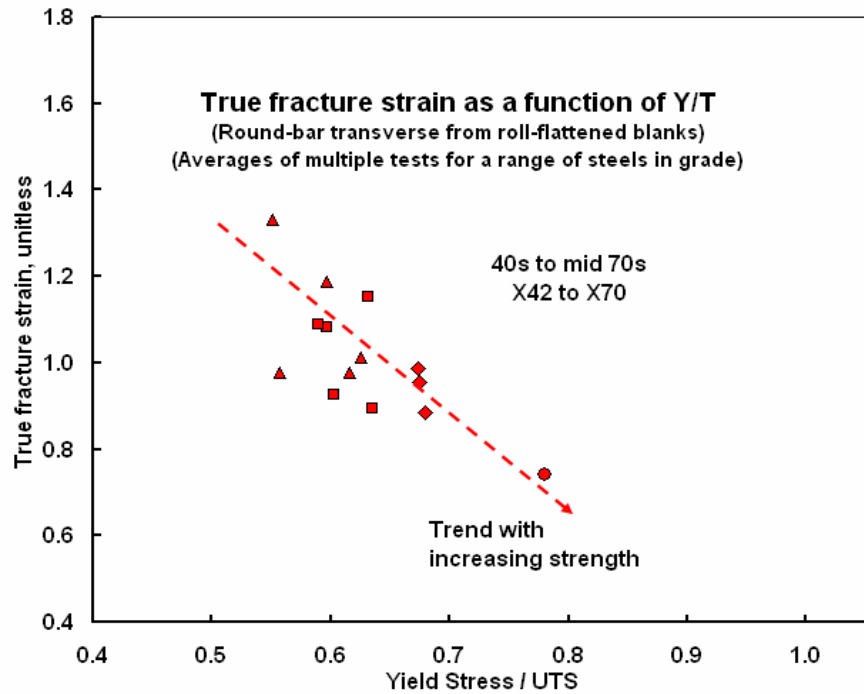


Figure 10. Decreased ductility with Y/T in C-M steels

phenomenon came by developing steels that were ductile at the service temperature, which reduced USE at that temperature at least initially^(e.g., 53). The tradeoff between strength and ductility (and implicitly toughness) characteristic of the C-M steels drove the evolution of modern high strength weldable steels beginning in the mid to late 1960s⁽¹¹⁾. The trends in Figure 9 indicate that this evolution resulted in a major increase in USE as compared to the differences apparent over the interval associated with the vintage pipeline system. These trends and the results of References 40-44 and 52 suggest the vintage system can be characterized by USE values that range from 10 to 30 ft-lb. However, where concern exists for anomalies in vintage weld seams, toughness an order of magnitude less can be anticipated for worst-case scenarios^(40,52).

Because the vintage steels had values of DBTT that often were above the line pipe's service temperature, the USE can overestimate the toughness available in service. The DBTT and related temperature dependence of the CVN energy through the transition region are essential to determine if the USE is applicable or transform the USE into a value that applies at the service temperature of the pipeline. Databases currently being collected⁽⁴⁰⁻⁴²⁾, which include these

properties for vintage systems will help diminish this knowledge gap, as will publications of work done to rehabilitate such systems where such properties are included^(e.g., 43,44,52,54). While technology exists to support quantifying mechanical properties specific to a given pipeline, field techniques designed to infer toughness properties from measured hardness of the pipe remain unproven through blind testing. Thus, care should be taken when considering such practices until commercial equipment evolving for this purpose is appropriately proven in blind tests.

The available data and the historical evolution of line pipe steels suggest that toughness be combined with the grades noted in Table 3 in the manner shown in Table 4. These combinations underlie the choice of toughness values for the analyses that follow much later. In using such results it must be noted that the toughness values added to Table 3 are considered representative of the decade and the grades indicated. However, exceptions exist across this table, with values lying well above as well as well below the tabulated values known to exist. Further, it is known that selected grades and specific production practices led to line pipe whose toughness falls well below the toughness levels tabulated. For example, X60 produced in Europe and elsewhere in the late 1960s exhibits quite low toughness and high transition temperatures⁽⁵⁴⁾. Other similar scenarios are known for selected grades, vintages, and steel chemistry/production practices. Suffice it to note that care must be taken in using the results that follow in applications to vintage pipelines, as toughness at service temperature controls the defect size for failure, which in turn influences the time over which the defect can grow stably. It also is appropriate to indicate that toughness levels well above those in the table exist, even for vintage line pipe. In regard to results indicated for the recent decades, toughness levels well above these also exist, as the values indicated as well as levels much higher were available in the 1990s without price penalty. The Alliance Pipeline⁽⁵⁵⁾ is a prime example, with toughness predicted and demonstrated for fracture control the order of 175 ft-lb⁽⁵⁶⁾ being produced in the 1990s without problem or price penalty.

Table 4. Summary of property combinations by decade for the pipe body

Decade	≤ 1930s	1940s	1950s	1960s	1970s	1980s	1990s
Grade	GrA/GrB	GrB/X42	X42/X52	X52/X60	X60/X65	X65/X70	X75
USE, ft-lb	15	15	15	30	40	65-90	80-120

Failing Defect Sizes for the Vintage Pipeline System

The first step in evaluating the long-term stability of a defect involves determining the sizes of defects that fail as a function of pressure-induced wall stress for axially oriented features and axial stress for circumferentially oriented features. Such results will be determined for each of the pipe geometries and grades identified in Table 3, subject to the corresponding toughness levels indicated in Table 4. This follows the next section, which outlines the methods used to determine the sizes of defects that fail as a function of pressure-induced wall stress.

Prediction Methods

Whether based on an empirical solution or theoretical fracture mechanics analysis, failing defect sizes depend on two parameters. One is the wall stress in defect-free pipe while the second is the

size, shape, and orientation of the defect. Equation 3 expresses their coupled effect in a simple form consistent with theoretical and empirical solutions:

$$S_f = S_R \cdot f(\text{defect geometry}). \quad (3)$$

In this equation, S_f denotes the stress at failure, and S_R is a reference stress whose value should reflect the defect-free failure stress and $f(\text{defect geometry})$ embeds the effects of the defect geometry. This form of equation applies uniquely to circumferential and axial defects. In this form, the value of $f(\text{defect geometry})$ tends to unity as the size of the defect decreases to zero.

NG-18 Equations

Early predictions of failing defect sizes in pipelines dealt with axially oriented defects through empirically calibrated expressions known as the NG-18 equations^{(23,57)5}. Defect size was embedded as function in terms of its area, and the effects of bulging due to the defect that involved the length of the defect, L , the line pipe radius, R , and wall thickness, t . The reference stress was termed a “flow stress”⁽²³⁾, denoted here S_{fs} , whose value was empirically calibrated in reference to data that included the effects of geometry. The NG-18 Equation has the form:

$$S_f = S_{fs} \left[\frac{(1 - A / A_0)}{(1 - A / A_0)(M^{-1})} \right], \quad (4)$$

with the bulging factor M represented as $((1 + 0.6275 L^2 / 2R t - 0.003375 L^4 / (4R^2 t^2))^{0.5})$. As time passed, Equation 4 was adapted for use with crack-like surface flaws⁽²³⁾ and also blunt defects, the latter in the form of ASME B31G⁽⁵⁸⁾, which transitioned to Modified B31G⁽⁵⁹⁾ for simple geometries and RSTRENG^(59,60) for use with complex defects.

Initially the value of S_{fs} was expressed as a function of the flattened-transverse-strap yield stress, S_y , in the form:

$$S_{fs} = S_y + 10 \text{ ksi} . \quad (5)$$

In the transition from NG-18 Equations to ASME B31G this gave way to:

$$S_{fs} = 1.1 \times \text{SMYS} , \quad (5a)$$

which was used in conjunction with $f(\text{defect geometry})$ expressed in terms of a modified value of M and a parabolic defect shape as $0.67 (d \times L)$, where d denoted the maximum defect depth. The transition to Modified B31G and RSTRENG reformulated the effective defect area and dealt with what was viewed as excessive conservatism, wherein the above definition of flow stress shifted back to the earlier form:

$$S_{fs} = \text{SMYS} + 10 \text{ ksi} , \quad (5b)$$

⁵ Much of the early work on transmission pipelines was done under the auspices of the American Gas Association (AGA) as part of their project Number 18, which historically has been referred to as Project NG-18. This was the forerunner to the Pipeline Research Committee, which today is the Pipeline Research Council International.

except here S_y is replaced by SMYS, which was necessary for field applications where strap test results are unknown. This flow stress was used with f (defect geometry) expressed in the form $0.85 (d \times L)$, with related forms of M . For details see the references indicated.

Fracture-Mechanics and Plastic-Collapse Based Formulations

Textbooks indicate that structures like pipelines can fail in two ways – if the strength is exceeded or if the resistance to crack extension is exceeded – with either causing failure in a pipeline when the pressure boundary is breached. Either a leak or rupture ensues.

Where failure occurs because the strength is exceeded, the failure process in structures made of ductile metals is known as plastic collapse, which occurs at a stress level corresponding to the UTS of the metal involved. Because pipelines are designed to remain elastic, and do so under normal operation through use of a design factor that keeps the stresses well below yield, plastic collapse under normal operation can occur only where the cross-section area is reduced as compared to design. As such, plastic collapse in applications like pipelines is often termed “net-section collapse”. And, as failure cannot occur under normal loadings because the stresses are limited to elastic levels, cases where failure occurs through the full cross-section are often termed “overload” failures.

Solutions for plastic collapse are unique to the orientation of the defect, which as noted earlier is herein taken as axial or circumferential, with the failure stress by definition being the lowest stress indicated for these extremes. General solutions for plastic collapse at circumferential defects are published for bending as well as tension loading^(e.g., 48,61,62), as are solutions for axial defects^(e.g., 63-65) for pressure loading, which include analyses for defect-free pipe as well as for defects⁽⁶⁶⁾. As under collapse conditions sharp defects blunt prior to failure due to the high toughness necessary to ensure collapse occurs, such solutions are viable for blunt as well as sharp defects, the difference associated with the blunting process being small. The general form of such collapse solutions is that of Equation 3.

As with plastic collapse, fracture solutions for pipelines are unique to the orientation of the defect, which again is taken as either axial or circumferential, with failure defined by the lowest stress indicated for these extremes. Fracture mechanics solutions are published for external surface defects in pipelines under linear elastic fracture mechanics (LEFM)^(e.g., 67,68) conditions and for nonlinear fracture mechanics (NLFM) scenarios^(e.g., 69). The driving force for LEFM fracture, D_f , can be written in general in the form:

$$D_f = S f(a/W) (\pi a / Q)^{0.5}, \quad (6)$$

where S = wall stress normal to the defect (considered to be axial or circumferential), a = crack dimension considered perpendicular to the surface, Q = shape factor that embeds crack length and assumes a semi-elliptical form, and $f(a/W)$ is a geometry-dependent function, which can be found in handbooks^(e.g., 18,70) or determined analytically or numerically^(e.g., 71-73).

Equation 2 is specific to LEFM, wherein the symbol D_f is the LEFM stress intensity factor, a universal measure of crack driving force⁶ more commonly represented by the symbol K .

⁶ The units evident on the right-hand-side of Equation 6 indicate the term driving force is a misnomer – nevertheless its use is conventional and so adopted herein.

References 67 and 68 present values of K of interest in transmission pipeline applications. A form comparable to Equation 6 exists for NLFM^(e.g., see 69), including large-scale plasticity^(e.g., 70), which are based on the J -integral and the theory of tearing instability⁽⁷⁴⁻⁷⁷⁾. Failure is indicated in reference to Equation 6 when D_f exceeds a critical value, which for this form is the critical toughness, K_c . This parameter can be measured under either quasi-static or dynamic loading rates according to standardized practices^(e.g., 78), with analogous standards to measure NLFM fracture resistance⁽⁷⁹⁾. All values of fracture resistance depend on considerations like crack-tip constraint, discussion of which is addressed elsewhere in detail^(e.g., see 80,81).

Selection of Failure Criteria Used Herein

Key considerations in the selection of a failure criterion include accuracy to the extent that overly conservative criteria lead to maintenance without value, with a bias to safety. Safety in the present context implies a conservative bias in predicted wall stress at failure and indicated defect size. Unfortunately, a failure criterion that is inherently conservative in predicting wall stress is non-conservative in predicting defect size. This follows from the form of Equation 3 (equally Equation 6). For example, Equation 3 indicates that a bias to decreased failure stress on the left-hand-side (LHS) must because of the equality include the same numerical bias on the right-hand-side (RHS). Thus, a factor introduced to reduce the failure stress to lead to conservative predictions must be present on both sides of the equation, thus leading to a similar reduction in the critical defect size.

The interplay between the LHS and RHS of Equation 3 is illustrated in regard to failure pressure for axial defects in Figure 11. This figure presents the usual plot of failure pressure on the y-axis as a function of failing defect length on the x-axis for a given depth defect represented by the contours shown on the plot. The upper contour shown as the solid line represents the actual failure pressure, which would be predicted if the failure criterion adopted were exact, or “accurate” as indicated in the figure. Any conservative prediction fails at pressures below this “exact” result, which for this illustration is represented by the dashed line. Also shown in Figure 11 is a horizontal trend that for this illustration indicates the actual failure pressure, which leads to indicated defect lengths shown in the figure. The disparity between the predicted and actual lengths at failure is highlighted by the dashed ellipse, and noted below in reference to the actual and predicted lengths on the x-axis. It is apparent from this illustration that this non-conservative error in defect length increases as the predicted failure pressure becomes more

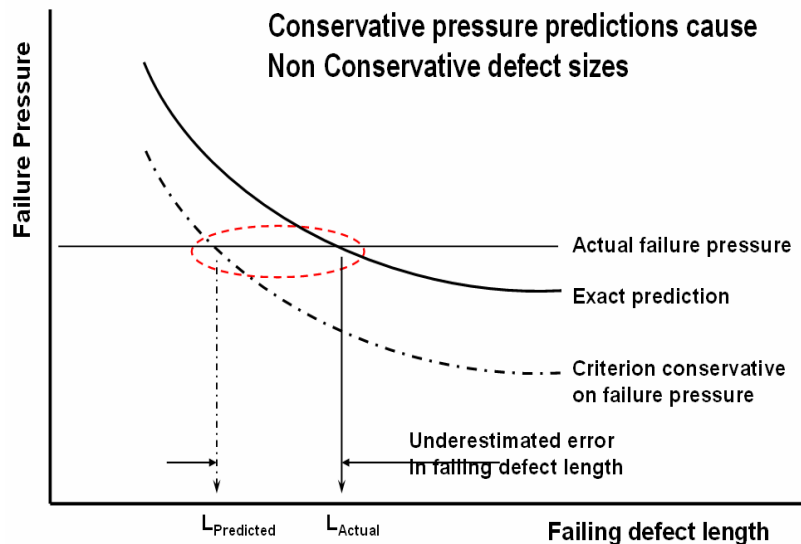


Figure 11. Underestimated crack size as a consequence of a conservative pressure prediction

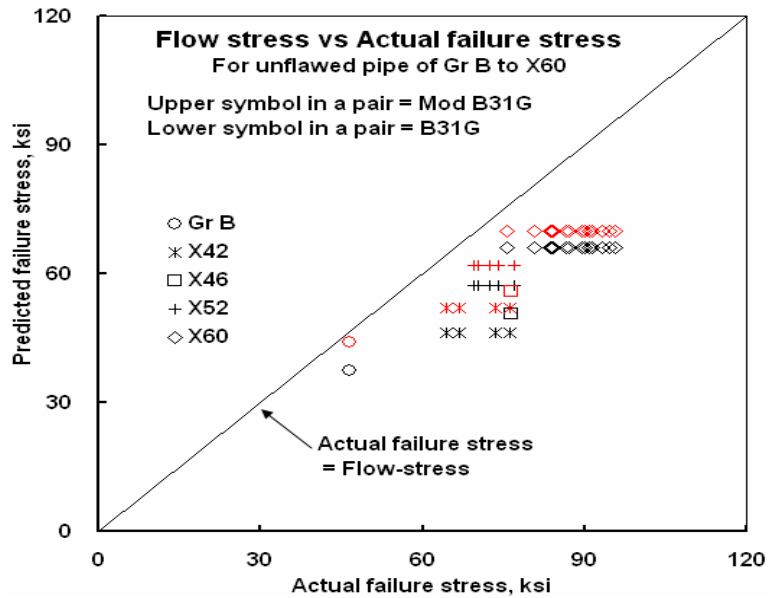
conservative. Moreover, this error increases as the slope of these predicted trends diminishes, as occurs for longer defects and for pressures more typical of service as compared to for example hydrostatic testing.

It follows that the basis for selecting the failure criteria used herein is accuracy, rather than a conservative bias in predicted failure pressure. Because the empirical versus fracture and collapse-based formulations differ in regard to their defect-free reference stress, the choice of criteria is assessed first in terms of reference stress.

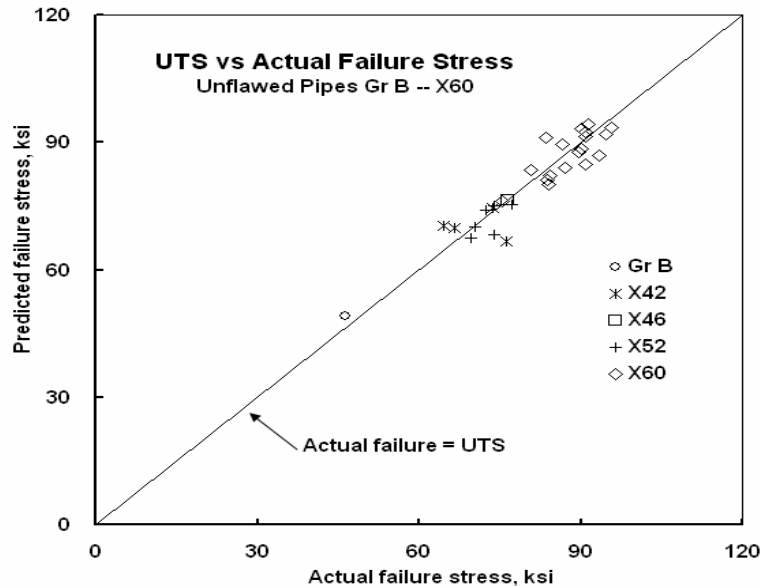
Reference Stress for Defect-Free Pipelines

Recall that the empirical NG-18 Equations and plastic collapse-based formulations share the same form, represented by Equation 3, while the fracture formulations are of the form of Equation 6. Equation 3 is written such that when the structure, which here is a pipe, is defect free, the value of the function of geometry tends to unity. Where toughness is sufficient or the pipe is defect free, fracture does not control failure as the critical fracture resistance is not reached before plastic-collapse occurs, which as indicated above occurs at a stress corresponding to the UTS. In contrast, for the NG-18 Equations, failure in a defect-free pipe is predicted at the flow stress defined by Equation 5. As more than one definition of flow stress has been suggested, values of flow stress from Equations 5a and 5b will be considered in contrast to the UTS associated with plastic-collapse formulations.

Figure 12 contrasts predictions of failure in defect-free line pipe for grades of steel from Gr B through X60, which are the grades that Table 2 indicates represent the vintage pipeline system. These results reflect file data for burst tests done on vintage pipe that was either removed from service or otherwise made available for testing at



a) flow stress predictions



b) UTS prediction

Figure 12. Failure in defect-free pipe

Battelle. Figure 12a presents flow stress predictions in comparison to actual failure pressure, while Figure 12b presents the same results in reference to UTS. It is clear from Figure 12b that the defect free failure stress is on average characterized very well by the UTS. The range of the ratio of UTS / actual failure stress for these data runs from 1.09 to 0.88, or data scatter of roughly ± 10 percent that lies uniformly about the one-to-one trend. In contrast, the range of the ratio of flow stress / actual failure stress for these data runs from 0.60 to 0.87 for B31G and from 0.68 to 0.95 for Modified B31G and RSTRENG. Data scatter here is roughly the order of 30-percent uniformly biased conservatively in regard to the one-to-one trend.

In reference to Figure 12b, the ratio of the UTS to SMYS is on average 1.48, while by code the maximum allowable stress is at its highest 72-percent of SMYS, which provides a factor of safety the order of $(SMYS / (0.72)) = 1.39$. This means that, on average, the difference between failure at the UTS and operating stress for Class 1 Locations is $1.39 \times 1.48 = 2.05$. Thus, even at the highest service stress, defect-free vintage pipelines operate with an average factor of safety of more than two on the pressure induced hoop stress.

The results in Figure 12 indicate the UTS will on average accurately predicts the defect-free failure response of vintage line-pipe steels, doing so with slightly less overall scatter and no bias as compared to the flow-stress-based NG-18 Equations. These results point to the utility of collapse and fracture based formulations, provided such are shown to accurately predict failure pressure for vintage pipeline applications. This is evaluated next, first in terms of failure pressure and thereafter in terms of defect geometry.

Validity of Collapse and Fracture Based Formulations

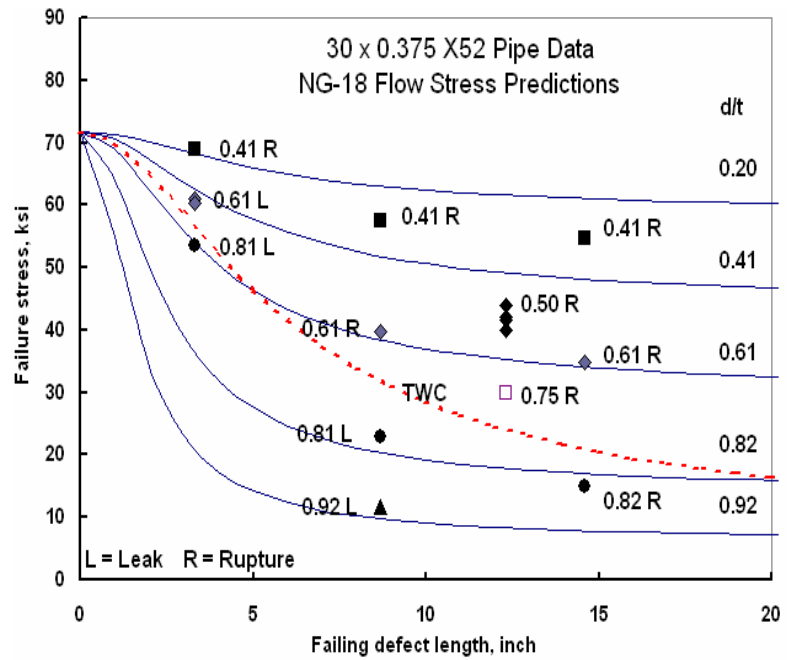
Perhaps the most comprehensive evaluation possible in reference to predicting failure at defects in vintage line-pipe steels comes in terms of axial defects through analysis of the almost 50 full-scale burst tests involving part-through-wall sharp axial slits cut into line pipe produced primarily in the 1960s. This database reflects X52, X60, and X65 grades, the latter representing a variety of high-strength-low-alloy steels.

In developing the empirical data used to “calibrate” the NG-18 Equations, some tests were done for conditions considered to be “flow-stress” controlled failures⁽²³⁾, wherein the toughness was sufficient to produce failure at or above the flow-stress. Figure 13 presents results for these flow-controlled scenarios, along with predictions based on the flow-stress form of the NG-18 Equations. Figure 13 also presents predictions made using the plastic-collapse solution embedded in the PRCI ductile flaw growth model (DFGM) developed at Battelle to predict failure at axial defects, through use of the software-based version of this technology termed PAFFC (Pipe Axial Flaw Failure Criterion). The y-axis in this figure is predicted failure pressure, while the x-axis is failing defect length, as was the case for Figure 11. Contours of predicted failure pressure are presented for four or more defect depths, with five shown for the NG-18 Equation and four shown for PAFFC. Results of the full-scale testing developed at several defect lengths representing defect depths of about 40, 60, and 80-percent through wall are shown as data points. Results of other select combinations of defect length and depth evaluated are also included as data points. These “flow-controlled” tests represent 12 unique combinations of defect length and depth, with four tests repeated for one of these, which provides some measure of scatter under flow-stress controlled conditions. In each case the depth of the defect is indicated, along with an L or R, which signifies failure as a leak or a rupture.

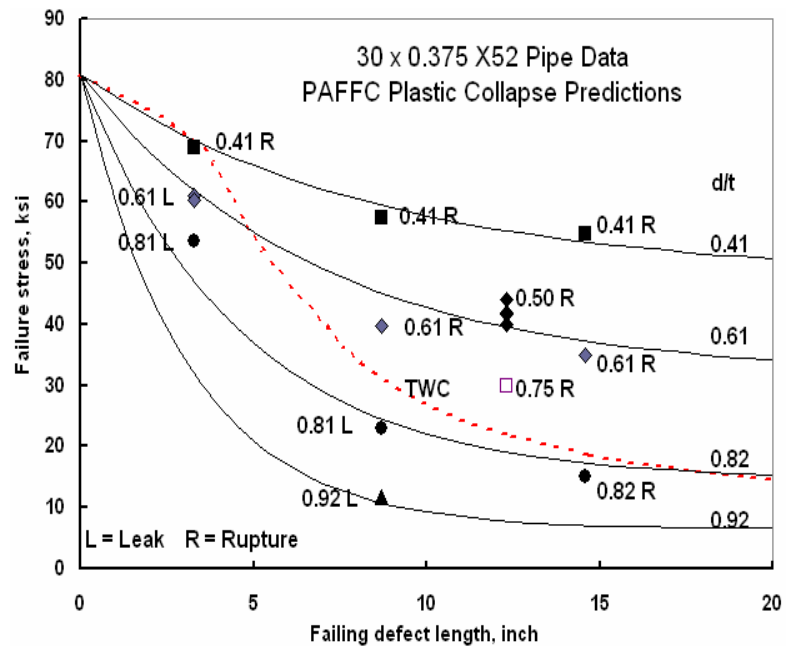
Predictions based on the flow-stress form of the NG-18 Equation shown in Figure 13a reflect predictions for full-scale testing also used to empirically calibrate these equations, so quality predictions are anticipated. However, the figure shows this approach gives quite conservative predictions for shallow defects. It is evident that this approach consistently under-predicts the result for each defect at 41-percent of the wall thickness, being conservative here in failure pressure by the order of 10 percent. In reference to the defect whose actual length is 14.6-inches, this 10-percent conservative prediction on failure pressure corresponds to an under-prediction on defect length the order of 7 inches – that is, it is non-conservative on defect length by roughly 100-percent, which underscores the need for accuracy made earlier in reference to Figure 11. In addition to being conservative on failure pressure for shallow defects, this equation also is conservative for short defects. Finally, while not an issue for vintage pipelines, this technology becomes increasingly conservative for higher-strength grades. However, the NG-18 flow-stress equation does an excellent job of predicting failure for longer defects, and usually is accurate for deeper defects.

Figure 13b presents the corresponding failure trends

predicted using the plastic collapse model in the DFGM / PAFFC. It can be seen that the DFGM / PAFFC more consistently predicts these so-called flow-stress controlled failures as compared to that achieved using the empirical model calibrated in reference to these tests. Suffice it to note that this more recent collapse-based model will therefore make more consistent predictions of failing defect size, which are essential in analyses of revalidation intervals that follow later in this report.



a) NG-18 flow stress predictions



b) DFGM – PAFFC plastic-collapse prediction

Figure 13. Failure pressure for axial defects

Finally, Figure 14 presents comparison of the DFGM and PAFFC in predicting failure pressure for the NG-18 database considered “fracture-controlled” failures⁽²³⁾. As can be seen, the fracture-mechanics based model in the DFGM and PAFFC accurately predicts these failure pressures and so can make consistent predictions of failing defect size, as required later in assessing revalidation intervals. It is noteworthy that similarly accurate predictions have been made for a variety of burst pressure tests, as well as defect growth and crack instability.

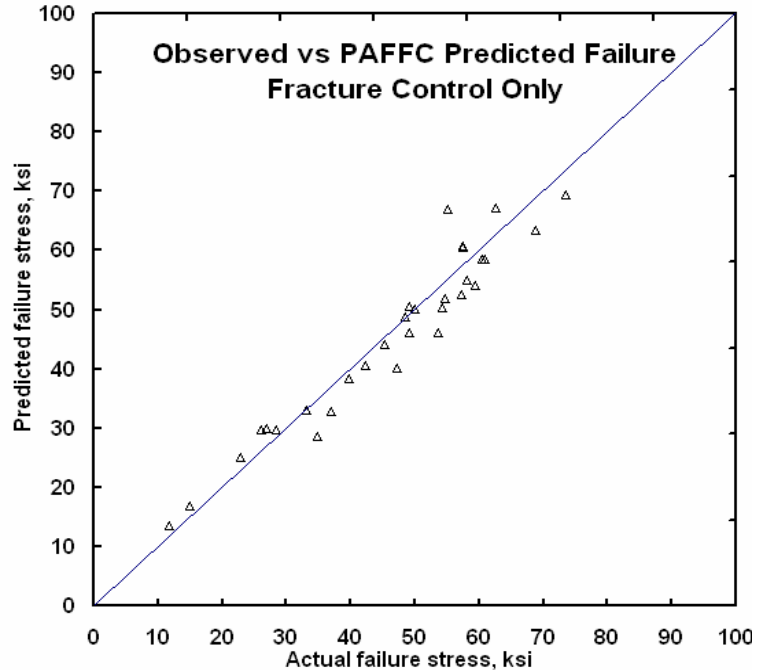


Figure 14. Predicted failure pressure for axial defects

Reference 82 provides a detailed evaluation of its validity and a comprehensive listing of references addressing validation for PAFFC. It

has been demonstrated to produce accurate predictions of failing defect sizes and defect criticality, which reflects the transition from leak to rupture based on axially stable versus unstable response for steels typical of vintage line pipe.^(14,82) This included pipe diameters ranging from 8 through 42 inches and grades from X42 through X80, for failures in the body of the pipe as well as in ERW long seams. Its accuracy also has been demonstrated in a blind round-robin comparison of such models, and through recent full-scale testing of higher toughness steels in grades through X80⁽⁸⁵⁾. For reasons evident in Figure 11, PAFFC does not include any embedded factors of safety, leaving the choice of an appropriate safety margin to be selected and applied on a case-specific basis.

Predicted Failing Defect Sizes

Experimental studies^(e.g., 57) indicate that axial part-through-wall (PTW) defects in a pressurized pipeline fail via plastic collapse or fracture, with growth through the wall occurring in a three-step failure process. Reference 44 details the steps in this process and essential differences for low toughness steels, through moderate to high toughness steels. Simulating the three-step failure process described in the following paragraphs is central to predicting whether fracture or plastic collapse controls failure, and the corresponding failure pressure and failing defect sizes. This is done here in reference to axial defects, although these steps are paralleled in the failure of all defects.

Full-scale experiments indicate failure of a sharp axially oriented defect first involves gradual bulging of the pipe local to the defect as the pressure is increased. Such bulging becomes more evident as the pressure increases and in tough steels can occur without measurable defect growth. For ductile thin-wall pipe and deep defects, bulging is noticeable to the unaided eye, but for heavier-wall pipe, shallow defects, or lower toughness steels, relatively less bulging occurs prior

to failure. The second step involves nucleation of cracking and its possible stable extension into the wall and along the pipe that continues as the pressure increases. The final step involves initially stable time dependent crack extension at constant pressure, which eventually transitions to unstable crack growth, and rapid penetration into and through the wall thickness.

The amount and nature of the crack extension depends on the steel's fracture resistance, measured commonly in terms of the CVN fracture energy, with the most complex response developing for modern higher-toughness steels, and least for the early vintage steels of interest herein. Higher toughness steels experience blunting along their initially sharp crack fronts that makes them very resistant to fracture. In the same way tough steels blunt initially sharp defects, their growth involves the extension along a blunted crack-tip. An upper-bound toughness exists beyond which failure pressure ceases to increase as toughness increases, with little difference evident beyond this toughness level⁽¹⁴⁾. Such behavior indicates the transition from toughness-controlled failure to plastic-collapse-controlled failure for a given line pipe geometry, although such behavior can occur at much lower toughness particularly for shorter defects, or very deep or very shallow defects. Whether the breach created in the pipe wall as the crack transitions through-wall leads to a leak or a rupture (and fracture propagation along the length of the pipe) depends on the length of the break, the geometry of the line pipe and its mechanical and fracture properties, and the properties of the pressurizing media⁽¹⁴⁾. Very short breaks and leaks are likely for very tough steels, while lower toughness steels are prone to longer splits and ruptures.

Failing Defect Sizes

As evident in the prior subsection, analyses methods have been developed that accurately recreate the experimental trends in defect failure and accurately predict failure pressure, which facilitate calculating defect sizes that fail by plastic collapse, common at blunt defects or in high-toughness steels, as well as fracture, which is more common at initially sharp defects in lower toughness steels. Results generated with PAFFC are used next to illustrate typical failing defect sizes and their dependence on the line pipe's properties and its loading.

Defect dimensions that lead to failure are a function of the type, magnitude, and manner in which loading is applied, the pipe geometry, and the material properties of the pipe steel. The most important line pipe properties affecting critical dimensions are the UTS and the toughness. Since there are property differences between vintage pipelines and modern pipelines, it is useful to illustrate this as an aid to formulating IMPs for vintage versus more modern pipeline systems.

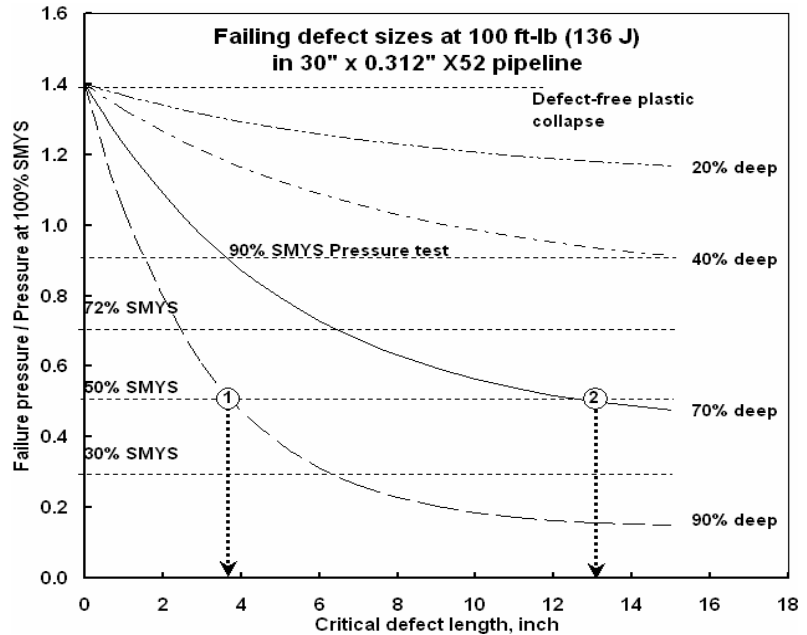
Effect of Toughness on Failing Defect Sizes

Examples follow that contrast a vintage scenario in terms of line pipe toughness with a situation where the toughness reflects more modern construction. The modern scenario is represented by line pipe with full-size equivalent (FSE) CVN USE energy (toughness) of 100 ft-lbs, which lies toward the upper end of conditions in Table 4, while CVN energy of 10 ft-lb is used for the vintage scenario, which according to Table 4 lies slightly below levels considered common for those applications. The vehicle used for this illustration is a 30-inch diameter pipeline made with a 0.312-inch-thick wall of X52 steel. This pipe geometry lies at the upper end of the sizes identified in Figure 6 in regard to pipe diameters representative of the vintage pipeline system, so this geometry is an effective bridge between vintage and more modern scenarios. In all cases failure stress is simulated in reference to sharp axial defects under pressure loading using software developed at Battelle (PAFFC).

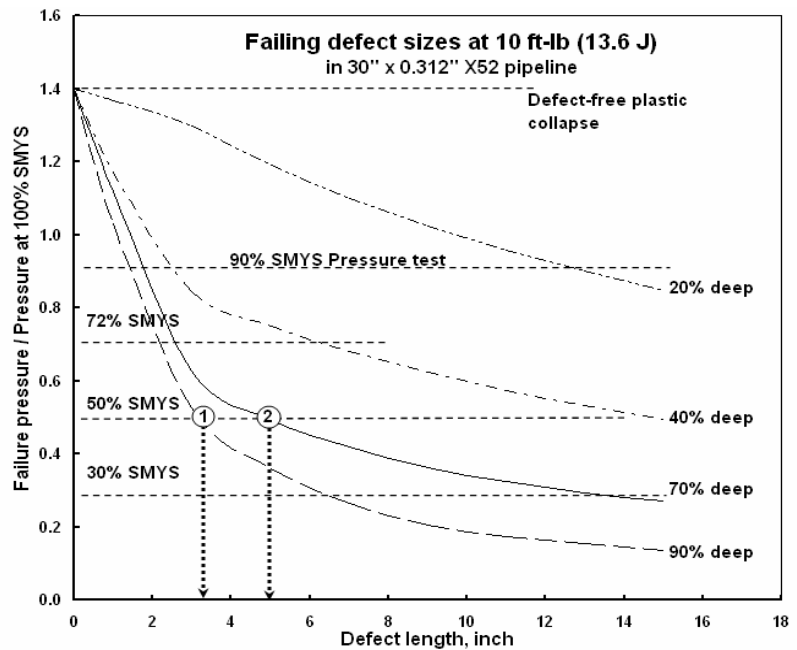
Figure 15a represents results for X52 steel with FSE USE of 100 ft-lbs, while Figure 15b addresses FSE USE of 10 ft-lb. As in Figures 11 and 13, the vertical axis is failure pressure, which here is presented as hoop stress normalized by SMYS. The horizontal axis is the axial extent or length of the crack-like defect, as it was in Figures 11 and 13. The curved lines represent defect depth relative to the pipe's wall thickness (e.g., the curve labeled 70 percent deep represents defects that have a maximum depth of 70-percent through the wall). The dashed horizontal lines correspond to low-wall stress operation (30 percent SMYS), operation in Class 2 (50 percent SMYS) and operation in Class 1 (72 percent SMYS).

The horizontal line at the y-axis value of ~1.4 corresponds to the ratio of the UTS to SMYS for this X52 pipe. Defect sizes associated with failure at MAOP are considered critical defects in the definitions introduced at the start of this report. Critical defect sizes corresponding to each of these class locations can be found by inspection of Figure 15 in reference to length and depth combinations that lie above the horizontal lines at the associated respective pressures noted in this figure.

Each point along a contour of constant depth in Figure 15 represents a combination of failing length and depth for a given pressure. For example, in reference to the higher toughness steel reflected in the trends in Figure 15a – at 50 percent SMYS, a defect that is 90 percent of the wall thickness deep and 3.7 inches long (point 1 in the figure) will fail, as will a defect that is 70 percent deep and about 13 inches long (point 2 in the figure). Similar values can be determined for other combinations of depth and pressure. At higher pressures, the critical defect sizes are smaller, and at lower pressures, they are larger.



a) at 100 ft-lb FSE CVN



b) at 10 ft-lb FSE CVN

Figure 15. Failing defect sizes vs. toughness

While not evident from the information supplied in reference to Figure 15a, the trends for defect depths 40-percent and 90-percent through wall represent failures that are controlled by the strength of the pipeline steel. This occurs for these depths because the toughness supplied (at 100 ft-lb) leads to toughness independent failure, or plastic collapse. If the toughness were much lower (as occurs for some vintage pipelines), the failure response of some defect depths and lengths would be controlled by toughness rather than strength. This is the case in reference to Figure 15b, which represents CVN energy of 10 ft-lb. Notice first that for this lower-toughness steel that defect-free failure is indicated at a y-axis value of ~ 1.4 , just as it did for the higher-toughness scenario in Figure 15a. Thus, defect-free lower-toughness pipe fails by plastic collapse.

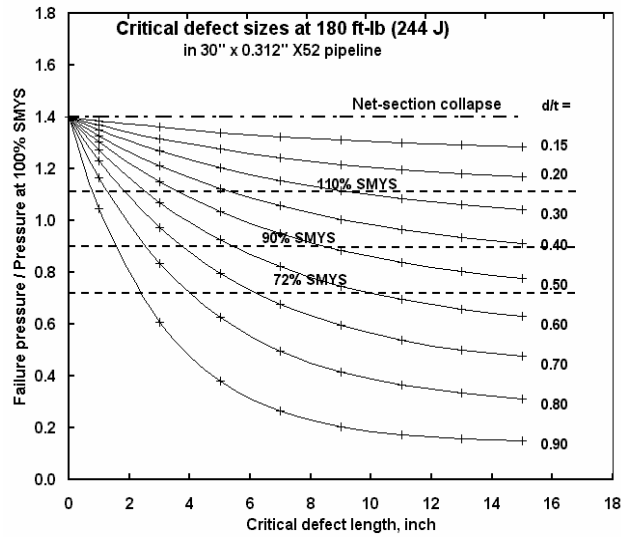
For the lower-toughness steel, Figure 15b indicates the critical defect length at 50 percent SMYS for a 90 percent deep defect is 3.3 inches long, while that for a 70 percent deep defect is ~ 4.8 inches long. In contrast to Figure 15a, lower toughness pipelines have smaller critical defect sizes, although there is little difference for very deep defects as these remain close to a plastic-collapse condition. Aside from somewhat smaller defect sizes and failure more often under fracture rather than collapse control, there is little difference in the performance between vintage pipelines and those made of modern steels.

Trends in Failures Controlled by Plastic Collapse versus Toughness

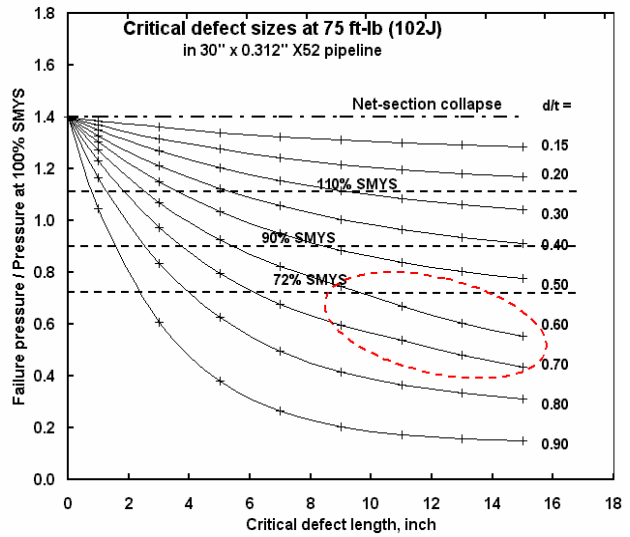
As the toughness increases, analyses discussed in reference to Figures 13 and 14 indicate there is a transition from fracture controlled failure to collapse controlled failure. Beyond this transition toughness, all failure boundaries evident in Figure 15 are independent of toughness. In addition to being independent of toughness, collapse-controlled failure boundaries are smooth and continuous, and are spaced uniformly as a function of defect depth. The uniform spacing between plastic collapse-controlled failure boundaries as a function of defect depth reflects the net-section limit-state for very long defects, which is determined simply from the plastic collapse stress and the net thickness. Where the collapse stress is taken as the UTS, the hoop stress at failure for longer defects is $(1-d/t) \times \text{UTS}$. For shorter cracks, the length of the crack also is a factor, which is obvious in reference to the defect-free limit state where the limit state has a constant value for all defect lengths.

Figure 16a, which considers the same 30-inch by 0.312-inch X52 pipeline considered in Figure 15, illustrates the just-noted collapse-controlled traits for sharp defects at toughness equal to 180 ft-lb (244 J) FSE CVP⁷. Comparing these failure boundaries to the trends in Figure 15a (100 ft-lb FSE) indicates these failing defect sizes are identical, which indicates for this line pipe geometry and grade that collapse controls failure at toughness levels as low as 100 ft-lb. Figure 16b, which reflects 75 ft-lb (102 J), broadens this illustration, where comparing the trends between Figures 16a and 16b all failure boundaries are the same with the exception of that for $d/t = 0.60$. Expanding this comparison to Figure 15b, which deals with 15 ft-lb toughness, shows that at this toughness all the failure boundaries differ from the collapse controlled boundaries

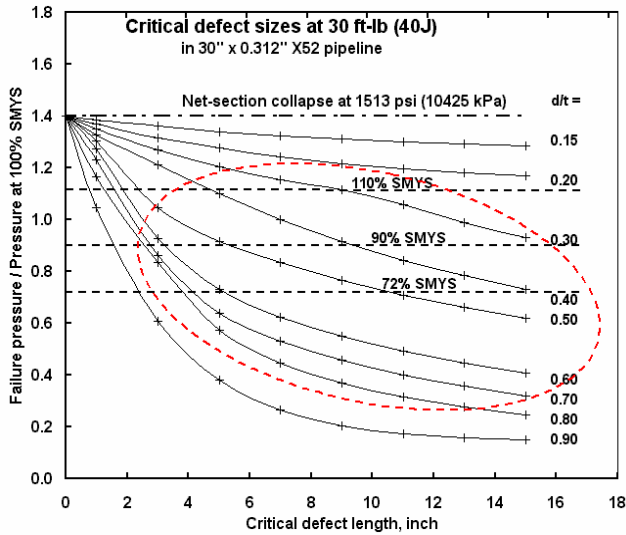
⁷ While extreme in reference to vintage pipelines, comparable and higher toughness levels have been built into pipelines constructed in the 1990s, and were available then without a price penalty. Their inclusion here is to illustrate differences in failure behavior for plastic collapse versus those controlled by toughness, whose practical value lies in the observation that toughness which is often unknown is not a factor where collapse controls.



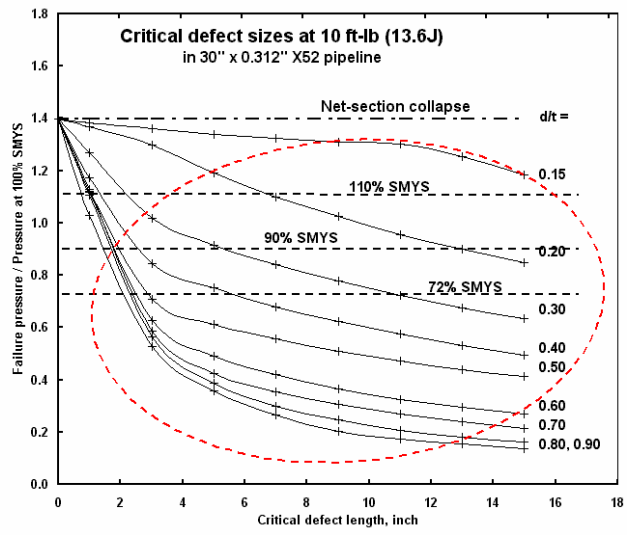
a) 180 ft-lb



b) 75 ft-lb



c) 30 ft-lb



d) 10 ft-lb

Figure 16. Trends in plastic collapse versus toughness controlled failure

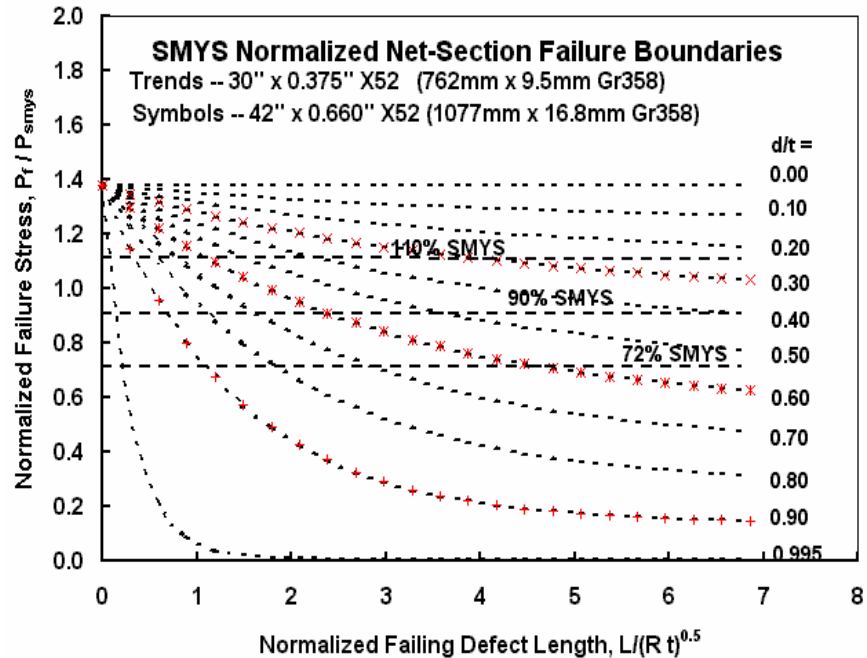
evident at 100 ft-lb and 180 ft-lb. Where the failure boundaries differ from those due to collapse, fracture must control. Portions of the failure boundaries where this occurs have been circled (as best as possible). As expected, comparing fracture-controlled failure boundaries to collapse-controlled boundaries shows that fracture-controlled failures occur at lower pressure.

The smooth, continuous, uniformly spaced appearance of failure boundaries for sharp defects evident in Figure 16a disappears where toughness controls. This is evident in contrasting the trends evident in Figure 16a to those in Figures 16c and 16d. Figures 16c and 16d present results for the same 30-inch by 0.312-inch X52 pipeline addressed above, but at toughness equal to 30 ft-lb and 10 ft-lb, respectively. This comparison indicates there is a gradual transition from collapse to fracture control that spreads across the range of defect sizes considered as toughness decreases. As can be seen by comparing the trends in Figures 16b to 16d with those in Figure 16a, this spread begins for longer defects whose depth is about mid-wall, moving

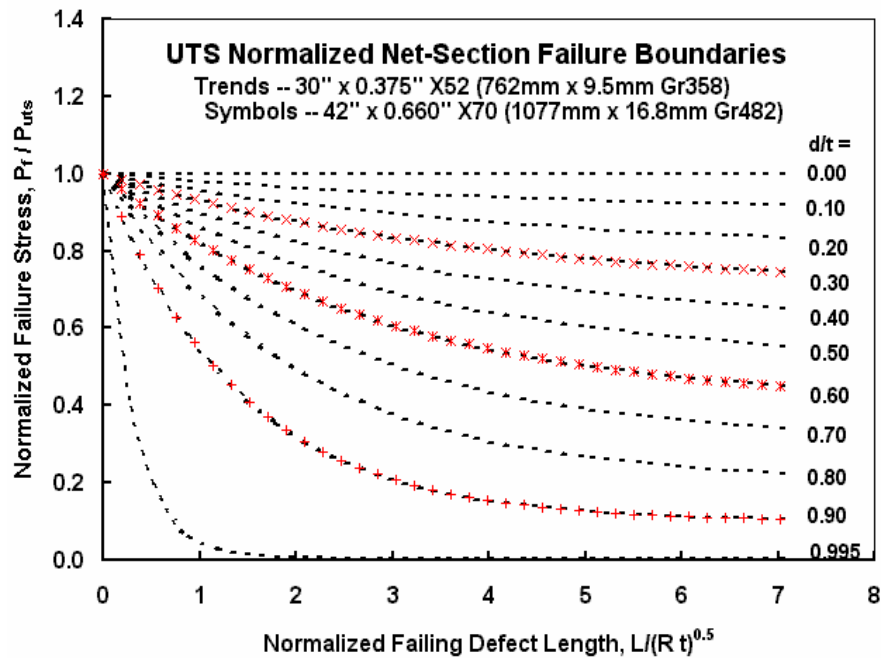
gradually toward comparable length defects that are either deeper or shallower. Likewise the spread moves toward shorter defects. Work reported elsewhere⁽⁸²⁾ indicates that while very deep defects do become fracture controlled at low toughness, such trends not occur for shallow defects. This can be seen in Figure 16d, which is comparable to Figure 15b except for that more failure boundaries are shown in Figure 16d. Comparison of the extreme trends for defect depth (i.e., at $d/t = 0.1$ and $d/t = 0.9$)

indicates slightly lower failure pressures at 10 ft-lb for $d/t = 0.90$, whereas the trend for 10 ft-lb for $d/t = 0.10$ shows collapse controls at shorter lengths, but gives way to fracture control for longer defects. As can be seen by comparing these figures, fracture-controlled failure can significantly shift the relative location of adjacent failure boundaries, significantly reducing both the length and depth available for stable growth.

Analyses similar to those discussed here have been conducted over the years to determine when plastic collapse controls failure^(e.g., see 82,83). Those results indicate the trends in these figures are typical of the behavior of a broad range of pipe sizes and grades, and so can be used to infer trends for a range of practical scenarios. These results indicate that at wall stresses that occur in cross-country service defects shallower than $d/t = 0.2$ fail by plastic collapse at lengths up to about 12 inches for toughness levels typical of much of the vintage



a) via SMYS and $L/(R \cdot t)^{0.5}$ across geometry



b) via UTS and $L/(R \cdot t)^{0.5}$ across grade and geometry

Figure 17. Consolidated collapse-controlled failure

system as defined in Table 4. Shorter defects likewise tend to experience collapse control, which can be traced to the reinforcement associated with the surrounding full pipe wall. Finally, collapse controls for most defect geometries and steels, except for defects with moderate depths in moderate to lower-toughness steels.

The practical significance of collapse control in contrast to fracture control lies in the observation that toughness which is often unknown is not a factor where collapse controls failure. Analysis of defect response for vintage pipeline systems is therefore more certain as well as simpler where collapse controls failure. Plastic collapse is a preferred failure mode, as it involves widespread plastic deformation and capitalizes on the reserve strength of steel, which provides an additional safety margin, well beyond that implied in WSD, as noted in reference to Figure 12b.

Consolidated Failure Boundaries Exist Where Collapse Controls Failure

The patterned response evident in Figure 16a suggests these failure boundaries can be consolidated, with the virtue of simply determining failing defect sizes under such conditions. The parameter $L / (R \cdot t)^{0.5}$ can be expected to consolidate the effects of defect length and line pipe geometry where collapse controls failure, but not fracture controls⁽⁸³⁾. As collapse controlled failures are most likely for all defect sizes in the transition from the vintage pipeline system into more modern construction scenarios, this section explores possible consolidation in reference to such scenarios. Results for plastic collapse in a 30-inch diameter X52 line pipe with a 0.375-inch-thick wall will be contrasted to a 42-inch diameter pipeline with a 0.660-inch-thick wall made of the same X52 line pipe steel. In regard to Figure 6, these line-pipe geometries reflect the upper end of what comprises the vintage system and so are well suited to present purposes.

Figure 17a illustrates the degree of consolidation achieved by the parameter $L / (R \cdot t)^{0.5}$ for these different pipe geometries when plastic collapse controls failure, and SMYS is used to normalize the failure response. Results for the larger diameter, heavier wall pipeline are represented in this figure by data points at three values of normalized defect depth – $d/t = 0.3, 0.6,$ and 0.9 . These depths are represented by the x, *, and + symbols, respectively. This figure demonstrates that exact consolidation is achieved in reference to net-section failure in these line pipes, which for purposes of this illustration are made of the same X52 line pipe steel.

In contrast, when this same comparison is made where the mechanical properties differ this consolidation is lost when SMYS is used to normalize the wall stress at failure. This occurs because plastic collapse occurs at the UTS, which does not scale linearly with SMYS. But, as might be anticipated, where the respective values of UTS are used to normalize the wall stress at failure, exact consolidation is again achieved. This is illustrated in Figure 17b for the same two pipelines, with this comparison made more extreme through evaluation of the 42-inch pipeline made of X70 rather than X52. Again, the results for the 42-inch-diameter X70 pipeline are represented by data points for normalized defect depths of $d/t = 0.3, 0.6,$ and 0.9 . As is evident, this figure shows exact consolidation when the UTS is used to normalize failure pressure. It follows that by appropriate substitution of line pipe properties Figure 17b could be used to predict failure of all possible scenarios where plastic collapse controlled failure – a true one-size-fits-all solution.

Leak versus Rupture

As alluded to in reference to Figure 13, pipeline failures can occur as either a leak or a rupture, depending on the defect size and the loading on the defect⁽¹⁷⁾. In a leak, the release of gas is small and controlled, and the consequences more limited as compared to a rupture. This is a critical aspect in risk analyses of pipelines, which might be done as a part of a system-wide IMP.

Figure 18 depicts the calculated demarcation between leak and rupture for the two cases discussed in Figures 15a and 15b. Below and to the left of each curve in Figure 16 the defect will fail as a leak, whereas defects that are above and to the right of the curves will rupture. Still higher toughness has a limited effect on the leak versus rupture boundary, as slightly higher toughness leads to plastic-collapse controlled failure for which toughness level is not a factor.

Longer defects are more likely to rupture than shorter defects, but the effect of material toughness can be relatively small, particularly at higher stress. As indicated in Reference 11, with the exception of weld-seam anomalies, most historic anomalies are short in length. Thus, these defects are more likely to fail by leak rather than by rupture. Weld-seam anomalies, which can be long, can fail by rupture.

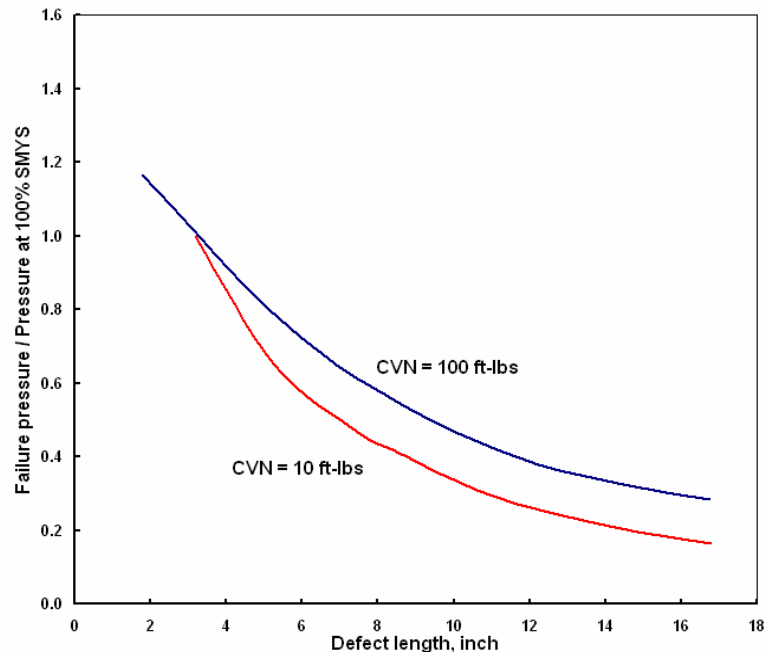


Figure 18. Leak versus rupture boundary

Lower pressure lines (e.g., lines in Class Locations 3 and 4, operated at their MAOP (40 and 30 percent, respectively) can in light of Figures 15 and 18 tolerate longer defects without rupturing as compared to higher-pressure pipelines. Consequently, pipelines operated at MAOP for Class Location 3 and 4 locations are more likely to leak than rupture for a given defect size as compared to the same scenario in lines operating at MAOP for Class Locations 1 and 2. On this basis, analysis results that follow later for pipelines operating in Class 1 Locations provide a conservative indication of consequences for pipelines that operate at lower pressure, all else being equal.

Brittle versus Ductile Fracture⁸

Whether pipe rupture behavior is brittle or ductile can affect the consequences of a failure if there is a likelihood of propagating brittle fracture. Brittle fractures are hard to contain because they run at speeds higher than the acoustic velocity, which means the pressure ahead of the crack

⁸ For a general overview of this topic and methods for control, see Reference 17.

remains high and arrest therefore is unlikely. For this reason propagating brittle fractures can open long distances of a pipeline without arrest as compared to running ductile fracture. For this reason running brittle fracture is considered more serious than propagating ductile fracture, as more pipe fails with greater exposure to the public in the wake of the fracture. Accordingly, the toughness for brittle fracture arrest is evaluated, with the results for an example vintage pipeline scenario shown here in Figure 19.

Public safety at a particular site along the right of way can be viewed in terms of the thermal exposure associated with a fracture. C-FER has developed a model⁽⁴¹⁾ that has been widely accepted to estimate thermal exposure. The model assumes a full guillotine fracture with jet fires impinging from both ends of the rupture. The intensity of the resulting fire if the gas ignites varies as the distance between possibly impinging jet fires. If ignited at the time of the rupture, the worst-case scenario develops so long as the impinging jet fires remain in close proximity, as this leads to the highest thermal exposure for the surrounding area. However, when fracture propagation ensues, the jet fires rapidly separate and for brittle fracture likely do so prior to significant local exposure. As the fractures propagate away from the origin, the ends of the pipe separate resulting in decreased thermal exposure at either site because of the reduced fuel available. It follows that the potential thermal exposure is greater for shorter fracture lengths, because of the proximity of the two fuel sources. Ductile fracture arrest can occur quickly, particularly for pipelines so designed, all else being equal. Thus, the thermal exposure in such cases can be more intense as compared to brittle fracture propagation that significantly separates the fuel sources. While brittle fracture produces reduced thermal exposure, the downside is such exposure threatens two sites. Retrofit arrestors are an option to control fracture propagation in such cases. Reference 86 reviews related issues and presents a design basis for arrestors.

The material property that controls whether a propagating fracture will stop is the arrest toughness of the line pipe steel. Figure 19 presents the minimum arrest toughness for steady-state running brittle fracture on the horizontal axis, as a function of wall stress plotted on the y-axis. The curves represent 16-inch diameter line pipe with a 0.250-inch thick wall made of one of three grades of steel – Grade B, X42, and X52. For this example, toughness equivalent to CVN FSE energy of 2 to 3 ft-lbs provides sufficient resistance to arrest a running brittle fracture for operation at 30 percent SMYS. At 72 percent SMYS, somewhat higher toughness is needed: between 6 and 16 ft-lbs. In reference to Table 4, very early vintage systems have toughness toward the upper end of this toughness interval such that designs such as this example are not at great risk. However, larger diameter or thinner wall pipelines

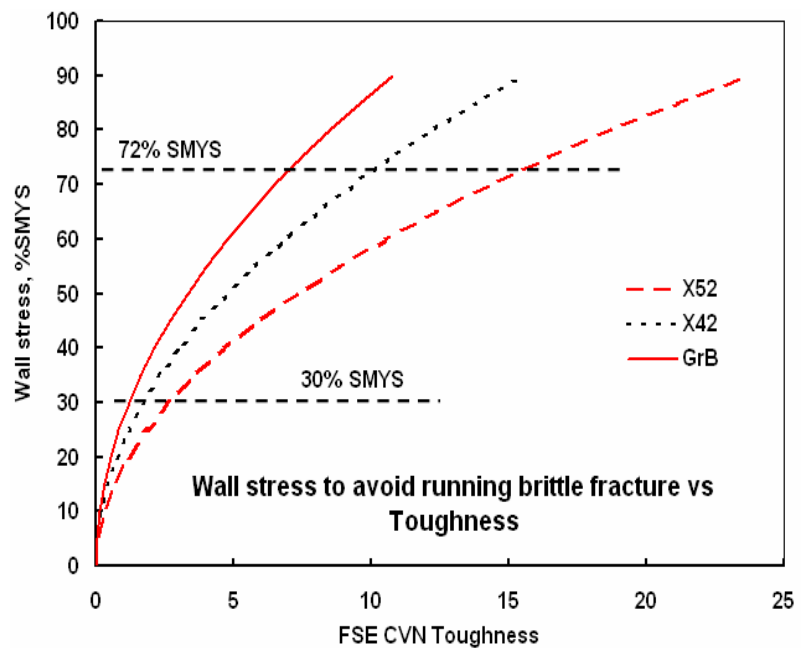


Figure 19. Toughness for brittle fracture arrest

require proportionally higher toughness, which means care should be taken in regard to possible brittle fracture in formulating IMPs for larger diameter, thinner wall vintage pipeline systems operating at pressures approaching MAOP. Some, but not all, early Class 1 and 2 pipelines have sufficient toughness to arrest propagating brittle fractures. Retrofit fracture arrestors are an option to control fracture propagation in such cases. Reference 86 reviews the issues in such applications and presents a design basis for such arrestors.

Many early pipelines in Class Locations 3 and 4 were of smaller diameter and were built from materials with lower strength (typically Grades A, B, X42). In light of the trends in Figure 19 and typical toughness available for such steels, these pipelines operate with limited concern for propagating brittle fracture. Consequently, brittle propagation is not considered a significant issue for such vintage pipelines.

Critical and Failing Defect Sizes for Vintage Pipelines

Whereas Figure 17b provides a general solution for all crack-like defect sizes where collapse controls failure, as the remaining parts of Figure 16 indicate it is necessary to develop critical defect sizes for fracture controlled failure. The present section uses the same approach to quantify failing defect sizes for blunt and sharp defects. Blunt defects are evaluated even though collapse controls their failure because results for collapse-controlled sharp defects are slightly conservative for such applications. Cases involving blunt defects are simulated using PCORRC (Pipeline CORROsion)^(e.g.,65,131), while PAFFC introduced earlier in regard to Figure 15 is used to simulate failure pressure for sharp defects. PCORRC has its foundation in plastic collapse, while PAFFC has its basis in plastic collapse and fracture mechanics. Failure has been simulated for PTW axial defects, which for pipelines free of secondary stress represent the worst-case scenario. Failing crack sizes have been calculated for present purposes for depths from zero up to 90 percent of the wall thickness and for lengths up to $L / (R t)^{0.5} = 7.5$ for the blunt defects and up to 15 inches for the sharp defects. Parametric studies have been made for the scope of vintage pipelines whose geometries are defined in Table 3, for the mechanical and fracture properties defined in Table 4. The plastic collapse limit state is taken as the UTS throughout these analyses, with SMTS used to represent specified minimum properties.

Blunt Defects

Figure 20 presents the results for failing defect sizes involving blunt defects in the format discussed in regard to Figure 16a. Thus, the y-axis presents the failure stress (or pressure) normalized by SMYS (or the pressure corresponding to SMYS). The x-axis presents the defect length normalized as $L / (R t)^{0.5}$, while defect depth is represented by contours of constant d/t. Results are presented in Figure 20, parts a), b), and c) respectively, for Gr B, X42, and X52 for the vintage pipeline scenarios summarized in Table 3 as representative of that system. Contours of constant d/t at failure are presented in each part of this figure for the 24-inch diameter pipeline, with results presented for the 4-inch diameter pipeline scenarios as confirmation of data consolidation for plastic collapse failures when using this figure format.

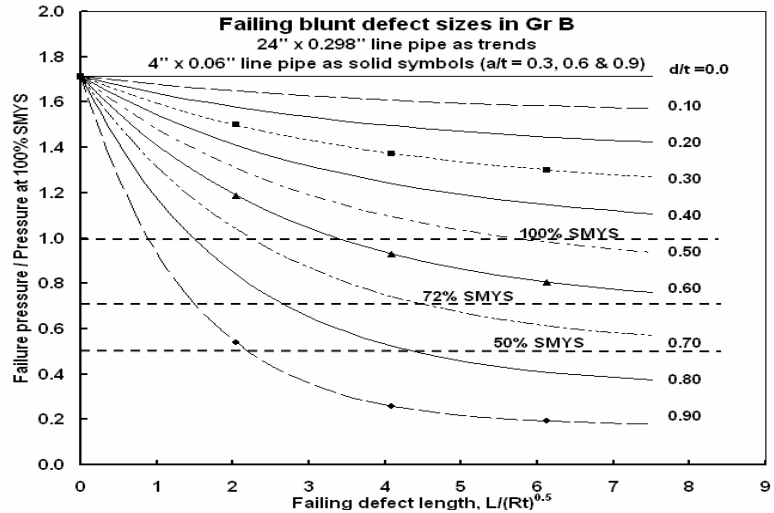
The upper-most contour in each part of Figure 20 is for d/t = 0, which is defect-free line pipe. In reference to the use of the UTS as the plastic-collapse stress as validated in Figure 12b, this contour at d/t = 0 lies at a value of the y-axis = SMTS/SMYS, as SMTS⁽¹³⁾ has been used in these analyses. As can be seen in these figures, $L / (R t)^{0.5}$ provides consolidation for plastic-collapse

controlled failures as the solid data points for the 4-inch diameter line pipe fall exactly on the appropriate trends for the 24-inch diameter pipeline. Failing defect sizes for defects 90-percent through the wall are found to be quite large even for the lower-strength grade at a wall stress corresponding to Class 1 Locations (y-axis value = 0.72). Inspection of the figure indicates values of $L / (R t)^{0.5}$ respectively for Gr B, X42, and X52 of about 1.5, 1.2, and 1, which for the 24-inch diameter pipeline correspond to lengths of about 4.7, 3.6, and 2.5 inches, respectively. At a depth of 20-percent of the wall thickness, these results indicate that defects more than a 12 inch long are unlikely to fail a high-pressure hydrotest, which lends credence to shallower depths being code allowable. In reference to the nine pipeline designs in Table 3, there is roughly a five-fold difference in values of $L / (R \cdot t)^{0.5}$ for these designs. All else being equal, this spread can be associated with significantly different failing defect sizes in light of Figure 20.

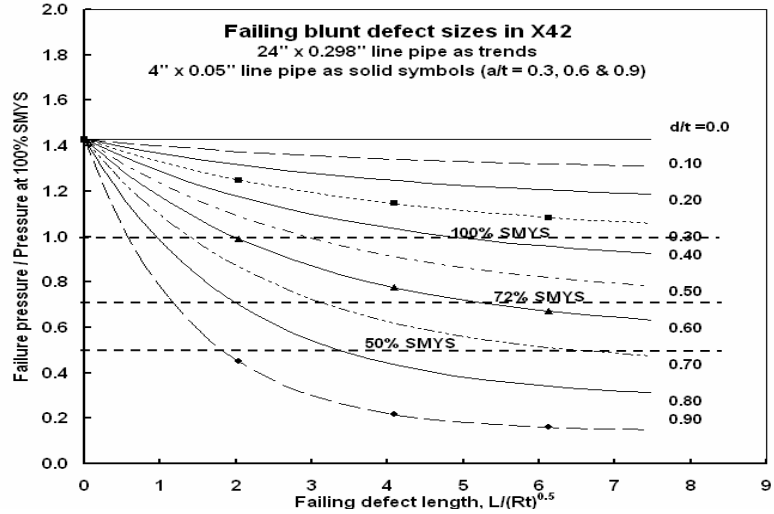
The trends in Figure 20 provide the basis to determine the limiting sizes of corrosion defects, but are equally valid for any blunt feature.

Sharp Defects

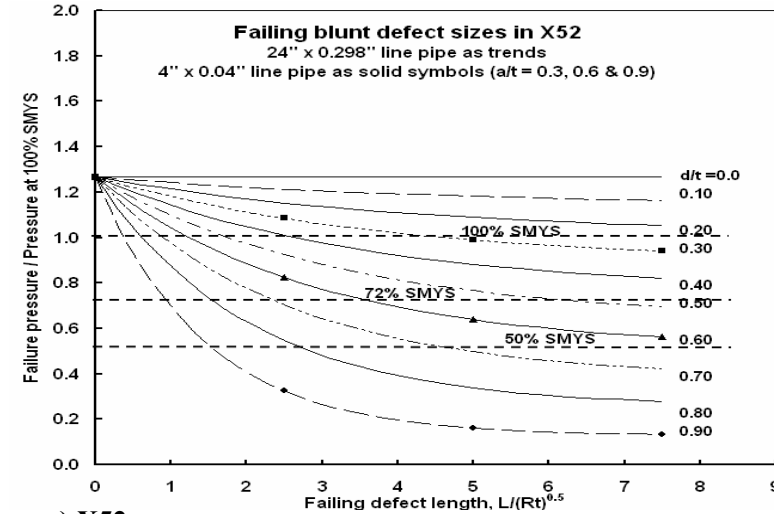
Results comparable to that for blunt defects shown in Figure 20, but for initially sharp



a) Gr B

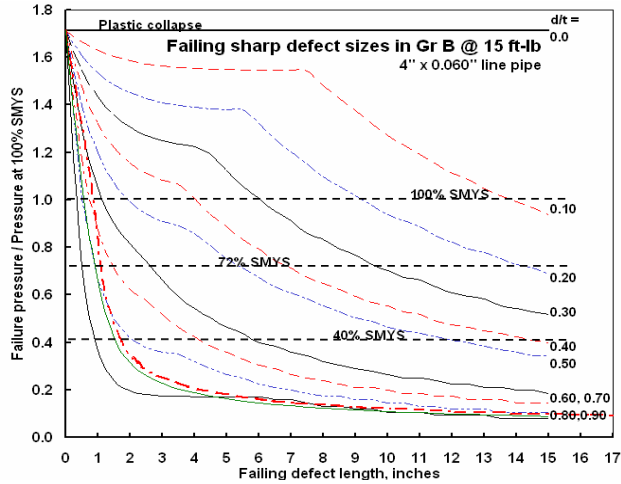


b) X42

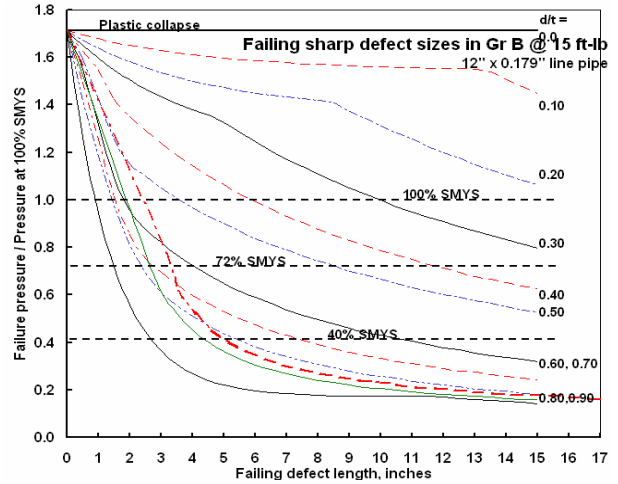


c) X52

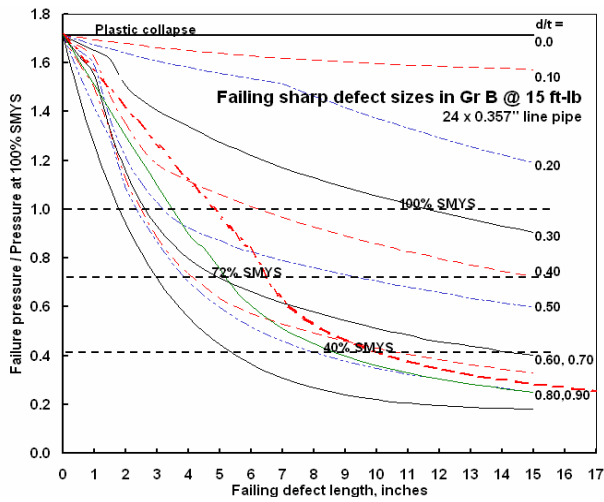
Figure 20. Failing sizes for blunt defects



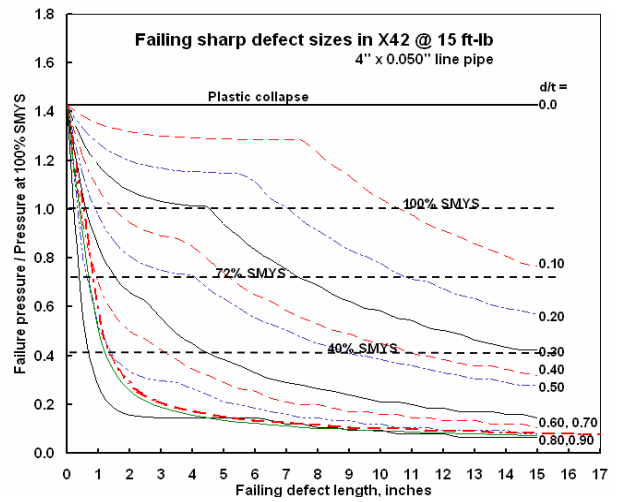
a) 4-inch diameter Gr B @ 15 ft-lb



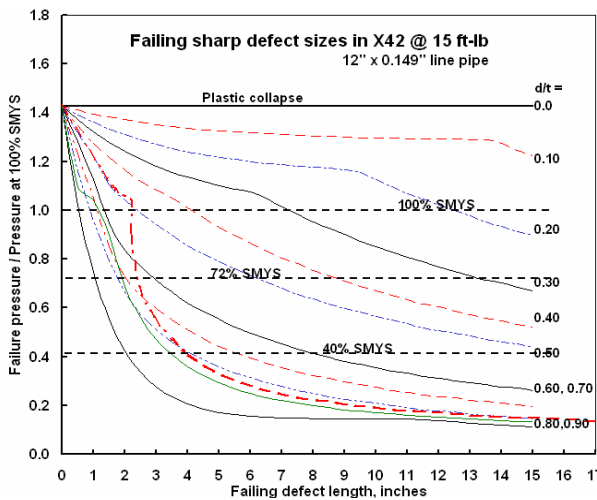
b) 12-inch diameter Gr B @ 15 ft-lb



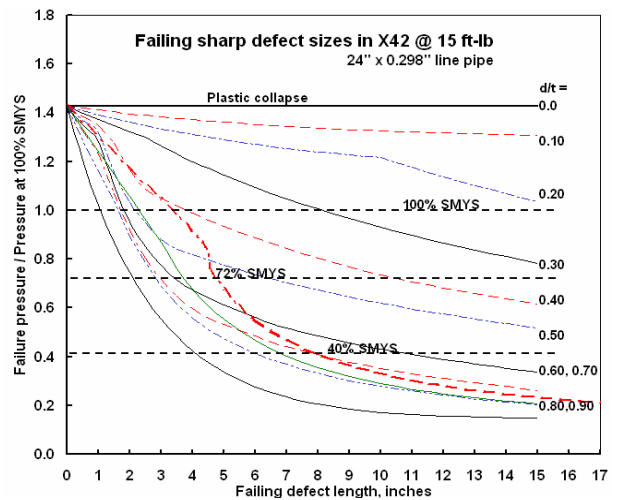
c) 24-inch diameter Gr B @ 15 ft-lb



d) 4-inch diameter X42 @ 15 ft-lb

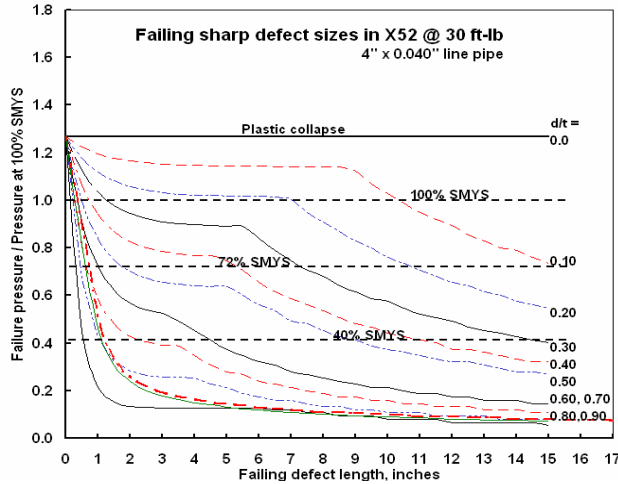


e) 12-inch diameter X42 @ 15 ft-lb

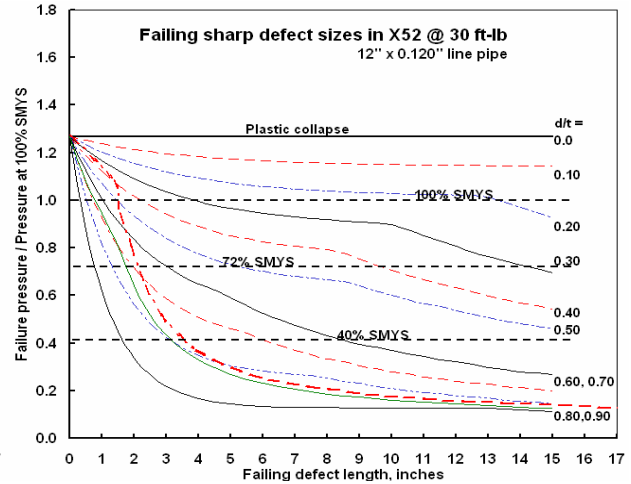


f) 24-inch diameter X42 @ 15 ft-lb

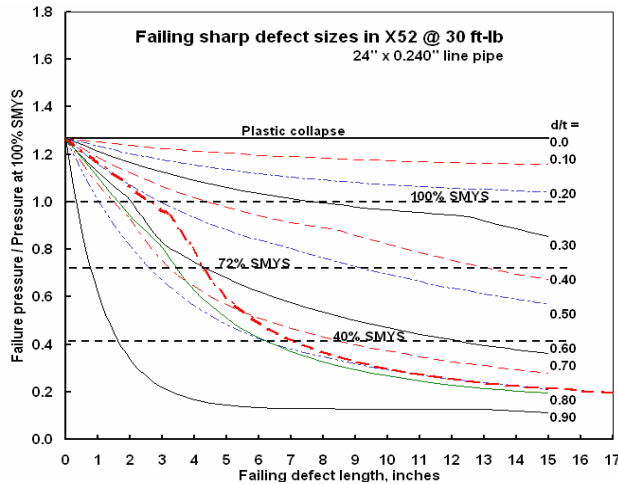
Figure 21. Failing sizes for sharp defects at 15 ft-lb toughness



g) 4-inch diameter X52 @ 30 ft-lb



h) 12-inch diameter X52 @ 30 ft-lb



i) 24-inch diameter X52 @ 30 ft-lb

Figure 21. Failing sizes for sharp defects at 15 and 30 ft-lb toughness, concluded

defects are presented in Figure 21. In contrast to blunt defects and their anticipated plastic-collapse controlled failure, fracture can occur for initially sharp defects. When fracture controls failure, the linear dependence of failure pressure on defect depth for long defects is lost. Instead, fracture mechanics as evident in Equation 6 indicates the influence of defect size and shape is nonlinear. It is for this reason that fracture-controlled failure boundaries cannot be simply consolidated by $L / (R t)^{0.5}$ and SMYS or SMTS. Accordingly, where three plots were suffice to represent collapse-controlled failure boundaries referenced to SMYS in Figure 20, and one would suffice based on SMTS, these boundaries are unique where fracture controls failure. Consequently, failure boundaries must be developed for the nine grade and line-pipe geometry combinations listed in Table 3.

The several parts of Figure 21 present failure boundaries for initially sharp defects in the same format used for Figures 15 and 16. The y-axis is the failure stress (or pressure) normalized by SMYS (or pressure corresponding to SMYS), while the x-axis presents the defect length, L . Defect depth is represented in these figures by contours of constant d/t . As for those figures, horizontal trends are used to indicate wall stresses or pressures that correspond to Class 1 and 3 Locations, as well as a value typical of high-pressure hydrostatic testing. As Table 3 indicates,

the combinations of pipe geometry and grade presented in Figure 21 represent pipelines designed for operation in Class 1 Locations at a pressure equal to 750 psi. Thus, the horizontal line at a design factor of 0.72 in each part of Figure 21 corresponds to a pressure of 750 psi, and failure at 100-percent of SMYS is in all cases 1042 psi. The collapse pressure for defect-free failure can be found for each part of this figure as SMTS/SMYS x 1042 psi, which gives 1786 psi, 1488psi, and 1322 psi, for the Gr B, X42, and X52, respectively. The results for all parts of this figure have been shown on identical scales to facilitate comparing failure pressure relative to that for represents this defect-free scenario. As expected in light of Figure 12, the y-axis value for $d/t = 0$ defect free line pipe. As in Figure 20, the upper-most contour in each part of Figure 21 corresponds to SMTS/SMYS, as SMTS⁽¹³⁾ has been used in these analyses.

Figure 21 presents results for the nine possible combinations of vintage pipeline geometry and properties that arise from Table 4. Two levels of toughness are used – with 15 ft-lb appropriate for the Gr B and X42, and 30 ft-lb appropriate for the X52. Recognizing the influence of toughness discussed earlier in regard to Figures 15 and 16, the trends evident in comparing the parts of this figure reflect four primary drivers – diameter, wall thickness, grade and toughness. Diameter to thickness ratio varies from ~70 to ~100, which is not a large range nor does it reflect other than a thin-wall scenario. In light of Figure 16, the effect of toughness can be significant where collapse does not control, while grade has an obvious influence as was evident above.

Comparison of trends as a function of geometry for a given grade indicates that the smaller diameter, thinner wall pipelines fail at smaller defects as compared to larger pipelines when fracture controls failure. While not evident in Figure 20 because of the normalized form of the x-axis, this same tendency occurs for plastic collapse, to roughly the same extent. As can be seen in the relative shapes of the failure boundaries in Figure 21, this can have a significant effect on the failing defect sizes for shorter defects in thinner-wall pipe as compared to what fails in heavier-wall pipe. Grade likewise has a strong influence on failing defect sizes when fracture controls failure, which likewise is paralleled for collapse-controlled cases. This is evident in Figure 21 as well as Figure 20 wherein higher strength grades that show characteristically lower yield to tensile stress ratio as compared to lower strength grades show a much broader spread of the failure boundaries. All else being equal, this leads to a larger increment of wall thickness that must be traversed for failure to occur. Accounting for the effect of grade, comparison of the trends as a function of grade for a given geometry indicates that line pipe with the higher UTS tolerates larger defects. This influence becomes increasingly significant as the defect becomes shallower. As expected, the influence of toughness can be significant, but is strongest for defect size and shape combinations that for the higher toughness fail by plastic-collapse versus toughness control at the lower toughness. Once the shift to plastic-collapse control occurs for a given defect size and shape combination, increasing toughness has no influence on failure pressure.

Failing defect sizes are longer for larger-diameter pipelines. For comparable depth defects, failing defect lengths are comparable to those for blunt defects where plastic collapse controls failure, as occurred for many defect sizes and shapes for the 24-inch diameter X52 and X42 line pipes, but to a lesser extent for the Gr B line pipe. For defects whose depth was 90-percent of the wall thickness, inspection of these figures indicate failing lengths of about 1.7, 2.1, and 2.5 inches, respectively for Gr B, X42, and X52 for the 24-inch diameter pipeline at a wall stress corresponding to Class 1 Locations (y-axis value = 0.72). These lengths are shorter than that for their blunt counterparts, significantly so for the Gr B, which serves to emphasize the influence of

fracture versus collapse controlled failure on failing defect size (equally pressure). At a depth of 20-percent of the wall thickness, these results indicate that such shallow defects are unlikely to fail a high-pressure hydrotest, and are stable at lengths of more than 12 inches. In the Gr B and the X42, this resistance is due to the significant difference between SMYS and SMTS, while for the X52 it reflects use of 30 ft-lb toughness versus the lower value used for the other grades.

The trends in Figure 21 provide the basis to determine failing defect sizes which when coupled with the initial defect size defines the increment for growth available for stable in-service growth. The remaining life of such crack-like defects is determined by the time it takes to traverse this increment of wall thickness subject to the kinetics and thresholds presented in Figures 24 and 25, with due consideration for the leak versus rupture boundaries evident in Figure 21 as the dashed trend from upper-left to the lower right of these figures. Significantly the failure boundaries in Figure 21 show significantly different increments of wall develop as a function of crack length. In some cases the failure boundaries reflect plastic collapse, whereas in other cases fracture controls. For all nine example vintage pipelines considered the design pressure corresponds to 72-percent of SMYS, which in these figures corresponds to a line across each figure at a y-axis value equal to 0.72. The complex nature of these failure boundaries indicates that predicted MTBF for crack-like defects will not necessarily follow simple or consistent patterns as a function of grade or pipe geometry. However, differences in the relative kinetics between corrosion, fatigue, and SCC should be evident subject to their respective thresholds and the above-noted effect of the failure boundaries on the available increment of wall to support in-service growth.

Summary for Failing Defect Sizes

Tools exist to accurately simulate defect shapes and sizes across the range of interest in formulating IMPs for vintage systems. The capability also exists to discriminate between leak and rupture, such that the significant influence of gas release can be addressed in evaluating the consequences of potential failures. Finally, while brittle fracture is a possibility particularly in the more highly stressed thin wall large diameter pipelines in the vintage system, the results do not point to this as a critical concern, a fact evident in incident experience.

Figures 15, 16, and 19 to 21 showed that critical defect sizes for in-service failures are quite large, even for anomalies in lower-toughness steels. Blunt anomalies and those that are not axially aligned have much larger critical dimensions^(e.g., see 82,83). A tolerance for relatively large defects, even in lower-toughness steels, implies that pipelines can operate safely with stable anomalies less than critical size. Use of high-pressure or code required hydrostatic testing could expose defects whose size lies above the test pressure. Thus, although as-produced vintage pipe contained anomalies, pressure testing, whose use began on a widespread basis in the 1960s^(e.g., see 84, 85), served to expose critical or near-critical defects and so limit their significance.

In reference to Figure 2b, consideration turns next to criteria to quantify thresholds for defect activation, and the kinetics of processes that can continue their in-service growth. Thereafter, typical loadings will be considered, followed by analysis to establish revalidation intervals. While the relative differences in kinetics between corrosion, fatigue, and SCC, should be evident in the MTBF, simple and consistent patterns are not expected as a function of grade or pipe geometry because of differences in their respective thresholds and the complex nature of the failure boundaries.

Growth Mechanisms, Thresholds, and Kinetics

Consideration of the incident database and detailed failure analysis of such incidents indicates that failure in pipelines has occurred most commonly as a result of corrosion, a time dependent mechanism involving dissolution⁽⁸⁷⁾. Hydrogen-induced cracking (HIC) also called HSC, which also is time dependent, and cycle-dependent mechanisms like fatigue also contribute as does the coupled time-at-stress- and cycle-dependent mechanism known as SCC.

The MTBF⁹ for mechanisms like those noted varies with the kinetics of the process. For environmentally dependent processes the kinetics depend on conditions that vary along the RoW, which control the ground-water chemistry, and the long-range electrochemistry when coupled with the cathodic protection imposed to limit corrosion, and ambient temperature. Operating circumstances enter through their influence on temperature, and the stress history induced by pressure as a function of time, which are factors for stress at time and cycle-dependent processes. The RoW also influences stress at time processes through external loading due to outside forces. The properties of the line-pipe steel, such as strength and toughness, also are factors as they condition the stresses and strains that develop due to the loading, and limit the critical crack size. Secondary factors include system maintenance driven by direct assessment, hydrostatic retesting, or in-line inspection (ILI), as these actions affect which defects remain in the pipeline, and can alter the stresses and strains at defects just as the in-service loads do.

Of the above noted factors contributing to the MTBF, prior sections have addressed issues like toughness and its influence on critical defect size, while the subsequent section will deal with the stresses and strains caused by pressure and external loads. Consequently, this section focuses on data that characterize thresholds for defects to become active, and the kinetics for their possible growth for the more common mechanisms that degrade the wall thickness provided according to elasticity theory and working stress design. Each mechanism is addressed in regard to the factors that control the degradation process, after which thresholds for defect activation are presented when they exist. Finally, kinetics data are presented. In all cases the data presented is drawn from the literature, with references cited as the data are introduced.

Possible Approaches to Assess Thresholds and Kinetics

It follows from the above discussion that determining thresholds that quantify activation and the kinetics that quantify a safe revalidation interval depend on details of the pipeline and its operations and its maintenance history. It follows that thresholds and kinetics generally cannot be determined from information on other pipelines, unless all measures of degradation resistance and all metrics driving degradation are identical. Given this fact, information that characterizes MTBF must have a rudimentary form that is easily transferable between pipelines, which hopefully also can be simply evaluated by pipeline engineers. The easiest and most transferable format is wall stress for stress-based applications and stress intensity factor for fracture-based situations. Plausible data sources to quantify thresholds and kinetics for use in assessing MTBF include:

⁹ Use of MTBF is appropriate, as average properties and typical circumstances are evaluated.

- review of the OPS incident database,
- surveys of pipeline companies,
- full-scale experiments,
- data generated by each pipeline company based on specific uniform guidelines, and
- synthesis using field-proven models of the degradation processes.

The literature indicates that the information needed to determine intervals have not been gathered by survey, nor have full-scale tests been done to generate necessary and/or sufficient data.

Two generic approaches exist to determine intervals for maintenance and revalidation of pipeline condition and serviceability. One generic approach is empirical, based on field experience, or available databases. To meet the present needs, this requires a database that is populated by serviceability problems as a function of the factors controlling the occurrence of these problems. Such could evolve from the current OPS database, but as yet such a database has not been considered. The second generic approach involves analytical simulation, supplemented or calibrated as appropriate with field data. As this second approach is the only viable one, it has been adopted, with the data presented next in this section used to support this approach. The ensuing sections first address factors controlling each of the above-noted mechanisms, and thereafter present thresholds and relevant kinetics data, considering corrosion first followed by fatigue, SCC, and HSC.

Corrosion Threshold and Kinetics

Controlling Factors

Corrosion-induced metal-loss on pipelines occurs by dissolution⁽⁸⁷⁾. First-order factors affecting the dissolution kinetics for pipelines include:

- Parameters that control the local environment at the steel's surface (soil, moisture, coating type/condition/disbonds, temperature, electrochemical conditions, etc) and
- Line-pipe wall thickness.

Second order factors involve the mode of failure, and include:

- Line pipe strength and toughness and pipeline operating pressure, which determine leak versus rupture and influences the consequences of failure.

Threshold

As long as the conditions necessary for dissolution are present, the process occurs, so a threshold for corrosion exists in reference to the above-noted first-order factors. Where these conditions are satisfied corrosion occurs, whereas where they are absent it does not. There is no stress level below which corrosion does not occur, although increased stress can enhance corrosion kinetics in reference to pitting as an example. Other interactions between stress and corrosion kinetics have been documented as for example the Reibinder effect⁽⁸⁸⁾, hydrogen-enhanced localized plasticity⁽⁸⁹⁾ (HELP), with indirect effects also evident on the open-circuit potential⁽⁹⁰⁾. NACE⁽⁹¹⁾ has published a handbook dealing with corrosion on pipelines that provides useful information.

Corrosion Kinetics

Much has been done to quantify the electrochemical reaction between steel and ground water, with textbooks^(e.g. 87) and handbooks detailing this process^(e.g., 92,93). Corrosion kinetics depend on a host of parameters that are unique to each type of reaction, and tend to be pipeline specific or site specific along a pipeline. Dissolution occurs on bare pipe, as well as on pipe that is under cathodic protection (CP), where this protection system fails because of local shielding, or other field-related complexities. Corrosion kinetics can depend on local stray currents or involve microbiologically influenced corrosion (MIC), or other case-specific processes that accelerate the degradation rate. Finally, corrosion kinetics also could involve reactions occurring on the inside of the pipeline involving moisture in the product, and acid forming gases present at low partial pressures in the product. In all cases, integrity is threatened as this corrosion grows and penetrates the pipe wall. Kinetics unique to such situations can be much accelerated in comparison to the more usual steel exposed to soil and ground water, as considered here in reference to typical data obtained from field coupon studies derived from Reference 92, and supplemented later by field results.

Figure 22 presents two sets of corrosion rate data for steels observed under field conditions. The data in Figure 22a are trends from results of field tests done with bare, unprotected coupons, with a view to simulate corrosion rates for buried steel structures^(92,93). The trends shown in this figure bracket the results reported, with the bounds being reinforced by the dashed lines. Corrosion “rate” as shown here has been calculated by dividing corrosion weight-loss averaged over a time interval on the order of a few days. Figure 22a shows the lower-bound rate is about 0.001 inch per year, while the upper-bound rate is stable at about 0.003 inch per year. For the higher-rate data the results imply the corrosion process was initially much more reactive, as compared to the stable behavior that developed after a few days. The bounds shown in Figure 22a represent general corrosion, and differ in rate by a factor of about three. This scatter in rate is indicative of the variability in the general corrosion process, even though these data reflect the same steel, in the same soil, with the same moisture conditions, under controlled testing conditions. A factor of three seems large until the variability for this process is compared, for example, to fatigue where a factor of ten can be viewed as “low” scatter.

For present purposes, data such as that in Figure 22a are credible only if they reflect the actual behavior of in-service pipelines. To this end, times to failure were determined for cases representing bare but protected pipelines using data in the OPS database¹⁰. Because data for bare pipelines have been considered, no “adjustment” is required to account for the time for coating failure. The rate has been calculated by dividing the full wall thickness by the pipeline’s time in service. The data representing bare but protected pipelines are split almost evenly between leaks and ruptures, with no pattern evident in rate as a function of failure mode. The results have been culled to exclude pipe with diameters smaller than 12 inches, and cases involving SCC. The

¹⁰ This database reflects mainly first-to-occur incidents for the pipeline segments involved, and covers lines put into service over more than a 50-year interval, that are operated and maintained differently. Because it represents primarily first-to-occur incidents, it reflects corrosion “hot-spots” along those pipelines, and provides a reasonable worst-case estimate of corrosion rate. For these same reasons, pooling these data for purposes of other analysis reflect an uncertain practice because most first-time incidents are cause for systemic response in terms of both operations and maintenance practices.

small diameter pipe has been excluded because steel and pipe making for smaller diameter pipe can be much different than for larger-diameter transmission line pipe. SCC has culled from the data as this process involves cracks, as opposed to metal loss corrosion that typically involves much blunter features.

Using corrosion kinetics derived from the OPS incident database means the kinetics reflect worst-case field corrosion conditions as compared to circumstances elsewhere in transmission pipeline systems, where degradation must be occurring at a slower rate over the pipeline's life. Because the kinetics used reflect the leading edge of the population of corrosion rates, this analysis has been made in regard to three specific corrosion rates. A worst-case rate has been determined that reflects the fastest rate for all of the incidents on bare, protected pipe. In addition, rates that reflect average kinetics for the bare, protected pipe incident population have been determined in reference to the 90th percentile¹¹ for the population. For the general corrosion data the rate-data scatter by about a factor of two, while the extremes for the pitting data differ by about a factor of five. The worst-case corrosion rate for pitting is found to be ~0.022 inch-per-year¹², while that for general corrosion is about half the pitting rate, at ~0.012 inch-per-year. The corresponding 90th percentile rate is found to be ~0.012 inch-per-year for both pitting and general corrosion, while the average rate for the worst-case situations is found to be 0.009 inch-per-year. The similarity between the average and 90th percentile rates for general corrosion and pitting corrosion is expected in light of the trends shown in Figure 22b, as is the difference in the upper-bound rates which reflects the differences in scatter at the extremes of

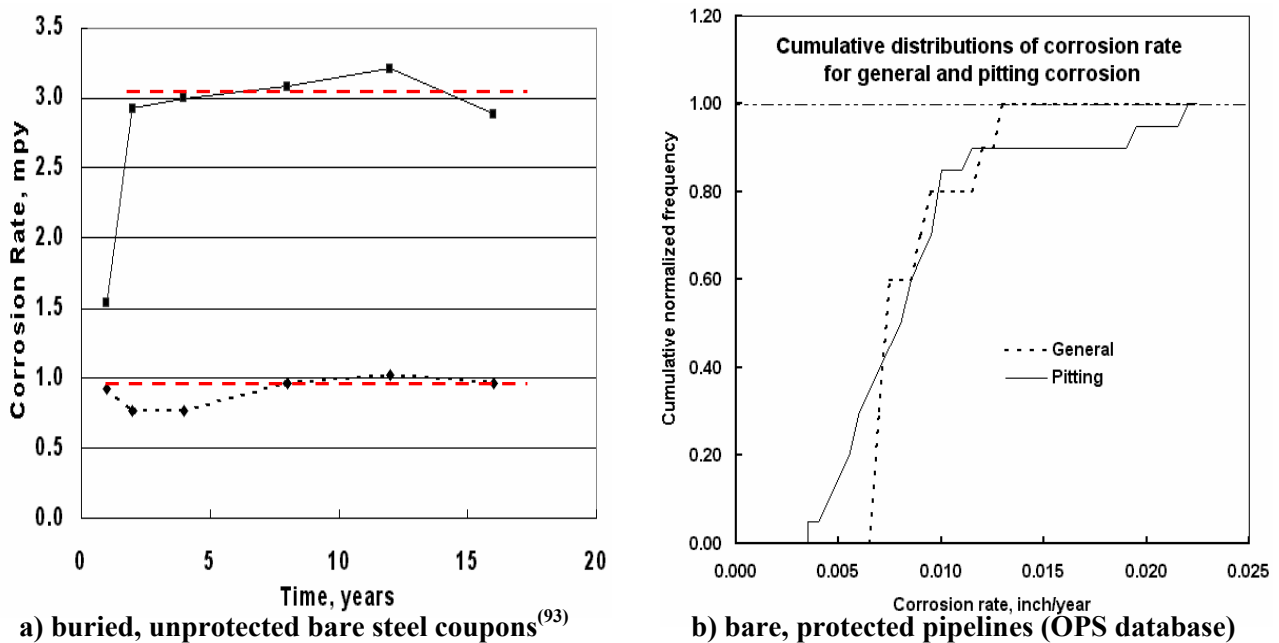


Figure 22. Corrosion kinetics trends for buried steel coupons and pipelines.

¹¹ That is 90 percent of the population had this rate, or a rate *slower* than this value. Thus, this value represents 90 percent of the worst-case corrosion scenarios that led to incidents.

¹² This rate reflects an upper bound, and should not be taken as typical.

these two populations.

Analysis of the OPS database for corrosion incidents leads to a maximum corrosion rate that is comparable to the upper bound for the bare, protected pipelines, while the average corrosion rate for all corrosion data is about a factor of three slower. The similar upper-bound values may reflect the fact that the first-to-occur field failures on coated lines happen at areas of poor coating, such that it takes little time for coating failure. Another factor is that where corrosion occurs on a coated line, the process tends to be “focused” there for cathodically protected pipelines. But, regardless of the cause, the results in Figure 22b remain credible worst-case values for the full database, and are even more so a worst case when compared to the rest of the pipeline system. This likewise is the case for the 90th percentile and average rates, as demonstrated by the fact that the average rate for these corrosion data are about three times faster as compared to the full OPS corrosion database.

Fatigue Thresholds and Kinetics

The fatigue process involves a period spent wherein damage accumulates in the microstructure that eventually precipitates the formation of a crack whose dimensions are physically measurable^(e.g., 94). Thereafter, this crack whose size can be measured continues to grow until it reaches a critical size. Like corrosion, the fatigue process is well characterized in textbooks and handbooks, from a microstructural perspective^(e.g., 94) through phenomenological approaches^(e.g., 15-17).

Factors controlling fatigue crack initiation and propagation are comparable, provided the fundamentally different scale of the processes they represent is considered. Crack nucleation is a bulk process and so can be represented by bulk parameters like wall stress or its equivalent in terms of pressure or other external loads like axial tension or bending to the extent they occur. In contrast, crack propagation is highly localized at a crack tip, which means the dimensions of the crack, its shape, and its location and orientation must be considered. But, as for nucleation, this process can be represented in terms of remote parameters like wall stress or its equivalent provided that the presence of the crack is considered.

Controlling Factors

Fatigue damage per cycle of loading during initiation develops in response to the maximum stress in a given cycle and the ranges of the stress and the strain⁽¹⁷⁾, which are proportional if the response is locally elastic. The amount of damage accumulated depends on the number of times that cycle is applied, with damage assessment and accumulation becoming complicated when dealing with variable-amplitude mechanical loading histories^(e.g., 95). First-order parameters in assessing the effect of increased wall stress on the kinetics (i.e., rate of fatigue damage accumulation during initiation) include:

- Pressure-cycle-induced stress range, mean stress, and strain range,
- Number of times that cycle is experienced,
- The size of the crack beyond initiation,
- Stress concentrations local to welds and other geometric features, and
- Inherent (line-pipe) fatigue resistance.

Second order factors that enter through their effect on critical flaw size include:

- Line-pipe diameter and wall thickness and
- Line-pipe strength and toughness.

The literature indicates that the fatigue mechanism exhibits a threshold stress level below which the kinetics diminish to the point they no longer are a practically significant concern^(e.g., 94,99). Such thresholds are evident for smooth-bar data for line-pipe steels, which reflect the fatigue resistance to crack initiation, as well as for pre-cracked specimens that reflect fatigue crack propagation behavior. Above the threshold, the crack initiation kinetics tend to depend on grade at longer lives, whereas fatigue crack propagation (FCP) rates tend to be largely independent of grade. Thresholds for use in pipeline applications are quantified shortly along with the kinetics data.

Driving Force for Fatigue Crack Initiation and Propagation

The influence of a given pressure cycle on fatigue crack initiation is measured through use of a fatigue damage parameter (FDP) that accounts for the effects of stress range, mean stress, and strain range caused by the cycling in a universal way. This FDP is taken in the form⁽⁹⁶⁾:

$$FDP = \{(\Delta s + s_{\text{mean}}) \cdot E \cdot \Delta \epsilon\}^{0.5}, \quad (7)$$

where Δs = stress range, s_{mean} = mean stress, E = elastic modulus, and $\Delta \epsilon$ = strain range. This parameter is evaluated in terms of local stresses and strains, such that it is evaluated after other factors like stress concentration are taken into account. Accordingly, analysis that addresses local geometric factors precedes use of this parameter. Such is referred to as the critical location approach^(e.g., 97).

Because pipelines operate at nominally elastic conditions, when dealing with nominal stresses and strains the quantity $E \cdot \Delta \epsilon$ is simply equal to the stress range, Δs . The slope of the fatigue-initiation resistance curve, m , expressed in terms of this damage parameter can be used to estimate the relative effect of differing stress cycles on the fatigue life. For fully-reversed cycling under nominally elastic conditions, the damage parameter has the form of the stress range, which means the slope of the fatigue-initiation resistance curve is negative one-twelfth. This value is typical of most C-Mn line-pipe steels, and most other steels at longer lives. Assuming, as is reasonable for elastic (linear) systems, that the range of the stress cycle decreases in proportion to the decrease in maximum stress, the relative service life can be determined from the damage parameter, which after raising both sides by the m^{th} power and implementing this assumption has the form:

$$FDP = \{(\Delta s + s_{\text{mean}}) \Delta s\}^{m/2}. \quad (8)$$

The factors controlling fatigue crack propagation are comparable to those for initiation, provided the fundamentally different processes they represent are accounted for. A damage rate parameter (DRP) is again used to account for the effects of stress range and mean stress, on fatigue crack-growth rate. This is in analogy to the approach applied to analyze fatigue-crack initiation kinetics.

A DRP is again used for the sake of illustrating the effects of stress range and mean stress on fatigue crack-growth rate. This is analogous to the approach applied to analyze fatigue-crack

initiation kinetics in Equation 8. For present purposes the form of the DRP adopted follows from the usual power-law expression^(e.g., 15-17) between crack-growth rate and Mode I stress-intensity factor, denoted K_I , whose form was introduced earlier in Equation 6. As noted in reference to Equation 6, values of this stress intensity factor are tabulated in handbooks for typical geometries^(e.g., 18), and evaluated for typical pipeline applications^(e.g., 31,67,68). Assuming the range of the pressure cycles increase in magnitude in proportion to maximum pressure increase as occurs for linear elasticity, the DRP has the form:

$$\text{DRP} = C_a \Delta K_I^n \propto C_e \Delta P^n. \quad (9)$$

The value of K in this equation reflects the effects of stress perpendicular to the axis of the defect and the defect size. In the worst case, the axis of the defect lies along the length of the pipeline, in which case the value of K is given in the form of Equation 6 as:

$$K = S f(a/w)(\pi a/Q)^{0.5}, \quad (6a)$$

where the symbols are as defined earlier. As indicated there, K denotes the LEFM stress intensity factor, which serves as a universal measure of crack driving force.

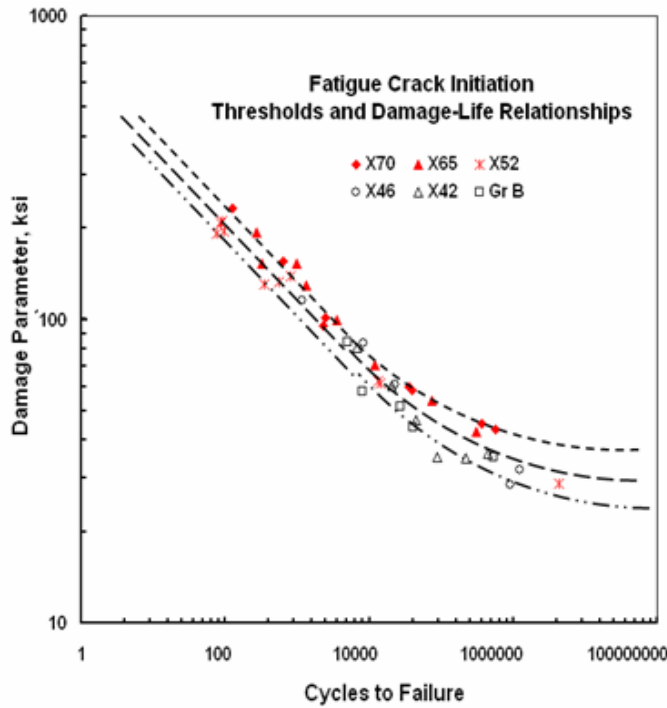
When the right-hand-side of Equation 6a is measured in the laboratory for a specific material, the corresponding value of K reflects the material's resistance, particularly in reference to thresholds for crack growth, usually denoted as K_{th} . In contrast, when S , the function $f(a/w)$, and the crack dimension represents the pipeline operating situation, the corresponding value of K represents the crack driving force.

Based on literature data^(e.g., 15-17,52), the value of the constant n in Equation 9 is about 3.5 for typical C-Mn and other similar steels. Fatigue life during crack propagation is obtained by integrating Equation 6a expressed in differential form. Where the threshold is a consideration, more complex forms of Equation 9 are required.

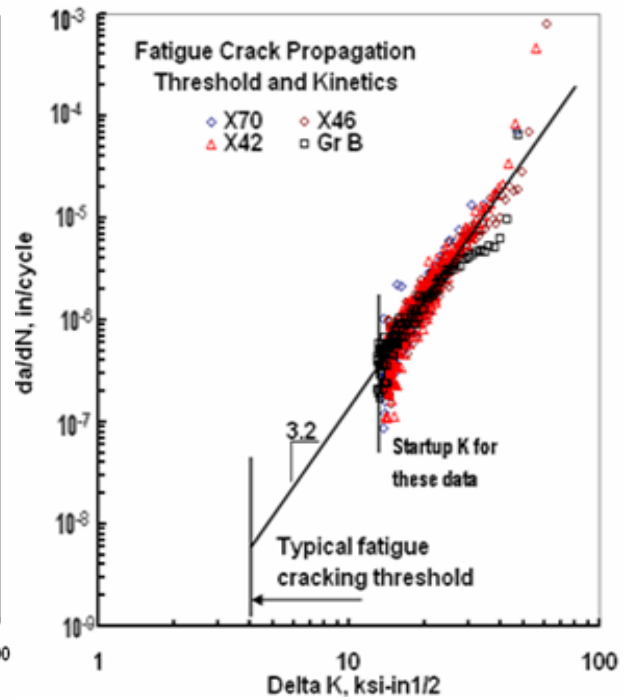
Fatigue Kinetics and Thresholds

Figures 23a and 23b present fatigue data typical of line-pipe steels generated using smooth-bar and pre-cracked specimens, respectively, while Figure 23c presents results for various welds for which it is usual not to discriminate between crack initiation and propagation. This figure makes use of the American Welding Society⁽⁹⁸⁾ (AWS) designations for typical weld configurations. Figures 23a and 23c presents the crack initiation resistance in terms of cycles to failure on the x-axis, while the y-axis presents corresponding values of the damage parameter expressed above in Equation 7. Figure 23b presents the crack growth resistance. The y-axis in these figures is the rate of cracking, while the x-axis indicates the driving force for cracking in terms of the stress-intensity factor of LEFM, defined earlier for Equation 6a.

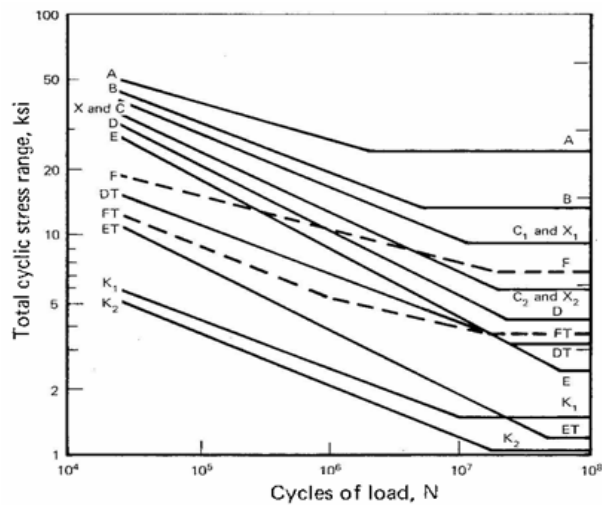
The damage parameter in Equation 7 is a function of stress range, mean stress, and strain range. It is adopted here because these variables influence fatigue initiation resistance, which can be reasonably consolidated through use of this parameter under different stressing conditions⁽⁹⁹⁾. Results are presented in Figure 23a in terms Equation 7 for three line pipe steels representing grades from Gr B through X42, X46, X52, X65, and X70. This figure indicates the fatigue resistance of these steels differs slightly. The X52 and X65 falls on the lower side of the scatter band compared to X70, while grades produced earlier tend to fall in a band below that for X65 and X52. Such banding is anticipated on both grade and vintage for these and other comparable grades and vintages of line pipe steels for two reasons. First, the long-life fatigue resistance



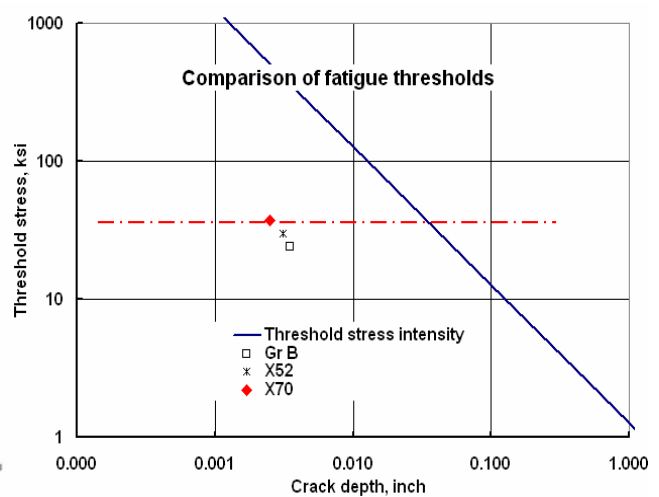
a) initiation



b) propagation



c) weldments, with AWS designations⁽⁹⁸⁾



d) threshold comparison

Figure 23. Fatigue resistance of several grades of line pipe steel

depends on strength, with increased resistance occurring with increased strength. Second, fatigue initiation resistance is imperfection sensitive. As indicated in Reference 11, the cleanliness of steels improved significantly in the 1960s and 1970s, such that more recent vintage steels such as the X70 evaluated here have fewer and smaller sites for crack nucleation, which leads to longer lives as compared to early vintage, lower-strength grades.

Figure 23c presents results for welds, which as the trends imply depend on the configuration of the weld and the manner it is loaded. Fatigue initiation and propagation at welds and stress concentrations in general is much less sensitive to steel imperfections, because the stress concentration and microstructure of the weld dominates imperfections at a micro level. Because the stresses are elevated by the stress concentration at the weld, local residual stresses or mean stresses imposed in the loading are diminished by the effects of local plasticity induced by the stress concentration. For this reason, such scenarios often are less sensitive to factors that can otherwise show a significant effect on smooth specimen data. Additional data on welds and the effects of certain treatments such as dressing can be found in Reference 100.

Figure 23b presents data for crack growth resistance for four line pipe steels representing early vintage Gr B through more recent X70. The y-axis in this figure is the rate of cracking, while the x-axis indicates the driving force for cracking in terms of the stress-intensity factor of LEFM, defined earlier for Equation 6a. As evident on this figure, the slope of this trend is 3.2, which lies in the range typical of construction steels. Also, these data show the usual power-law cracking response. The kinetics for the more recent line pipe grades is similar to that of earlier grades, apparently because the scale at which cracking occurs is above that affected significantly by changes in steel cleanliness. This too is typical of literature trends. On this basis, the resistance of line-pipe steels is comparable to that of other similar steels. Note that these cracking kinetics indicate a stress intensity below which the rate of cracking tends to zero, which indicates a threshold level of K below which crack growth is imperceptible. Such a value can be used to judge whether crack-like defects will become active due to fatigue (i.e., have a size large enough under a given loading to continue to propagate).

As implied above, thresholds for the effects of fatigue can be inferred in reference to stress levels below which continued cracking leading to failure no longer occurs. For the crack initiation results in Figure 23a, this threshold beyond which failure no longer occurs defines the so-called fatigue limit. The stress level that defines the fatigue limit can depend on the nature of the loading. For example, periodic overloads in otherwise constant amplitude cycling can reduce the stress level evident in Figure 23a⁽¹⁹⁾. This “overload” scenario is unlikely a practical factor in regard to pressure loading for compressible systems like gas transmission pipelines, as pressure overloads are controlled by regulators and fail-safe limits. Figure 23b also implies a threshold below which failure does not occur, and indicates a typical value of the so-called threshold for crack propagation¹³. Again, this threshold for crack propagation can depend on the nature of the loading and the length of the crack and related stress level, whose effects are potentially more complex than experienced with the fatigue limit. For example, an overload can arrest cracking while a significant compressive “under-load” can accelerate cracking or activate otherwise

¹³ Note as evident in Figure 23b that the stress intensity at which crack-propagation testing starts also produces a “tail” of data that has the appearance of a threshold, but actually reflects the “start-up” stress intensity factor. Care should be taken to distinguish between this artifact and the actual threshold.

dormant cracks, with both effects reflecting the near-crack-tip residual stress fields and so-called load-interaction effects^(e.g., 17). Constraint and the scale of plasticity at the crack tip, which contribute to the so-called “short-crack effect” also influence the threshold value for crack propagation. Such aspects are reviewed in the literature^(e.g., 101,102) and can significantly confuse the utility of typical testing practices⁽¹⁰³⁾. However, with care use can be made of the apparent thresholds evident in Figures 23a and 23b.

Figure 23d combines threshold data for crack initiation and propagation evident in reference to Figures 23a and 23b. The y-axis in the figure is the stress at the threshold or fatigue limit plotted on a logarithmic scale as a function of the crack depth at these conditions plotted on the y-axis on a logarithmic scale. In light of the form of Equation 6a, the LEFM threshold result in Figure 23b whose value is about 4 ksi-inch^{0.5} lies along a line whose slope is minus one-half. This trend and the corresponding data pair from Figure 23b are shown in Figure 23d along with the fatigue limit stress level for X70 from Figure 23a, whose value projected as a horizontal line from the y-axis. Also shown are the corresponding data pairs for Gr B, X52, and X70 at crack depths roughly corresponding to the grain size of these steels. The intersection of the two lines representing respectively crack nucleation and crack propagation thresholds can be viewed as a measure of the transition between control of the failure process by nucleation or propagation. At crack sizes smaller than that for their intersection, crack nucleation controls, whereas at larger sizes crack propagation according to LEFM controls.

Stress-Corrosion Cracking Kinetics and Thresholds

Controlling Factors

For SCC to occur, three concurrent conditions must be mutually satisfied:

- Operating environment that can develop a cracking environment adjacent to the pipe wall,
- Susceptible pipeline steel in that cracking environment, and
- Tensile stress (applied or residual), which exceeds the threshold for cracking in that cracking environment.

A fourth condition must be satisfied for SCC to threaten pipeline integrity:

- Multiple, adjacent, small cracks, which taken alone are effectively benign, must coalesce axially creating a crack length and depth that cause a break.

Because three concurrent conditions must be mutually satisfied for SCC, the first-order factors affecting SCC include:

- Parameters that produce and control the cracking environment at the steel’s surface (soil, moisture, coating type/condition/disbonds, temperature, electrochemical conditions, etc),
- Parameters that control the cracking response to that environment (steel temperature, or effectively the product and soil temperatures, the local electrochemical potential), and line-pipe susceptibility, and
- The stressing conditions (pressure and pressure cycles) expressed in terms of stress range

and mean stress for a given cycle, and stress concentrations local to welds and other geometric features.

Second-order factors that enter through their effect on critical flaw size include:

- Line-pipe diameter and wall thickness, and
- Line-pipe strength and toughness.

Two cracking environments have developed within the ground-water operating environment of a pipeline that are known to cause and support continued SCC for the stressing conditions and steels typically encountered in transmission pipeline systems. One of these is termed high-pH SCC because the pH for this environment is high – around 9.3 – as compared to the second environment that is near-neutral – with pH slightly less than 7 – such that this cracking is termed near-neutral SCC (NNSCC).

References 104 and 108 are excellent resources detailing the SCC process as it develops on pipelines. These references detail the environments known to produce SCC, and provide features to distinguish between high pH SCC and NNSCC. Reference 106 defines the mechanism for high pH SCC as anodic dissolution, which is elaborated in regard to slip-dissolution and other basic phenomenological models^(109,110). A mechanism for NNSCC has been recently postulated⁽¹¹¹⁾, which relates the process to non-electrochemically generated hydrogen, although other mechanisms are likely involved⁽¹¹²⁾.

While NNSCC was once considered a problem for northern climates, the recently developed mechanism for this process indicates conditions supporting such cracking can occur even in the Southern US⁽¹¹¹⁾. Of the above-listed factors, only maximum pressure, pressure cycles, and product temperature can be simply changed or controlled – the rest are fixed for existing pipelines. How these factors affect SCC kinetics and pipeline integrity is reasonably understood and characterized for high-pH SCC, but still somewhat undeveloped for near-neutral SCC. For this reason, kinetics are presented only in reference to high pH SCC. Suffice it for NNSCC to note that evidence based on trending cracking kinetics for field incidents discussed at the Canadian National Energy Board (NEB) hearing on SCC⁽¹⁰⁴⁾ indicates the kinetics underlying field failures led to similar cracking rates for high pH SCC⁽¹¹³⁾.

SCC Kinetics

To date, virtually all line-pipe steels exposed to typical ground water environments under sufficient stress have been found to be susceptible to SCC to some degree. Differences in susceptibility depend on the extent of microplastic strain that develops under the stressing conditions of typical pipeline operation. The nominally elastic response of line pipe steels at all regulatory-accepted operating stress levels limits the extent of this microplastic straining as compared to the conditions developed in the laboratory. For example, the slow-strain-rate test⁽¹¹⁴⁾ (SSRT) practice involves loading that while initially elastic eventually exceeds the yield stress and continues through stress levels that can reach the UTS. This is illustrated in Figure 24a, which presents a trace of the stress versus strain (time) in two typical SSRTs. One result marked “ambient” in this figure represents the stress-strain curve of the steel, while the second noted “SCC” indicates the response under environmental conditions that promote SCC. Results of similar testing interrupted part of the way through this straining history indicate that cracking, whose effects are evident in Figure 24a in the reduced elongation to failure, occurs

well after the yield stress is achieved. On this basis, the SSRT is highly accelerated in contrast to the nominally elastic response in a pipeline.

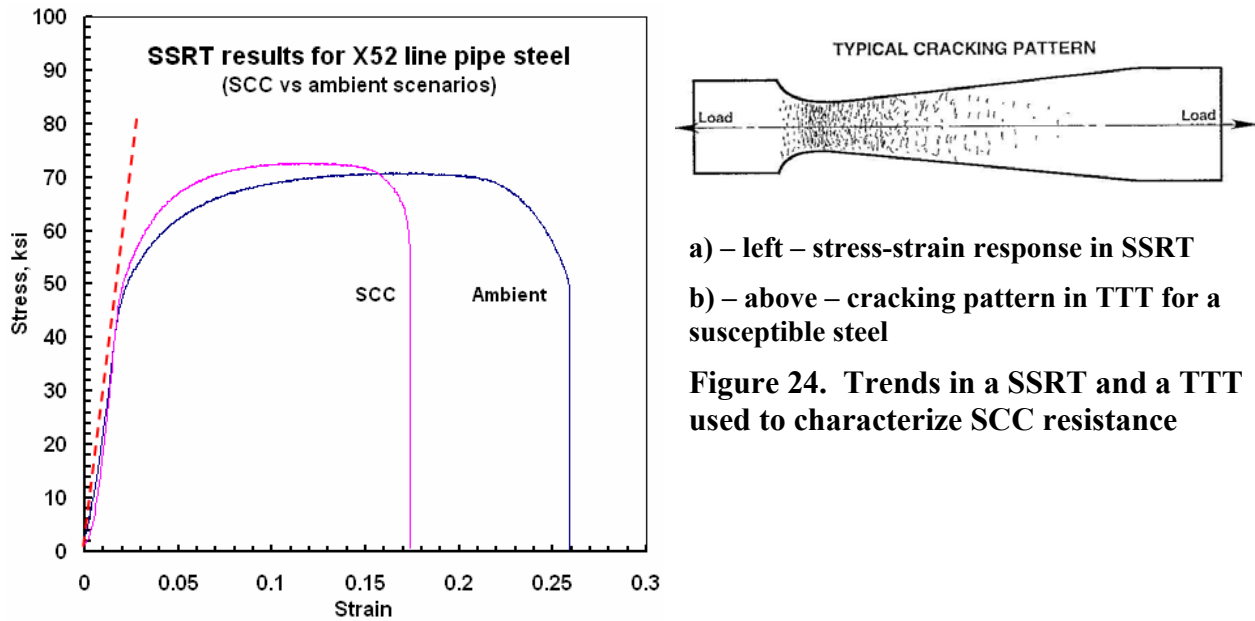


Figure 24. Trends in a SSRT and a TTT used to characterize SCC resistance

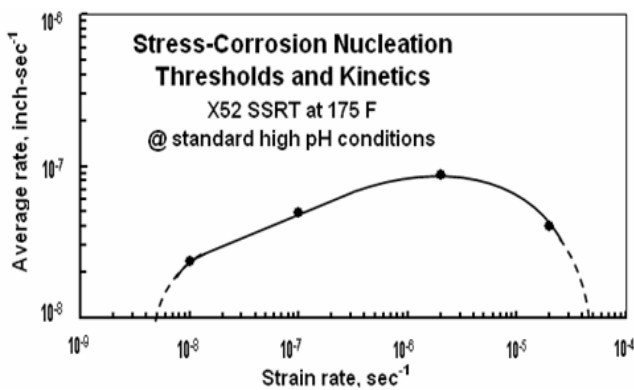
Experiments involving similar tensile loading, with instrumentation designed to detect electrochemical response to freshly exposed surface, indicate pre-yield microplastic strain develops. This pre-yield microplasticity is enhanced on the surface of such test specimens⁽¹¹⁵⁾ because grain-to-grain compatibility is limited there⁽¹¹⁶⁾. The effects of microplasticity on SCC nucleation as well as the more extensive flow that occurs with yielding are evident in Figure 24b⁽¹¹⁸⁾. This figure illustrates the pattern of cracking that develops in a tapered-tension test⁽¹¹⁷⁾ (TTT) specimen. As shown in Reference 118, the depth and frequency of the cracking increase as the stress increases along the TTT specimen, which indicates the spacing between the cracking decreases. Such results indicate a threshold stress exists below which SCC does not occur. More on thresholds follows later.

Laboratory data characterizing SCC kinetics as an analog to fatigue and Figure 22 are presented here for high pH SCC in Figure 24. These results reflect conditions that maximize cracking, as the temperature, the cracking environment, and the electrochemical potential used for this testing reflect circumstances much more severe than occur in the field. This results in accelerated kinetics, although it is unlikely to appreciably affect the thresholds for crack nucleation or for propagation. The accelerated conditions used are the so-called “standard test conditions” for the high pH environment⁽¹²⁰⁾. This involves a 1N carbonate - 1N bicarbonate aqueous solution at 75 C (167 F) with the potential controlled at -0.65V SCE, which leads to a current density the order of 5 to 10 mA/cm². According to Faraday’s second law, this corresponds to a penetration (cracking) rate of 2 to 4 x 10⁻⁶ mm-second⁻¹, or ~7.9 to 15.8 x 10⁻⁸ inch-sec⁻¹).

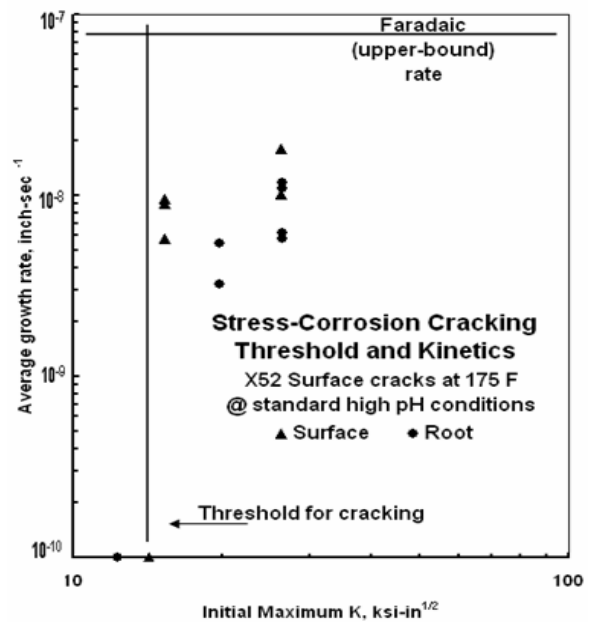
Figure 25a⁽¹¹⁹⁾ presents cracking speed as a function of straining speed based on SSRT results. These data, which reflect upper-bound speeds because they represent the deepest of the many cracks observed, indicate speeds that at the highest value are comparable to the above noted rates due to Faraday’s second law. It is apparent from this figure that thresholds exist for cracking at either very low strain rates, where repassivation limits penetration, and at very high strain rates,

where ductile tearing moves faster than dissolution occurs. Theoretically, such thresholds could be used to identify operating conditions to avoid or limit cracking. Unfortunately, operation under such conditions is impractical, as the stress levels are quite low in comparison to that for Class 1 Locations.

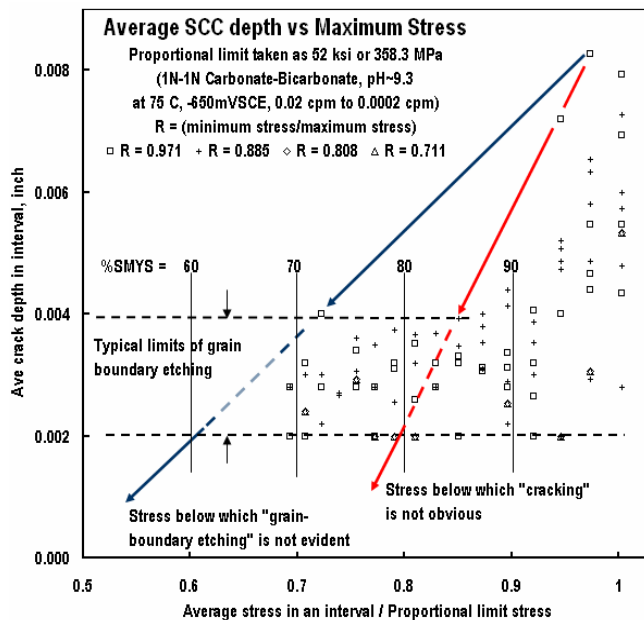
The maximum cracking rate evident in smooth specimens is often faster than that observed in pre-cracked specimens, which is evident in Figure 25b⁽¹¹⁹⁾. This figure presents the cracking speed developed from tension loading of surface-cracked plates, which more closely simulates a pipeline scenario than do the SSRT results. These results reflect the standard testing environment of Reference 120. Results are shown for cracking that occurred at the bottom of the crack (denoted root) and at the point where the crack reached the surface (denoted surface). Differences in speed between the pre-cracked and smooth specimens are anticipated even though the testing conditions in both cases were identical, because the smooth specimen generates many



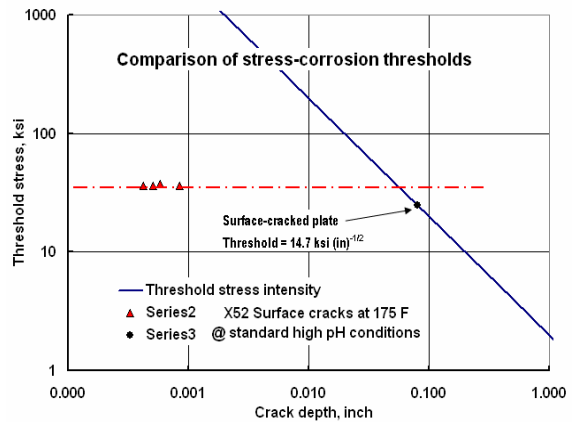
a) nucleation and early growth behavior



b) propagation resistance



c) cracking as a function of maximum stress



d) comparison of thresholds

Figure 25. SCC resistance of several grades of line pipe steel

cracks while the pre-cracked geometry generates one or two dominant cracks.

The kinetics evident in Figure 25a and 25b indicate that if the process characterized by these figures were continuously active in service, failure would occur within weeks of the onset of SCC. Service data, where in SCC speed can be identified between the ductile tearing marked by hydrostatic testing indicates in-service speeds orders of magnitude less than the kinetics in these figures imply. Obviously, a key to using these data is knowledge of the acceleration factor in these tests as compared to field scenarios. This aspect is addressed later in the section dealing with MTBF and pipeline revalidation intervals.

SCC Thresholds

Earlier discussion involving the phenomenology of SCC indicated that microplastic straining was required for SCC to occur, which implies that stress levels less than those that develop such microplasticity will not support SCC. This points to the existence of a threshold stress for SCC – as at low enough stresses microplastic strain ceases to develop to a practically significant level.

Figure 25c⁽³¹⁾ presents results from TTT specimens that likewise were developed using the standard testing conditions for the high pH environment⁽¹²⁰⁾. These data are typical of the response for a broad spectrum of steel grades typical of vintage construction. Two important trends are evident in these data. First, the results at lower stresses give rise to a band of data representing “cracks” whose depth is no greater than is typically observed with the grain-boundary etching that occurs in this environment in stress-free specimens. As such, this band of data is not associated only with stress-induced cracking, but rather is the anticipated effect of grain-boundary etching. The left-most diagonal trend brackets the lowest stress associated with evidence of crack-like features at all stresses. The second trend involves the development of deeper cracking as the stress increases along the TTT specimen, whose plan-form was illustrated in Figure 24b. These data can be seen toward the right margin of this figure, and bracketed by the right-most trend, which runs from the top right down toward the middle of the figure. Continuing this trend to the x-axis indicates the threshold for cracking for this test is the order of 70-percent of the actual yield stress for these specimens. Recognizing these data reflect testing that lasts for seven days, whereas pipelines operate for decades, consideration should be given to the possible effects of in-service growth. Evaluation of tests run up to four times longer than the typical short-term week-long test indicate little difference in this threshold. Likewise, analytical models of SCC do not point to significantly lower thresholds for in-service pipelines⁽¹²¹⁻¹²³⁾. Field data that support these model predictions^(124,125) likewise indicate a threshold exists at a stress level the order of 60 percent of SMYS, possibly higher. Finally, limited experience with significant SCC on pipelines other than those in Class 1 Locations supports such threshold levels.

Finally, consider the comparison of the thresholds evident in Figures 25a and 25b, as plotted in Figure 25d. As for fatigue, the y-axis reflects the stress for the smooth specimen threshold plotted on a logarithmic scale as a function of the crack depth at these conditions plotted on the y-axis on a logarithmic scale. Again, the form of Equation 6a indicates the LEFM threshold in Figure 25b whose value is about $14.7 \text{ ksi-inch}^{0.5}$ lies along a line whose slope is minus one-half. This trend and the corresponding data pair are shown along with the smooth specimen threshold stress level whose values are projected on a horizontal line from the y-axis. Crack sizes below that for the intersection of the lines representing crack nucleation and propagation thresholds

indicate crack nucleation controls the structural response, whereas at larger crack sizes LEFM propagation controls.

Hydrogen Stress Cracking Kinetics and Thresholds

Controlling Factors

Three conditions must be mutually satisfied for HIC to occur:

- Hardness above a critical level (20 R_c or 230 BHN),
- Tensile stress above the threshold level, and
- A source of atomic hydrogen and a gradient to drive it into the steel to a critical level.

Failure of a pipeline due to HIC occurs following a time period over which conditions develop at the surface of the line pipe that lead to the generation of atomic hydrogen. The ensuing ingress of atomic hydrogen is also time dependent. Continued exposure to atomic hydrogen can lead to a reduction in the apparent ductility of the steel, known as hydrogen embrittlement (HE). It can also lead to the initiation of cracks, that with time can grow until a critical size is reached, either for growth from a single crack origin, or by the coalescence of cracking from several adjacent origins.

Parameters with a first-order significance in terms of HIC include:

- Hardness of the line pipe, and presence of hard spots due to steel making,
- Areas of cold work, and the presence of cracking due to re-rounding, and
- Pressure and pressure cycles.

Second-order parameters include:

- Pipe diameter and wall thickness and
- Pipe steel strength and toughness.

Because the availability and diffusion of atomic hydrogen are both first-order factors and are very situation specific, it is very difficult to assess where and at what rate this process is active, which complicates generalizing trends for this mechanism.

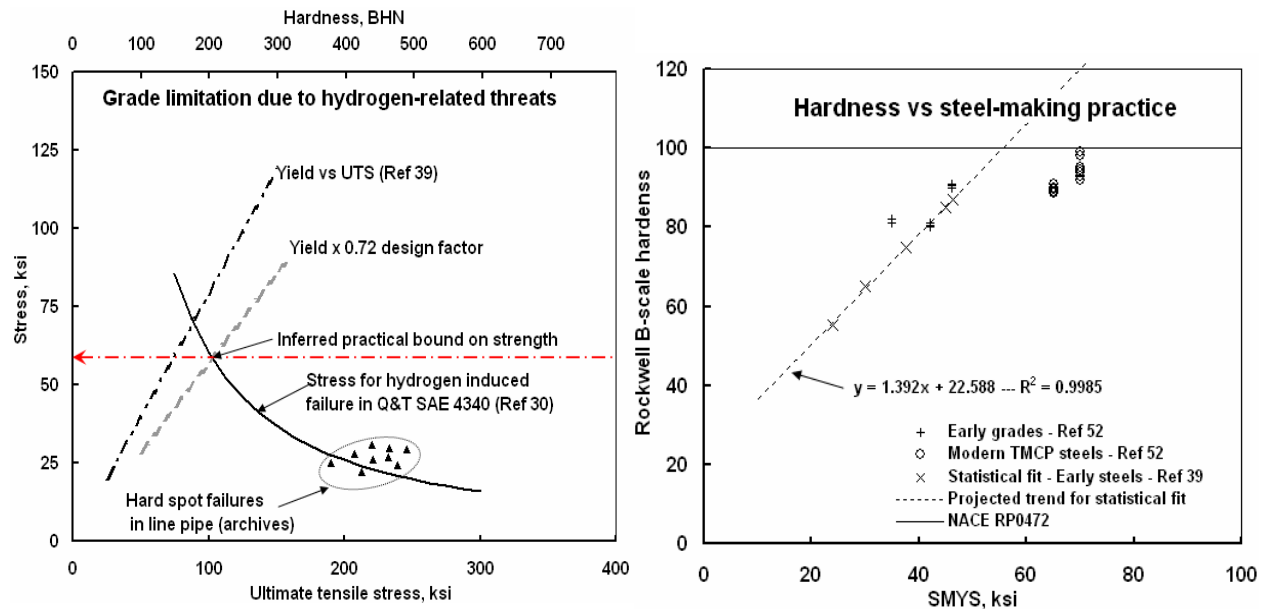
Susceptibility to Hydrogen-Related Mechanisms

Upsets in the CP system used to avoid corrosion on pipelines can induce hydrogen-related cracking or embrittlement. The severity of the resulting problem depends on the strength level and hardness for the early steels that were strengthened by alloying along with quench-and-temper (Q&T) processing. The pipeline industry recognized the potential problem associated with hydrogen-related mechanisms and chose steel making and strengthening practices to avoid or limit this mechanism. In general, steels not susceptible to hydrogen cracking have been employed.

Figure 26⁽⁵¹⁾ presents a plot that provides practical perspective for some of the key factors that control hydrogen-related susceptibility and cracking, which helps identify circumstances where

cracking could be problematic in pipelines. The format of Figure 26a presents yield strength on the y-axis and the ultimate tensile stress on the x-axis, along with correlations between hardness and the UTS. Literature data^(e.g., 30) are added to this, where the curved trend represents the threshold for hydrogen cracking in Q&T 4340 steel over a range of hardness levels and the data (triangular symbols) represent hard-spots in pipelines. It is evident from this figure that the data for the hard spots correspond to the trend for the Q&T steel used to infer the threshold for cracking in reference to the UTS of the steel. Such is expected, as the microstructure of Q&T alloyed steels depends strongly on hardness, such that steels of similar hardness would behave in like manner.

Also shown in Figure 26a is a trend that reflects the usual correlation between the yield stress on the y-axis and the UTS on the x-axis. The Y versus T trend used follows from Reference 39, being shown in the figure as a dashed trend labeled accordingly. Finally, offset to the right of this Y versus T trend is another dashed trend developed by multiplying the yield stress from the Y versus T trend by 0.72, which is the maximum design factor allowed for pipelines in the US. The intersection of the curved threshold representing hardened steels as a function of hardness and the trend for the maximum design factor of 0.72 lies at 60 ksi. Thus, these trends point to Grade X60 as the upper bound on SMYS to avoid cracking due to hydrogen-related mechanisms. This observation is reinforced by a number of pipeline company line-pipe specifications that limit sour service applications for conventionally processed steels to X60 and below.



a) threshold for initiation

b) susceptibility versus hardness

Figure 26. Aspects of hydrogen-related cracking behavior of line-pipe steel

Figure 26b contrasts behavior of a range of data for the early line pipe steels, such as those representing the hard spot data in Figure 26a, with the current approach to strengthen steels that relies on thermo-mechanical-controlled-processing (TMCP). The y-axis here is hardness whereas the x-axis is grade expressed as SMYS. The trend between hardness and strength for the early grades is indicated in this figure as the dashed line, which is projected to the bound on hardness established by NACE RP0472⁽¹²⁶⁾ to avoid such cracking. The intersection of this trend and the NACE limit comes at SMYS of 60 ksi. In contrast to the trend for the early steels,

literature results for TMCP⁽⁵²⁾ steels, shown as the circular symbols, fall on an independent trend. Significantly, these data for higher strength TMCP steels fall below the NACE limit. Thus, modern processing facilitates use of higher-strength grades in reference to their inherent hardness and the related NACE limit on hardness⁽¹²⁶⁾. Accordingly, such higher-strength grades can be anticipated to remain free of hydrogen-related cracking and concerns for effects of CP so long as pipeline design and operation continue as has been historical practice.

Thresholds and Kinetics

Because the industry reacted to the threat posed by hydrogen-related mechanisms through an avoidance approach, there are few instances where this mechanism is a concern, aside from hard spots due to an upset in steel making or arc burns introduced in pipeline construction. This fact, coupled with Table 2 that indicates the grades involved in vintage pipeline system are not inherently susceptible to this mechanism, suggests this mechanism is a secondary concern for the vintage system. The kinetics of hydrogen-related mechanisms are complicated for reasons that involve the evolution of atomic hydrogen on the pipeline's surface, the ingress (adsorption) of this hydrogen, and the microstructure's response to the hydrogen. The microstructure's response dictates the integrity implications. In some cases blisters form, which as their size increases relaxes the blister pressure, which lessens the integrity threat – but is often followed by further hydrogen ingress. In other scenarios the ingress of hydrogen focuses at microstructural stress raisers leading to embrittlement, and depending on the stress level, cracking. In this context, some forms of ingress are more benign than others.

As detailed in the literature^(e.g., 127,128), the complexity of hydrogen-related mechanisms is case specific in regard to each of the formation of atomic hydrogen, its ingress, and its interaction with the microstructure. Case-specific factors drive the kinetics and control the integrity threat to an extent well beyond the present scope. It is because of this complexity that data generic quantifying the kinetics for hydrogen-related mechanisms from formation of hydrogen, through its ingress and influence on integrity are sparse.

Given this complexity it is fortunate that the pipeline industry reacted to the threat posed by hydrogen-related mechanisms through an avoidance approach, which means there are few instances where this mechanism is of concern, aside from hard spots due to an upset in steel making or arc burns introduced in pipeline construction. This fact, coupled with the observation that the grades involved in vintage pipeline system are not inherently susceptible to this mechanism (see Table 2) suggests this mechanism is a secondary concern for the vintage system.

Suffice it here to note that where hard spots or arc burns pose a potential problem, their management may be case-specific as anticipated in terms of the factors that control the formation of atomic hydrogen, its ingress, and its interaction with the microstructure. The approach of Reference 11 addresses this complexity in reference to thresholds relevant to pipelines. These thresholds reflect the earlier-noted factors controlling hydrogen-related mechanisms – no cracking absent a source of hydrogen and its likely ingress, and no cracking absent steel that had hardness beyond critical levels. Accordingly, screening in Reference 11 occurred first in terms of sources of hydrogen that can embrittle the steel or promote blistering. If a source was present, assessed in reference to coating condition, and the steel was susceptible steel based on a hardness threshold level that depends on the severity of the hydrogen source, Reference 11 considered “activation” of the threat in reference to Figure 2a. As little can be added here because of the

case-specific nature beyond the approach taken there, this report hereafter focuses on corrosion, fatigue, and SCC.

Service Loadings and Operating Environment

The last data input needed to facilitate analysis of MTBF and pipeline revalidation intervals as outlined earlier in Figure 2b is the loadings experienced in normal service and under the action of outside forces. Because design provides adequate pipe wall thickness to function safely under normal service conditions, failures during normal operation occur at defects. In contrast, because the magnitude of outside forces can be extreme, failure can occur due to outside forces at sites that are otherwise defect-free as designed. Regardless of the cause, even unusual loadings develop nominally quasi-static conditions.¹⁴ Thus, the usual quasi-static material mechanical properties discussed earlier are appropriate, as are the usual mechanics analysis that relates the loading to the local conditions where failures occur.

The primary stress on buried pipelines is pressure induced. For a given pressure, hoop stresses in the pipe wall are a function of the diameter and wall thickness of the pipeline. Unanticipated loads and the secondary stresses that they develop are most commonly due to earth movement (i.e., landslide, earthquake), heavy rains, or floods (see Table 1), although these are beyond the present scope. Unintended events that could increase the pressure beyond the normal operating pressure can in theory also occur, but such are of little practical consequence because of redundant pressure controls and the compressibility of the gas.

For present purposes, information is needed to characterize the temperature and pressure in the pipeline segment of concern. Gas-transmission pipelines operate over long distances. Because of the compressibility of natural gas and frictional losses along the pipeline's length, compressor stations are distributed as demand requires along the length of the pipeline to maintain gas-flow. The heat of compression increases the gas temperature, the extent to which depends on the amount of compression. It follows that the gas at discharge is warmer than at suction at the next compressor station, as is shown for typical behavior in Figure 27¹⁵. There is an associated pressure drop, which also reflects frictional losses in-route, as is apparent for typical operation in Figure 27. It follows that the average pressure and gas temperature along a typical natural-gas transmission line varies appreciably.

¹⁴ Dynamic loading, from the perspective of pipeline failures, refers to loading that occurs on the order of milliseconds. Because of the compressibility of gas, pressure always is a quasi-static load. Loading due to weather and outside forces also typically develop slow loading rates.

¹⁵ These trends reflect cross-country operation where compression adds significant heat to the gas, which warms the pipe wall to roughly the gas temperature. This added heat is a negative factor in regard to SCC. However, it is a potentially positive factor in terms of fracture behavior, as it promotes ductile response. For steels with high fracture-appearance-transition temperatures, it also can increase the apparent fracture resistance. For this reason, the behavior considered here is not indicative of lines fed from liquid natural gas, or some intrastate lines downstream of pressure regulators where temperatures can be much reduced as compared to this example.

Before SCC was recognized as a potential problem and the role of temperature understood for high pH SCC, discharge temperatures are known to exceed 150 F⁽¹²³⁾. However, since the early 1970s when the role of temperature in high pH SCC became apparent (e.g., 106), gas-compression practices have changed, and some companies have installed after-coolers to reduce discharge temperatures. This has led to a marked reduction in discharge temperature on pipelines susceptible to SCC. On this basis, a temperature on the order of 110°F is taken as representative of typical operations for major companies with pipelines known to suffer SCC.

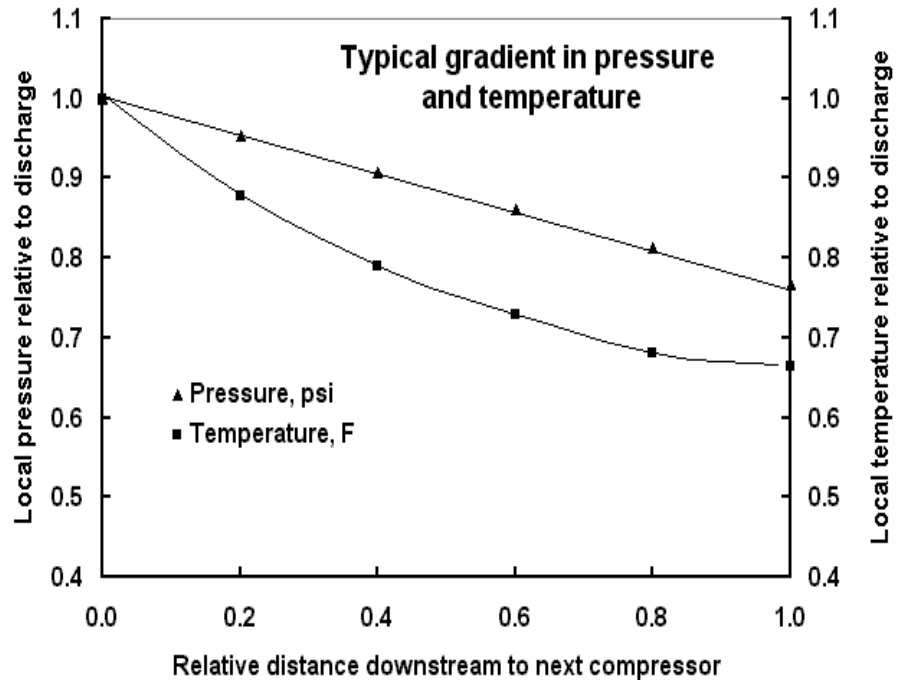


Figure 27. Typical pressure and temperature gradients between compressor stations

Because the minimum burial depth per regulatory requirements places pipelines well below the surface, thermal swings due to changes in ambient diurnal changes are not anticipated nor is the related heat capacity sufficient to overcome the metal temperature induced by the steady flow of compressed gas. For purposes of SCC analysis consideration should be given to the maximum discharge temperature, whereas from a fracture perspective the minimum temperature is relevant. As both pressure and temperature diminish along the pipeline as indicated above, risk-related analysis along a pipeline segment would logically address this decay.

Pressure and Temperature Histories

Pressure and temperature histories have been documented for a variety of pipelines, some of which are discussed in the literature^(e.g., 108,129), others for which have been sanitized and published in summary form^(e.g.,123). Typically, such data is gathered as input to SCC sensitivity studies, or related analyses. As not all lines run at maximum pressure, pressure data tend to be analyzed using cycle-counting algorithms, whose development began in the aircraft industry in the 1960s and before⁽¹³⁰⁾, and were further developed in the 1970s⁽¹³¹⁾, and now have been standardized⁽¹³²⁾. For the present a matrix of pressure, pressure range expressed as the pressure or stress ratio, $R_\sigma = \text{minimum value} / \text{maximum value}$, and temperature are evaluated in reference to fatigue and SCC, with temperature also considered in reference to SCC. Regulatory limits bound wall stress at 72-percent of SMYS, while literature data noted indicate stress ratios of concern in gas-transmission pipelines are in the range $0.70 \leq R_\sigma \leq 1$, while temperatures are in

the range $90 \leq \sigma \leq 140$ when dealing with SCC. This range of parameters has been investigated in reference to the growth of axial defects due to fatigue and SCC. Failure at constant wall stress (pressure) up to and beyond hydrostatic test levels has been previously considered in reference to Figures 20 and 21.

Axial Poisson-Induced Stresses

Because pressure-induced tension creates uniform axial stress remote to the defect in an earth anchored pipeline, it is appropriate to consider its effect on circumferentially oriented defects. For this reason, fracture controlled failure at circumferential defects has been evaluated in terms of the pressure-induced tension stress as it develops in earth-anchored pipelines at a pressure of 72-percent of SMYS. However, the general effect of outside forces are not addressed, as this threat is outside the scope of this project. While the UTS due to outside force has the same effect on defects, results that follow for pressure-induced tension should not be used to infer defect response under the action of axial stress due to outside forces tension as these results cannot be simply scaled or interpolated.

MTBF and Revalidation Intervals

Where evaluation of the company files in reference to Figure 2a indicates a threat can be activated, Figure 2b points to comparison of pipeline's operation in contrast to critical defect sizes quantified in Figures 20 and 21 and the threshold levels quantified in Figures 21 to 24. If the operation-induced wall stress exceeds the threshold indicated in these figures, then Figure 2b indicates consideration of MTBF. The resulting MTBF becomes a consideration in assessing the revalidation interval for the pipeline, along with the consequences of a failure and other issues such as the absolute factor of safety or risk that underlies related decisions.

Where blunt defects like corrosion are present, the kinetics of Figure 22 implies a gradual decrease in the remaining wall thickness, as illustrated in reference to revalidation intervals elsewhere^(7,8). Where crack-like defects are anticipated and operation-induced wall stress exceeds the relevant threshold, Figure 2b indicates MTBF becomes a consideration in assessing the revalidation interval for the pipeline, along with the consequences of a failure and other issues such as the absolute factor of safety or risk that underlies related decisions. Finally, where hydrogen-related mechanisms are involved, the process indicated herein in Figure 2 defaults to Figure 13 and the guidance of Reference 11.

Realizing that pipelines are not redundant in their design the question to be answered is whether defects potentially present in the pipeline can grow and if so at what rate and certainty.

Where defects are small in comparison to the transition to LEFM controlled growth as presented in Figures 23d and 25d, or their growth rates are near or below the thresholds for growth shown in Figures 23b and 25b, consideration should be given to MTBF. In contrast, where the size of the defect leads to values of crack driving force that point to high rates of growth, MTBF is not a practical concern as the resulting interval will be too short. For such cases, safety dictates repair on a timeline commensurate with the indicated kinetics, which in many cases will require immediate response. The results that follow address this full range of scenarios. Prudence must dictate how the results are used in regard to whether the defect can grow and if so at what rate and certainty.

The ensuing sections present the model formulation and the format used to present the results, for each of corrosion, fatigue, and SCC. Finally, the results are presented as contours of MTBF and related measures useful in assessing defect severity as part of a pipeline IMP.

Model Formulation

Model formulation relies on the observation that pipeline integrity is controlled by the formation and growth of features that can be considered either blunt as for corrosion or sharp as for fatigue or SCC. The difference between one sharp defect and another reflects the kinetics used to characterize its growth. On this basis, failing defect sizes reflect the nature of the defect (length, depth, orientation) and the properties of the line pipe (grade, UTS, diameter, wall thickness, and toughness). This generic framework facilitates use of failing defect size or stable penetration of the wall thickness as the limiting condition for MTBF, and permits characterizing safe operation as a function of parameters that can be measured in the field, and understood in reference to pipeline operation.

Regardless of the kinetics, MTBF represents the time required for the through-wall ligament to be breached, or for the defect to grow in length until failure occurs at the corresponding depth or the length for rupture is reached. The time before the defect becomes critical depends on the kinetics, and on the least of the absolute distances over which growth occurs. The absolute distance in the through-wall direction is the difference between the current depth, d_c , and the failing depth, d_f , which in the limit is the net wall thickness, t_n . The absolute distance in the length direction is the least of the difference the current length, L_c , and the failing length is a leak, L_f , or the rupture length, L_r . An algorithm is used to interpolate between adjacent failure boundaries like those in Figure 20 for blunt defects and those in Figure 21 for initially sharp defects, with leak versus rupture determined for both in reference to the bounds shown in Figures 20 and 21. This interpolation is done in two dimensions as a function of the operating pressure. Thereafter, another algorithm calculates the lesser of the length increments, ΔL , between L_c and L_f or L_r , which defines the controlling growth increment in the length direction. Likewise, the smallest difference in depth, Δd , between d_c and d_f or t_n defines the controlling growth increment in the depth direction. Thereafter, MTBF is determined as presented next in reference to the lesser of ΔL or Δd . The algorithm used to complete this analysis involves integrating the results from several software packages developed previously at Battelle.

As the relative amount of pipe wall thickness available for in-service growth decreases as the wall thickness decreases, either with increasing grade or increasing diameter for a constant design pressure, much different values of MTBF can be anticipated for applications with highly contrasted wall thickness when the increment of growth in the through-wall direction controls leak or rupture. This tendency will be clearly evident for cases where the wall thickness available to support in-service growth is rapidly traversed by a high-rate degradation process, as is evident shortly for SCC in the thinner-wall designs.

Because of differences evident in the kinetics as discussed in the section on presentation format, different mathematical models are formulated specific to the kinetics. Corrosion as represented in Figure 22 involves constant kinetics – so long as the factors controlling corrosion remain unchanged, the corrosion rate is a constant. In contrast, fatigue as represented in Figure 23 exhibits a rate of damage or crack propagation kinetics that is a function of stress, which for crack propagation also depends on the depth and shape of the crack. SCC as characterized in

Figure 25 is unlike corrosion or fatigue, but does show traits of both – thresholds are evident as in fatigue, but rather than being stress or crack length dependent, its kinetics once active are constant as evident for corrosion. Formulations follow that reflect the kinetics for each of these mechanisms.

Corrosion

The trends in Figure 20 define sizes and shapes of defects that fail. The MTBF for corrosion is the least of the times for corrosion to traverse the remaining wall as indicated in Figure 20, or for its length to reach that for rupture as indicated in Figure 21. These times are determined in regard to ΔL , between L_c and L_f or L_r , and Δd , between d_c and d_f or t_n , as indicated above. The MTBF that limits life is the lesser of ΔL or Δd divided by the corrosion rate.

MTBF based on this analysis and corrosion kinetics derived from the OPS incident database¹⁶ means the kinetics reflect worst-case field corrosion conditions as compared to circumstances elsewhere in transmission pipeline systems. As discussed in reference to Figure 22, these kinetics reflect the leading edge of the population of corrosion rates, which generates values of MTBF that reflect a worst-case as compared to all of the incidents on bare, protected pipe. Other kinetics can be used, which simply scale MTBF in direct proportion to the ratio of the corrosion rate. As indicated earlier, analysis of the OPS database for all corrosion incidents leads to a maximum corrosion rate that is comparable to the upper bound for the bare, protected pipelines, with the average corrosion rate for all corrosion data is about a factor of three slower. As these kinetics are otherwise independent of pipeline operation, there is no need to address operational parameters when dealing with MTBF for corrosion.

Fatigue

In parallel to the formulation for corrosion, the trends in Figure 21 determine failing defect sizes to assess the remaining life of crack-like defects, which again are coupled with the kinetics and thresholds of Figures 24 and 25, and consideration of the leak versus rupture boundaries evident in Figure 21. As for corrosion, MTBF is determined by the lesser of the difference in length, ΔL , and the difference in depth.

Because corrosion kinetics were invariant of defect size or stress, the ensuing calculation of MTBF is quite simple. However, as evident from Equations 6, 8, and 9, the damage done or the increment of crack advance depend at least on the wall stress (pressure), and for crack propagation also depend on the instantaneous crack depth and length. As MTBF here involves a known or estimated defect size based on field measurements or ILI data for some scenarios, the MTBF is determined in reference to fracture mechanics and Equations 6 and 9. The number of cycles to traverse the lesser of ΔL or Δd is determined by integrating Equation 9 (or a similar equation) expressed in differential form, with integration done between the limits of L_c and L_f or L_r or d_c and d_f or t_n as indicated by the lesser of ΔL or Δd . Because this result depends on

¹⁶ As noted earlier, the OPS database reflects mainly first-to-occur incidents for the pipeline segments involved, and covers lines put into service over more than a 50-year interval, that are operated and maintained differently. Because it represents primarily first-to-occur incidents, it reflects corrosion “hot-spots” along those pipelines, and provides a reasonable worst-case estimate of corrosion rate.

operating history through the pressure cycling experienced, results for MTBF are presented subsequently for a worst-case operational scenario, results for which are later generalized as a function of the pressure ratio. Equation 8 can be used to scale such results to estimate MTBF for pressure histories other than those considered.

MTBF based on the kinetics in Figure 23 reflect typical results for line pipe steels, which in turn have kinetics comparable to most construction grades of steel. In this context, textbooks note little difference in crack propagation kinetics, although the threshold can vary as a function of microstructure and other factors⁽¹⁵⁻¹⁷⁾. The present analysis has used “average” kinetics, so MTBF does indeed represent a mean in regard to these kinetics. Other kinetics could be used, but unlike the simple linear scaling for corrosion, rates scale nonlinearly in the manner indicated by Equation 8. Finally, note that MTBF for fatigue leads to results expressed in cycles. Central to translating a cycle-based measure of MTBF into units of time is the frequency of cycling, which is specific to each pipeline operation, the same way the pressure history is specific. For this reason, users should gather and analyze pressure histories, processing cycles in accordance with published standard cycle-counting algorithms⁽¹³²⁾. Note that typical gas pipelines are considered to experience one large cycle per day based on an evening peak and day-time demand, such that 50 years of service corresponds to just 18,250 cycles.

SCC

In the introduction to this section, SCC as characterized in Figure 25 was noted to differ from both corrosion and fatigue, although SCC was also noted to show traits of each. For example, thresholds are evident for SCC as they are for fatigue. But rather than being stress or crack length dependent, once cracking becomes active as occurs for fatigue, the kinetics for SCC indicate a constant rate as was the case for corrosion. Because of these differences, MTBF has been evaluated with constant kinetics as was done for corrosion. Likewise, it has been evaluated in reference to trends calculated for SCC from nucleation through failure.

In parallel to the formulation for fatigue, the trends in Figure 21 determine failing defect sizes as input to calculating the remaining life of crack-like defects, which are coupled with the kinetics and thresholds of Figures 24 and 25 and the leak versus rupture boundary from Figure 21. MTBF is again determined by the least difference in length, ΔL , between L_c and L_f or L_r , and the least difference in depth, Δd , between d_c and d_f or t_n . As above, these crack increments and MTBF, which reflects the lesser of ΔL or Δd , have been calculated.

Because the kinetics in reference to Figure 25b are invariant of defect size or stress, the ensuing calculation of MTBF could be done using the same “time = rate/distance” approach used for corrosion. The key question in evaluating MTBF for SCC lies in the value of the “rate” to use in the simple calculation of time = rate/distance. Comparing the rates evident for corrosion in Figure 22 with kinetics for SCC shows high-end corrosion rates at ~ 0.022 inch-year⁻¹, whereas the kinetics for SCC in Figure 25b lead to ~ 2.5 inch-year⁻¹ when SCC is “turned on.” On this basis, SCC can occur about 100 times faster than worst-case corrosion rates. SCC at such rates penetrates the thickest of plausible vintage pipelines in a matter of months, but requires only weeks for more typical values of wall thickness. MTBF so calculated is impractical because the indicated lives reflect weeks to months, while such is not observed in the field^(e.g., 104). Two choices exist to address the acceleration embedded in laboratory kinetics:

- the maximum theoretical rate in Figure 25b can be replaced by the kinetics typical of pipeline service, and
- MTBF can be estimated in reference to the SCC kinetics associated with the process from crack nucleation through failure, which involves the kinetics in Figures 25a and 25b and addresses directly the embedded acceleration.

The first of these options was formulated in parallel to the approach for corrosion, with the maximum theoretical rate in Figure 25b replaced by kinetics typical of pipeline service. Kinetics for this option were based on trending cracking evident in field incidents, as discussed at the Canadian NEB hearing on SCC⁽¹⁰⁴⁾. That work indicated the kinetics underlying field failures leads to similar cracking rates for both NNSCC and high pH SCC. This trending assumed steady cracking that reflects the continuous presence of cracking environment, and steady-state environmental drivers, neither of which is considered realistic. Rates so calculated indicated crack advance of ~ 0.024 inch-year⁻¹, which implies an acceleration factor the order of 100 for pre-cracked test geometries subject to the suggested standard high pH laboratory test conditions in Reference 120. Other kinetics could be used, which simply scale MTBF in direct proportion to the ratio of the rates. As these kinetics are otherwise independent of pipeline operation, there is no need to address operational parameters when dealing with MTBF for SCC determined in this fashion. However, care should be taken to ensure results developed with this measure of MTBF are consistent with the service experience for each pipeline. This approach is best implemented in reference to empirically determined kinetics based on data gathered from hydrostatic retest failures for pipelines that experience recurrent cracking. Examples of such analyses can be found in Reference 113. Once the service-based empirical kinetics are established, MTBF follows in reference to the initial defect size just as was done for corrosion.

Trends on MTBF have been evaluated by the second option in reference to the SCC kinetics shown in Figures 25a and 25b. This was done through analysis that continues from SCC nucleation and early growth through eventual failure. This analysis builds on the observation that high pH SCC is controlled by anodic dissolution, as characterized by Faraday's second law, which indicates the penetration rate due to this mechanism is proportional to the local peak current density, i_0 . Where the cracking environment remains fixed, the value of i_0 remains constant. Such penetration requires fresh (unfilmed) surface otherwise penetration ceases as the surface passivates. *The surface or crack-tip strain and strain-rate are critical parameters determining the time interval over which the conditions for dissolution at the Faradaic rate are satisfied.* It is for this reason that the kinetics in Figure 25a show thresholds at low strain rates, whereas the threshold above reflects cracking faster than driven by dissolution. It is also for this reason that the kinetics in Figure 25b show a threshold at low values of K, and thereafter a constant rate above that threshold. On this basis, still higher rates and a return to K dependent cracking are expected at still higher K levels, as is observed for line pipe steels⁽¹³⁴⁾. It follows that the kinetics in Figure 25a could be used to predict the range of rates evident in Figure 25b, whether they occur in a pre-cracked laboratory test or pipeline, which has been done as follows.

Fundamental models evolved to relate "free-surface" enhanced microplastic strain⁽¹¹⁵⁾ and strain rate to the nominally elastic deformation that occurs in smooth laboratory test specimens, or on the surface of a pipeline. These models were developed first for smooth laboratory SSRT⁽¹³⁵⁾ and TTT⁽¹²¹⁾ specimens, whose blind validation led to its adaptation for pipeline applications^(122,124). Similar models were developed to relate nominally elastic loadings to the strain and strain rate at crack tips. Again, this was done first for pre-cracked laboratory test

specimens⁽¹³⁶⁾, whose validation led to its adaptation to crack growth in pipelines^(122,124). These crack nucleation and growth models were subsequently coupled to represent the SCC process in pipelines, from nucleation through final failure, addressing such complexities as dormancy and reactivation⁽¹³⁴⁾, as well as crack coalescence⁽¹³⁷⁾. MTBF so derived is used later to trend the effects of pipeline operation on SCC, as opposed to presenting absolute life – as this aspect is obtained from the first of the above-two options.

Presentation Format

Presentation format is driven by several factors, which include the range of defect sizes and shapes to be addressed and the nature of the kinetics evident in Figures 22, 23b, and 25b. The presentation format for MTBF must illustrate the role of these, subject to the design and operating parameters typical of vintage pipelines. Because MTBF depends on crack or defect size and shape as a function of pipe design and operating parameters, the presentation format reflects crack or defect size and shape. For the present, the crack or defect length is presented on the y-axis, normalized by the diameter of the pipeline with a view to facilitate comparison between results for different pipeline designs. The crack or defect depth is presented on the x-axis, normalized by the wall thickness of the pipeline, again with a view to facilitate comparison between results for different pipeline designs. Crack or defect shape is thus a consequence of selecting a value of length and depth from the y-axis and x-axis, respectively. As pipeline operation can affect significantly different values of MTBF, it is necessary to create results as a function on pipeline operation. As the kinetics and thresholds differ for fatigue, SCC, and corrosion, results must be developed for each degradation mechanism, for each pipeline design and operating condition. It follows that this report could embody a wide range of plots, each representing a specific degradation mechanism, operating condition, and pipeline design. As operation can differ significantly from pipeline to pipeline, there potentially are an endless number of plots characterizing MTBF for each of fatigue, SCC, and corrosion as a function of pipeline design and operating conditions. As noted much earlier, this scenario has been addressed herein by evaluating the vintage pipeline system as typified by the three pipeline designs in Table 3, subject to the property combinations in Table 4.

Calculated Crack-Growth Intervals and Trends

Results generated in reference to the kinetics shown in Figures 22, 23b, and 25b are presented as contours of MTBF as a function of the defect size and the shape in Figures 28, 29, and 30 for degradation at axial cracks or defects due respectively to corrosion, fatigue, and SCC for kinetics representing typical field kinetics. Corresponding results for circumferential cracks are presented in Figure 31. Finally, results also have been developed to trend SCC response as a function of operating pressure and temperature history, and life as a function of probability of failure in reference to specific temperature histories, so these results are presented in related formats. Likewise, results have been developed to trend fatigue response as a function of the pressure cycle. These results are presented in Figures 32 and 33 for SCC and Figure 34 for fatigue.

Subparts are included for each figure to address the vintage pipeline system in reference to the pipeline geometries presented in Table 3, for the combinations of pipeline design and line-pipe

steel properties presented in Table 4, for pipeline operation at MAOP = 72-percent of SMYS. On this basis, subparts a, b, and c for each figure consider the 24-inch, 12-inch, and 4-inch diameter pipeline designs. Letter-numbered subparts (i.e., i, ii, iii) to each of these figures address each of Gr B, X42, and X52 for toughness represented by a CVN FSE-USE equal to 15 ft-lbs. A fourth letter-numbered subpart (i.e., iv) presents results for FSE-USE at 30 ft-lb for the X52 design.

The results in the figures can be applied directly for the specific parameters considered in that figure, or be used to illustrate the effects of parameters such as operation or design by comparing or contrasting the results between each figure. As noted previously, such results reflect the critical crack sizes discussed previously in reference to Figures 20 and 21.

Axial Defects

Figure 28 presents contours of MTBF for pipelines suffering corrosion in operation at 72-percent of SMYS. Consistent with the above discussion, part (a) of this figure represents the 24-inch diameter design in Table 3, while parts (b) and (c), respectively represent the 12-inch and the 4-inch diameter designs. Part (i) of each lettered subpart reflects GrB for which SMYS is 35 ksi with a corresponding wall thickness, while parts (ii) and (iii) correspond respectively to X42 and X52, for which SMYS is 42 ksi and 52 ksi, respectively. Consequently, Figure 28(a)(i) presents results for the 24-inch diameter Gr B design in Table 3 whereas Figures 28(b)(i) and 28(c)(i) respectively present results for the 12-inch diameter Gr B design and the 4-inch diameter Gr B design in Table 3, for which the wall thicknesses reflect operation at 750 psig. Likewise, Figure 28(a)(ii) presents results for the 24-inch diameter X42 design in Table 3 whereas Figures 28(b)(ii) and 28(c)(ii) respectively present results for the 12-inch diameter and the 4-inch diameter X42 designs in Table 3, where again the wall thicknesses reflect operation at 750 psig. Finally, Figure 28(a)(iii), 28(b)(iii), and 28(c)(iii) respectively present results for the 24-inch, 12-inch, and 4-inch diameter designs in Table 3 for X52, for which the wall thicknesses again reflect operation at 750 psig. For each of these scenarios, results for the same design except that the FSE-USE is 30 ft-lb are presented in part (iv) for each of Figure 28a, 28b, and 28c.

A similar numbering scheme is used in Figure 29, which presents contours of MTBF for pipelines operating with pressure cycling that can lead to fatigue crack initiation, growth, and possible failure. Likewise, a similar scheme is used for Figure 30, which addresses degradation due to SCC. As for Figure 28, these results represent operation at MAOP of 72-percent of SMYS. For all cases involving fatigue pressure cycling the minimum pressure is taken as 70-percent of MAOP, which for operation at 72-percent of SMYS is close to the worst-case maximum pressure cycle, namely $R = 0.7$. In accordance with earlier discussion, the kinetics for the SCC results in Figure 30 reflect typical high pH field cracking considered to represent typical operation with pressure cycling the order of 7.2-percent of SMYS at a temperature of ~ 125 °F, for which cracking is taken to occur at a rate of 0.024 inch-year⁻¹.

Cracking is taken to be external as is typical of pipelines. If internal cracking is a concern, the corresponding MTBF will be reduced because the pressure acting on the crack faces shortens the life somewhat in comparison to external cracking. Calculations indicate internal cracking rates are on a worst-case basis for typical pipeline scenarios the order of 3 times faster than those for cracking independent of the effects of pressure.

The results in Figure 28ai indicate the MTBF for corrosion occurring at a quite conservative rate of 0.009 inch per year at defects with depth 20-percent of the wall thickness (minimum depth requiring maintenance based on ASME B31G⁽⁵⁸⁾) is more than 10 years at defects 24 inches long (length = diameter). Shorter-length corrosion leads to lives the order of 20 years. In spite of this conservative corrosion rate, even deep defects have a MTBF the order of years. In all cases the tolerance for corrosion reflects the heavy wall thickness for this Gr B design. Of course, corrosion at lower rates more typical of service conditions would lead to proportionally longer lives. In all cases evaluated the failures occur as ruptures.

Comparing the results in the corresponding subparts of Figures 28a, 28b, and 28c shows that designs in higher strength grades lead to proportionally smaller MTBF, which reflects the decreased wall thickness needed as the grade increases. In all cases evaluated the failures occur as ruptures. Thus, the economic benefits that accrue in some applications associated with the use of a stronger grade lead to a diminished tolerance for corrosion. Comparing these figures also indicates that thinner-walled smaller-diameter designs have much shorter MTBF as compared to the heavier wall designs that result for larger-diameter pipelines, all else being equal. This reflects the fact that a thinner wall is required to achieve the same stress level relative to SMYS in designs that involve the same maximum pressure, which in these cases is 750 psig. Comparing results in subparts (iii) with those in subparts (iv), which reflect respectively 15 and 30 ft-lb FSE-USE, indicate no difference in corrosion response, which is anticipated in that corrosion failure occurs via plastic collapse, which leads to failure boundaries that in Figure 20 are independent of toughness.

The results in Figure 28 indicate that re-inspection intervals for corrosion targeted at the order of seven to ten years appear to be viable. It is apparent in comparing the many parts of Figure 28 that where plastic-collapse controls failure the MTBF does follow simple consistent pattern as a function of grade and wall thickness. The many parts of Figure 28 indicate this occurs for all nine vintage pipeline designs outlined in Table 3. This simple consistency reflects the corresponding simple consistent pattern evident in the failure boundaries presented earlier in Figure 20.

Comparing the results in Figure 29 with the corresponding subparts of Figure 28 indicate that similar trends develop in reference to the role of diameter and wall thickness for fatigue as were evident for corrosion. Where this similarity develops for fatigue it does so because diameter and wall thickness had a comparable influence on critical crack size derived from the failure boundaries in Figure 21. While similar in reference to the effects of diameter and wall thickness, the trends for fatigue differ from corrosion in two essential ways. First, MTBF for fatigue is expressed in reference to cycles, while it is expressed in terms of years for corrosion, which reflects the dependence on fatigue life on the nature of the cycling (frequency and magnitude), while corrosion is independent of these parameters. This shift from MTBF in years to cycles leads to values of MTBF that now lie between the threshold for fatigue, which is approached by trends for MTBF at a very high number of cycles to failure, and the critical crack size, which is approached by trends for MTBF at a very low life. Second, while the corrosion results were independent of toughness because failure was controlled by plastic collapse, there are scenarios where fatigue failure is or can be controlled by fracture toughness. This is evident in comparing the results in subparts (iii) with those in subparts (iv), which reflect respectively 15 and 30 ft-lb FSE-USE, wherein higher toughness leads to longer MTBF, all else being equal. That is, pipelines made of tougher line-pipe steel will show larger critical sizes and longer MTBF. In

cases where MTBF shows an influence of toughness, the fatigue life was controlled by fracture mechanics. Recall that where toughness controls the critical crack size the failure boundaries in Figure 21 lost the consistent simple pattern evident clearly in Figure 20 for plastic collapse. In spite of this added complexity, trends in MTBF show reasonable consistency across the nine vintage pipeline designs.

The present results indicate that re-inspection intervals involving fatigue will depend on the pipelines operating pressure history. For the high-stress ratio infrequent cycling that is typical of most gas-transmission pipeline service fatigue is an unlikely cause of failure, such that fatigue is not a viable threat for such gas-transmission pipelines. However, where the stress ratio falls below about 0.7 fatigue does become a concern. Re-inspection intervals for such pipelines should be evaluated as a function of the current condition of the pipeline and its operating pressure history.

Consider now the results for SCC in Figure 30. Comparing the results in Figure 30 with the corresponding subparts of Figures 28 and 29 indicates SCC shows many of the same tendencies evident for fatigue. For several of the vintage pipeline designs the results for SCC show a similar role of diameter and wall thickness as was apparent for both corrosion and for fatigue. This is particularly true for the 24-inch and 12-inch diameter cases, and marginally so for the 4-inch diameter results. However, because the larger threshold stress intensity for SCC as compared to fatigue triggered propagation at much larger initial crack sizes, and cases where the critical sizes were fracture controlled, a rather small increment of wall remains for some designs. This coupled with the much higher kinetics for SCC means that the MTBF can be quite short, or occur over rather small wall segments. Slightly different design parameters could promote such response for smaller diameter designs, whereas the nature of the failure boundaries for the larger diameter pipelines makes them less prone to such behavior.

As for fatigue, diameter and wall thickness have an influence on the critical crack size that parallels that for fatigue cracking, which in turn determines when failure as either a leak (through-wall penetration) or rupture (critical length) occurs. As for fatigue, the trends for SCC differ from corrosion in two essential ways. First, like fatigue MTBF can be expressed in reference to the number of cycles to failure multiplied by the period of the cycle to compute MTBF in units of time, while corrosion is otherwise independent of cycling. (SCC can in some ways be viewed as a time at stress phenomenon) As will be shown later in reference to Figure 33, SCC does depend on the nature of the cycling (frequency and magnitude), while corrosion is independent of these parameters. Second, as for fatigue, failure can be controlled by fracture mechanics for which toughness controls the critical crack size, while for corrosion the results were independent of toughness because failure was controlled by plastic collapse. Thus, as for fatigue, comparing the results in subparts (iii) with those in subparts (iv), which reflect respectively 15 and 30 ft-lb FSE-USE, show higher toughness leads to longer MTBF, all else being equal. That is, pipelines made of tougher line-pipe steel will show larger critical sizes and longer MTBF for SCC.

Comparing the kinetics for SCC typical of field observations indicates rates slightly faster than those for corrosion. As such, values of MTBF for SCC kinetics are comparable to that observed for corrosion, as evident in comparing Figure 28 with Figure 30. The exception to this is due to scenarios driven by the significantly different thresholds for fatigue and SCC, coupled with differences in critical crack size. As for fatigue, the present results indicate that re-inspection intervals involving high pH SCC depend on the pipelines current condition, past experience with

SCC, the pipelines RoW, and its operating pressure history in reference to pressure as it affects temperature and pressure cycles. For Class 1 Locations, the wall stress at MAOP is above typical high pH SCC thresholds such that this threat should be evaluated, whereas where the pressure or RoW-induced stresses are well below apparent thresholds this threat is diminished.

Contrasting Faradaic SCC kinetics with SCC for kinetics typical of field observations indicates the values of MTBF at Faradaic rates will be orders of magnitude shorter than evident when typical field kinetics are used. Because the Faradaic rate of cracking is so high, much less time is predicted between the onset of SCC and the time taken to grow the crack to a critical size if this rate is considered to be continuously active. Thus, use of the Faradaic rate would lead to tightly compressed trends for MTBF and quite short periods for stable crack growth.

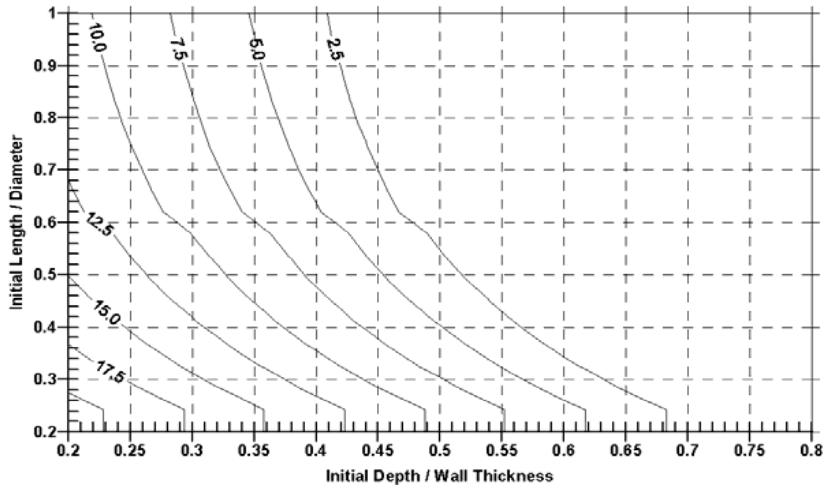
While acceleration of test time in the laboratory is useful and essential to evaluate factors controlling SCC, care must be used where such data are considered to guide integrity management decisions. RoW and operational factors have a first-order effect on SCC kinetics and must be addressed when making integrity management decisions. Consideration of threshold crack sizes for current or developing ILI crack tools coupled with growth rates typical of Faradaic kinetics suggests that once SCC begins it would be difficult to control unless the conditions that drive cracking are changed as compared to laboratory conditions. Such occurs in reality, as field cracking does not occur continuously at the rate seen under accelerated laboratory conditions, because the mechanical loading in the field and the environment do not support continuous cracking.

Control of SCC kinetics for high pH SCC can be achieved in practice by reducing the wall stress below the threshold, or by altering the cracking environment in reference to temperature of potential. It also can be accomplished by hydrotesting, with the added benefit that the increased wall stress serves to blunt cracks, or exhaust available microplasticity that underlies SCC nucleation. Where growth rates are high, ILI will have diminished value, while hydrotesting remains effective with the just-noted benefit of blunting deeper cracks and diminishing the microplastic strain essential for SCC nucleation.

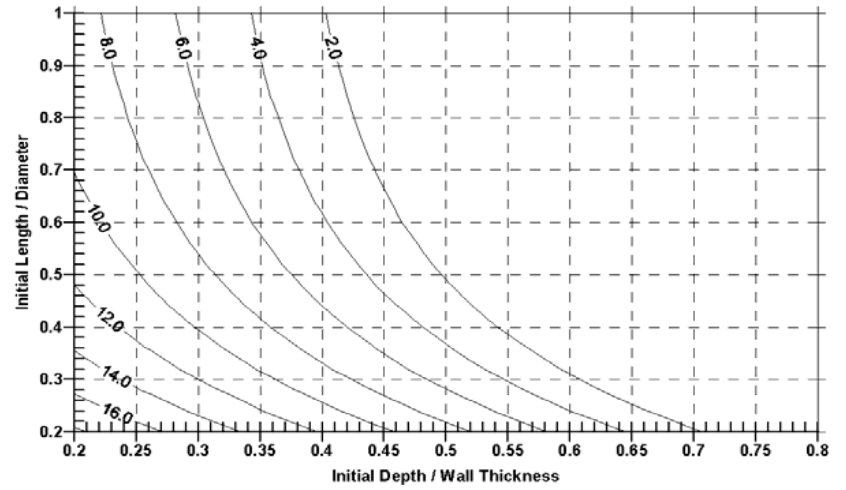
Circumferential Defects

Figure 31 presents results for circumferential cracking driven by the axial stresses developed in a soil-anchored pipeline due to the Poisson-induced tensile stress developed under the same worst-case pressure cycling considered for axial defects, which used a maximum pressure corresponding to 72-percent of SMYS and $R_\sigma = 0.7$. The presentation format is the same as that used for axial defects. As with the axial defects, the same pipe geometries considered typical of vintage pipelines have been evaluated over the same range of line-pipe property combinations.

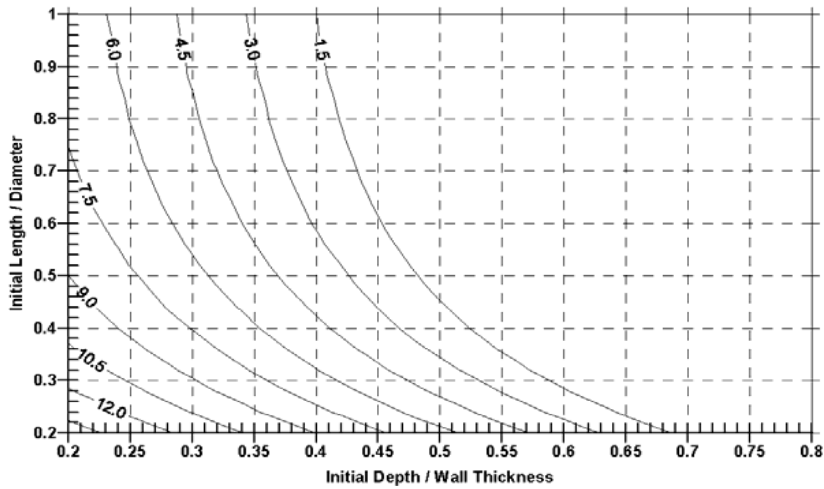
As is evident from Figure 31, quite large PTW circumferential cracks can be tolerated without failure for quite large numbers of cycles, indicating fatigue growth is unlikely a problem for circumferential defects under such circumstances. As such, where circumferential cracks exist, due for example to the presence of vintage girth-welds or SCC activated by axial loading, pressure cycling can cause crack growth but only to a limited extent unless other externally applied axial loads are present.



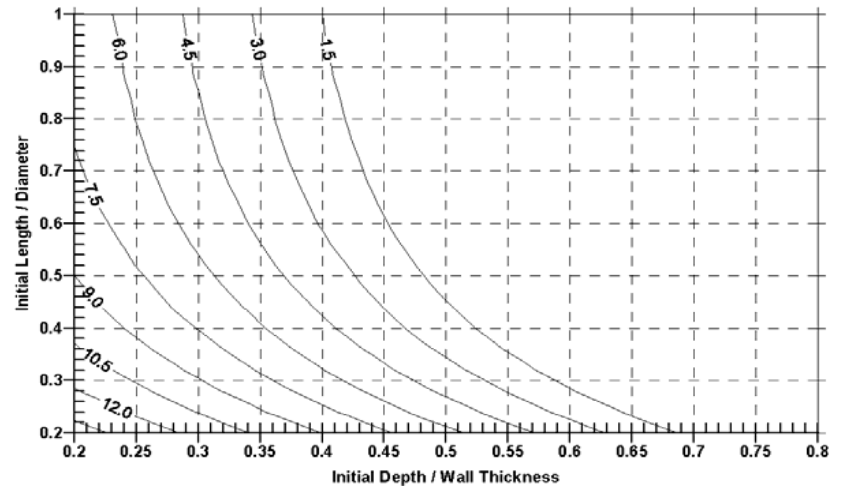
i) Gr B, Charpy Full-Size Toughness = 15 ft-lbs



ii) X42, Charpy Full-Size Toughness = 15 ft-lbs



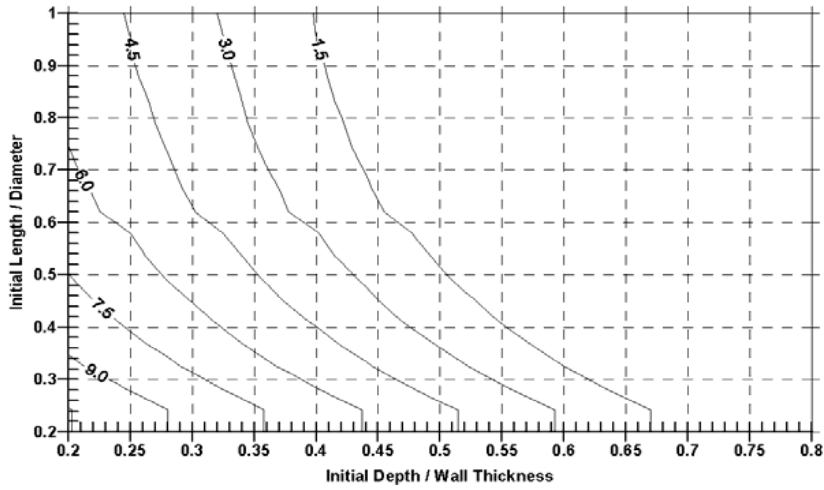
iii) X52, Charpy Full-Size Toughness = 15 ft-lbs



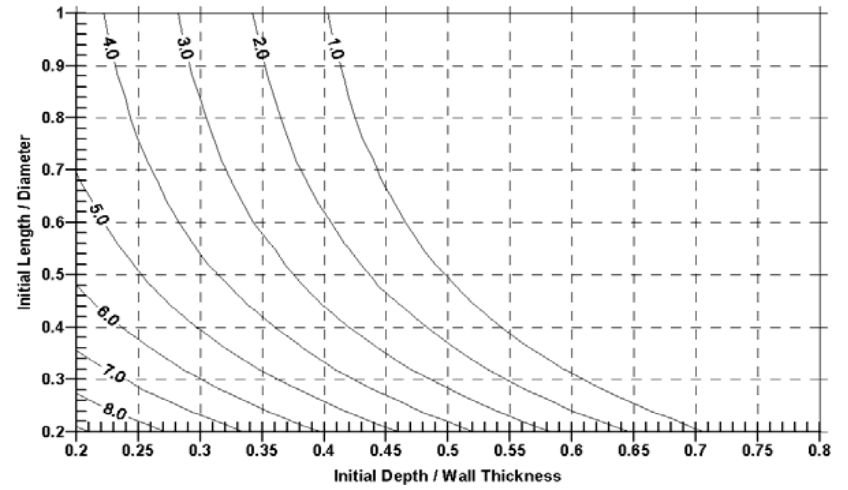
iv) X52, Charpy Full-Size Toughness = 30 ft-lb

a) 24-inch diameter design

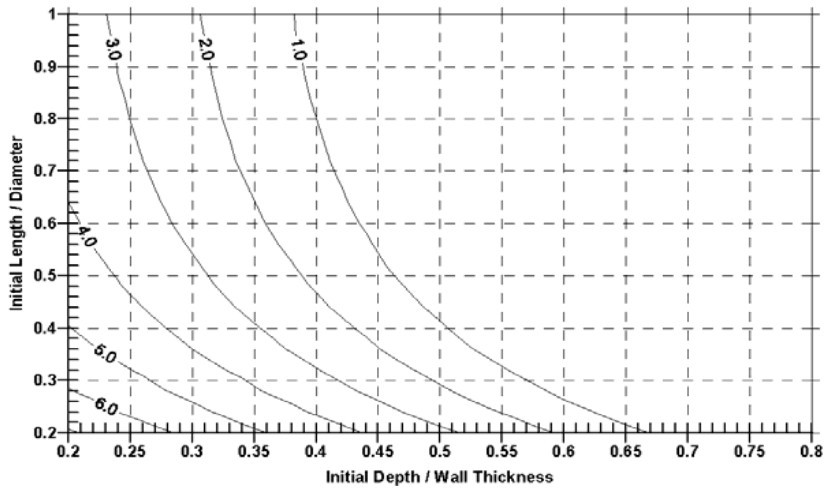
Figure 28. MTBF in years for axial corrosion(continued)



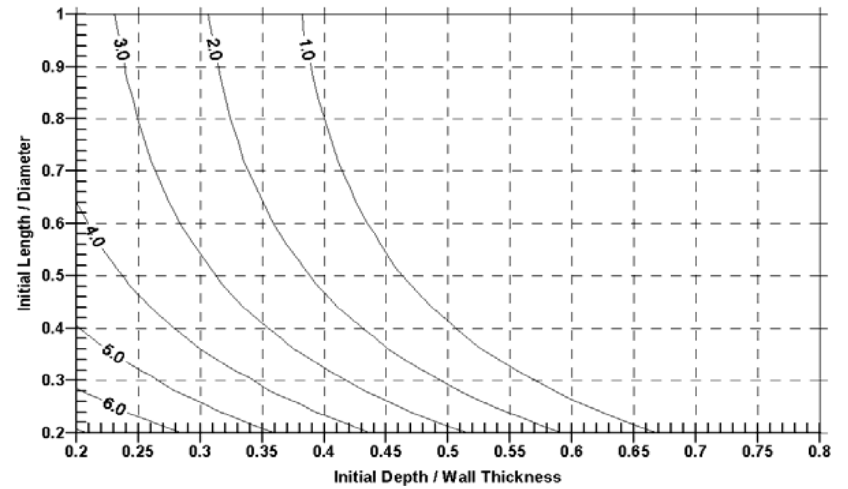
i) Gr B, Charpy Full-Size Toughness = 15 ft-lbs



ii) X42, Charpy Full-Size Toughness = 15 ft-lbs



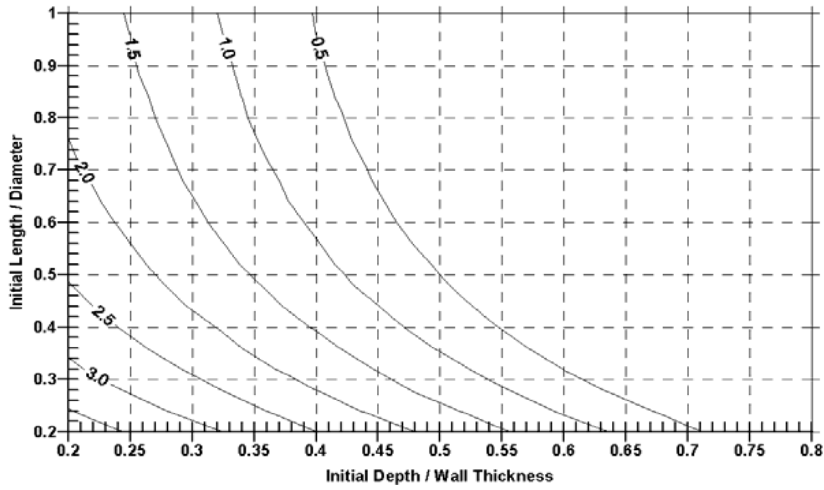
iii) X52, Charpy Full-Size Toughness = 15 ft-lbs



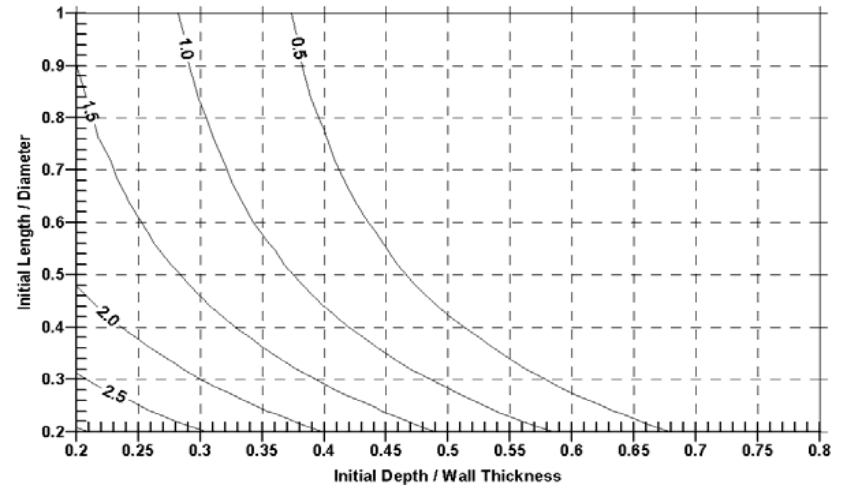
iv) X52, Charpy Full-Size Toughness = 30 ft-lb

b) 12-inch diameter design

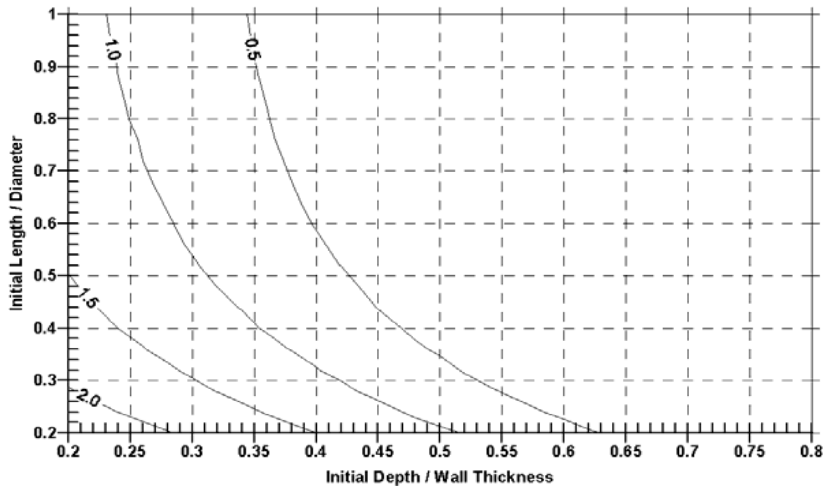
Figure 28. MTBF in years for axial corrosion (continued)



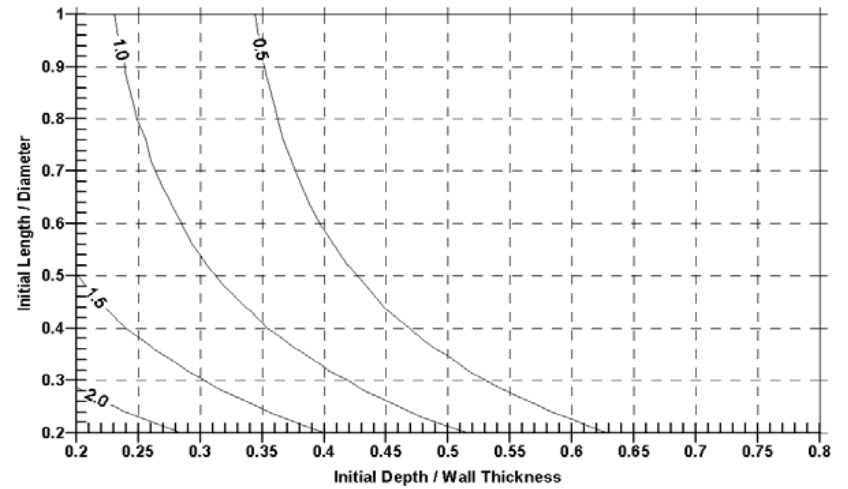
i) Gr B, Charpy Full-Size Toughness = 15 ft-lbs



ii) X42, Charpy Full-Size Toughness = 15 ft-lbs



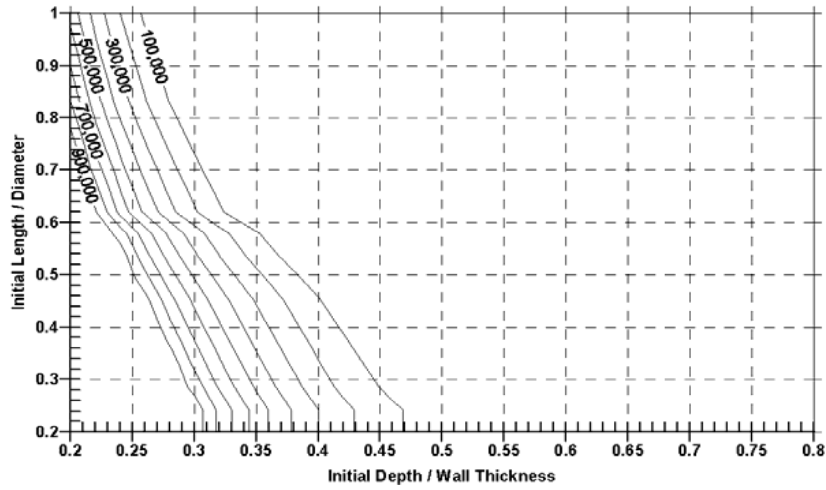
iii) X52, Charpy Full-Size Toughness = 15 ft-lbs



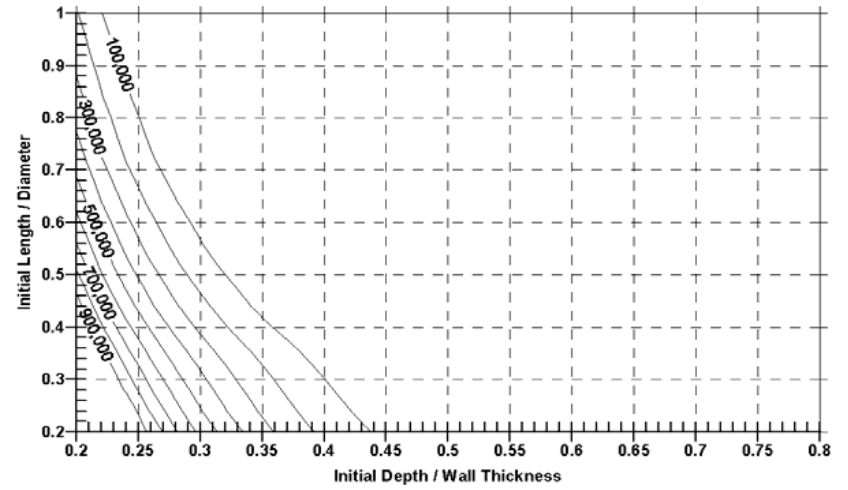
iv) X52, Charpy Full-Size Toughness = 30 ft-lb

c) 4-inch diameter design

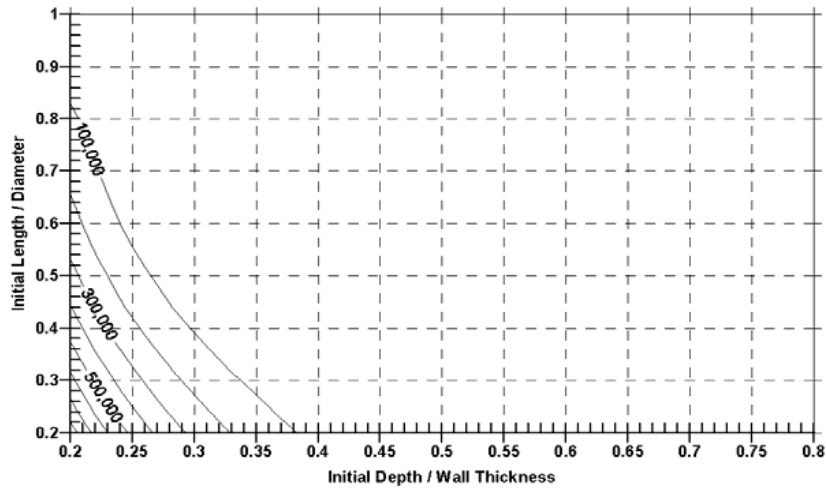
Figure 28. MTBF in years for axial corrosion (concluded)



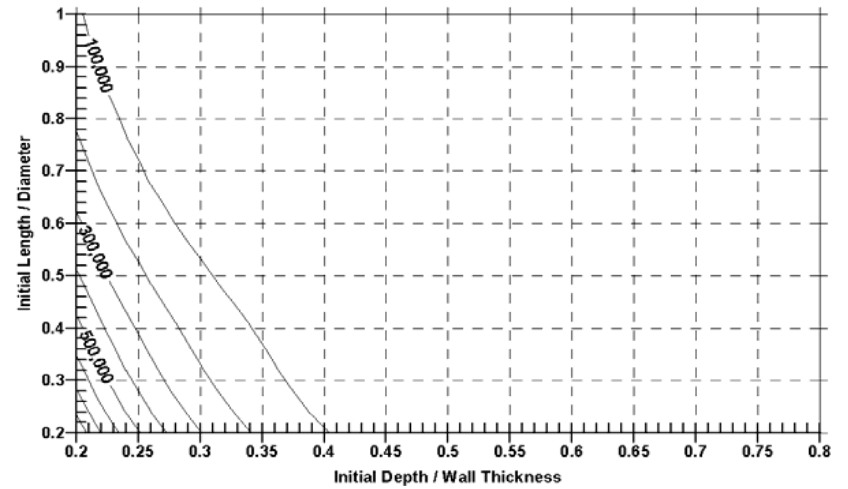
i) Gr B, Charpy Full-Size Toughness = 15 ft-lbs



ii) X42, Charpy Full-Size Toughness = 15 ft-lbs



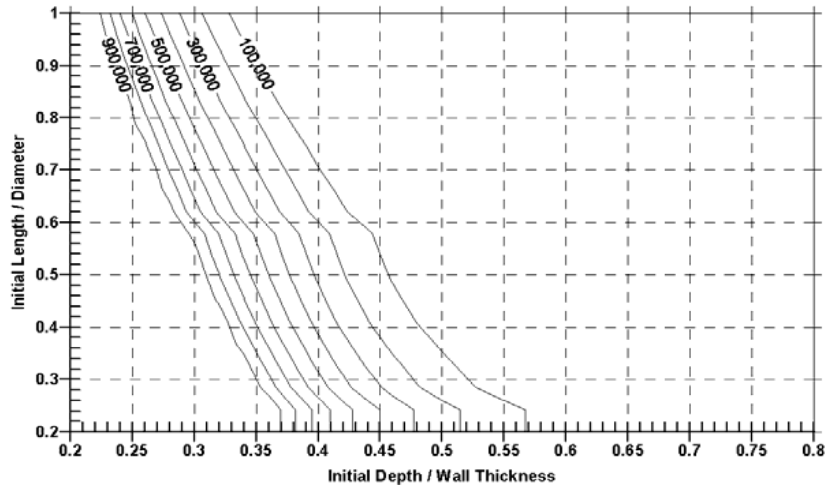
iii) X52, Charpy Full-Size Toughness = 15 ft-lbs



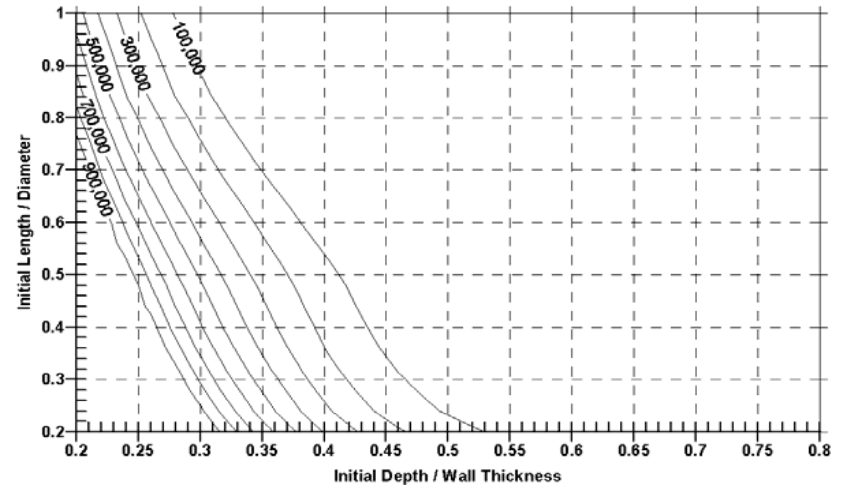
iv) X52, Charpy Full-Size Toughness = 30 ft-lb

a) 24-inch diameter design

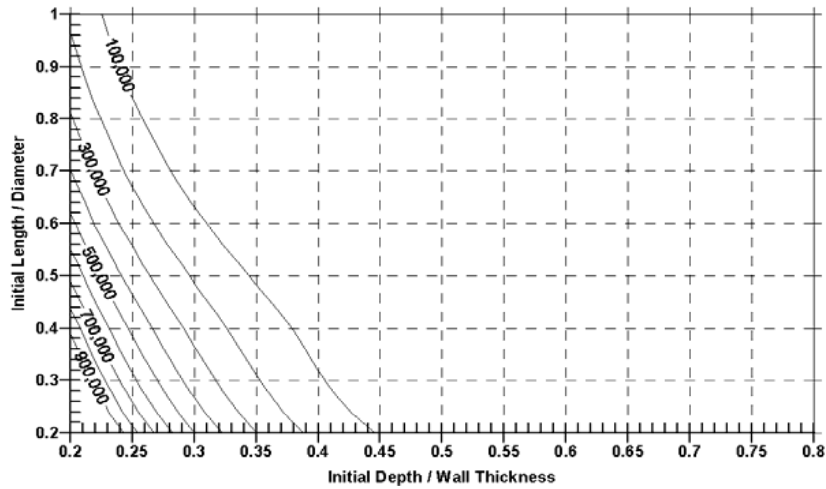
Figure 29. MTBF in cycles for axial fatigue cracking (continued)



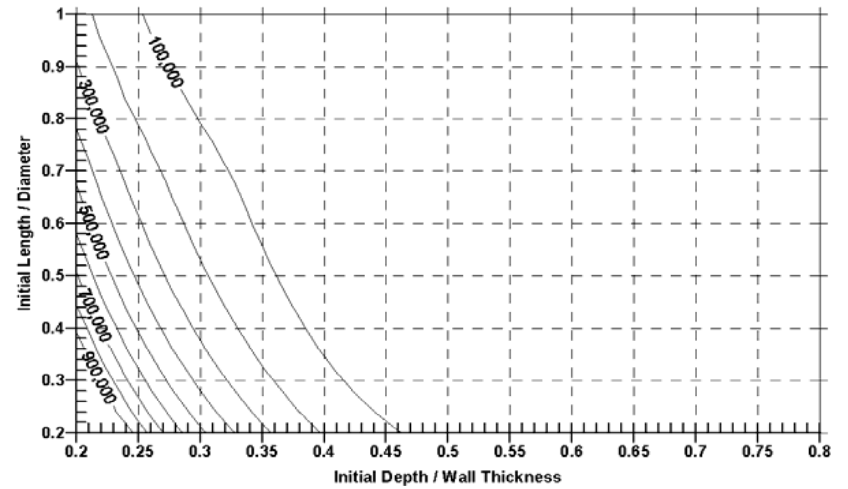
i) Gr B, Charpy Full-Size Toughness = 15 ft-lbs



ii) X42, Charpy Full-Size Toughness = 15 ft-lbs



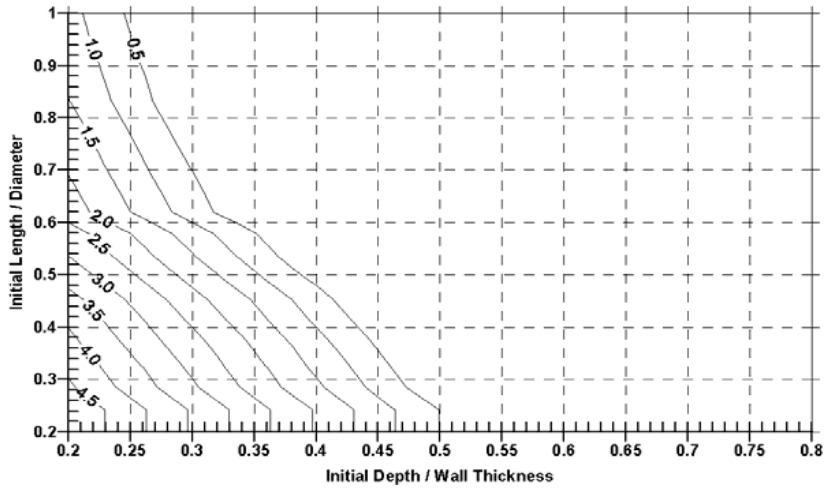
iii) X52, Charpy Full-Size Toughness = 15 ft-lbs



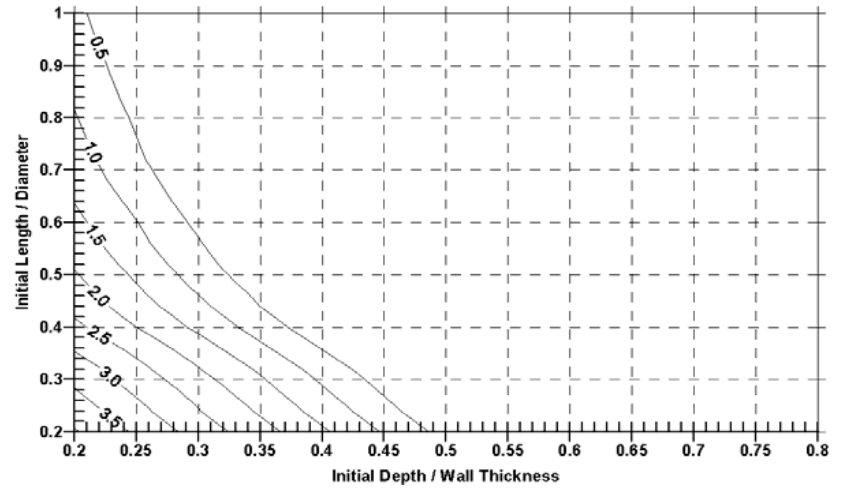
iv) X52, Charpy Full-Size Toughness = 30 ft-lb

b) 12-inch diameter design

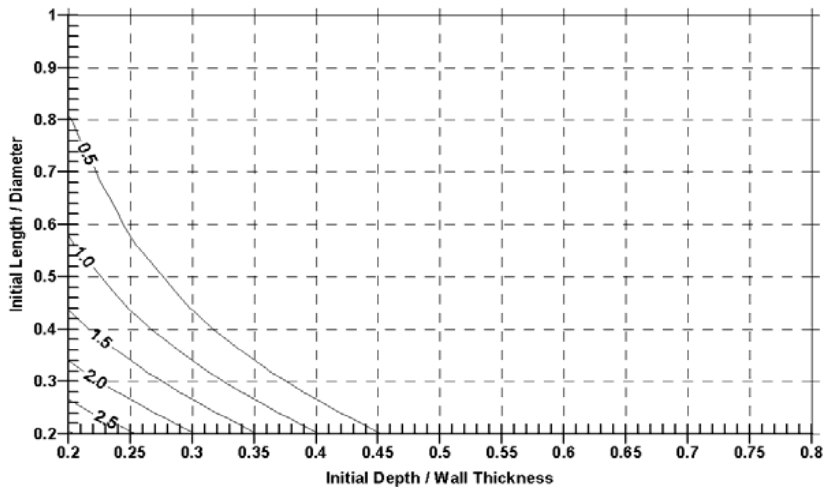
Figure 29. MTBF in cycles for axial fatigue cracking (continued)



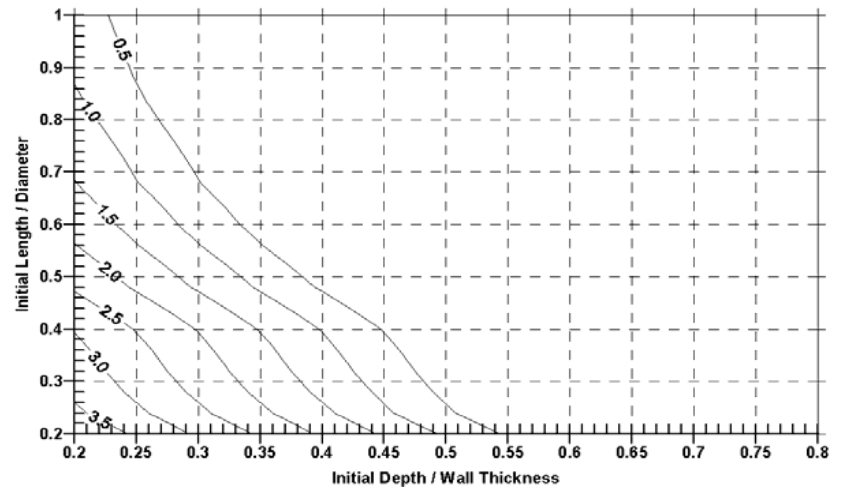
i) Gr B, Charpy Full-Size Toughness = 15 ft-lbs



ii) X42, Charpy Full-Size Toughness = 15 ft-lbs



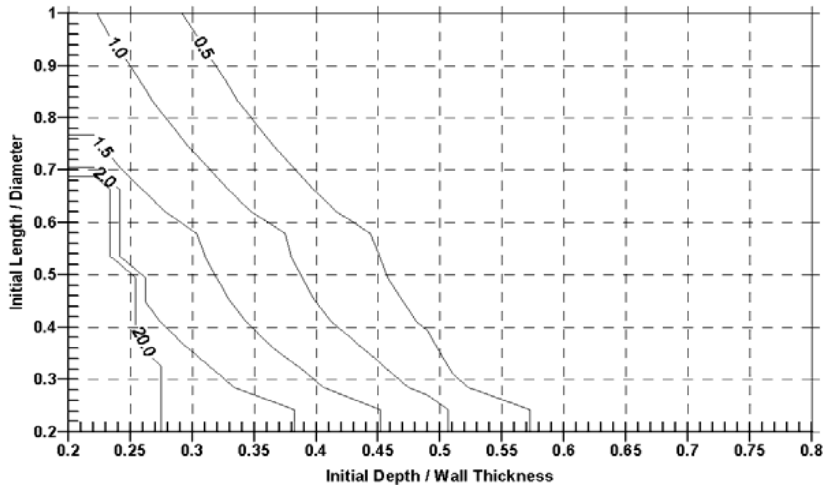
iii) X52, Charpy Full-Size Toughness = 15 ft-lbs



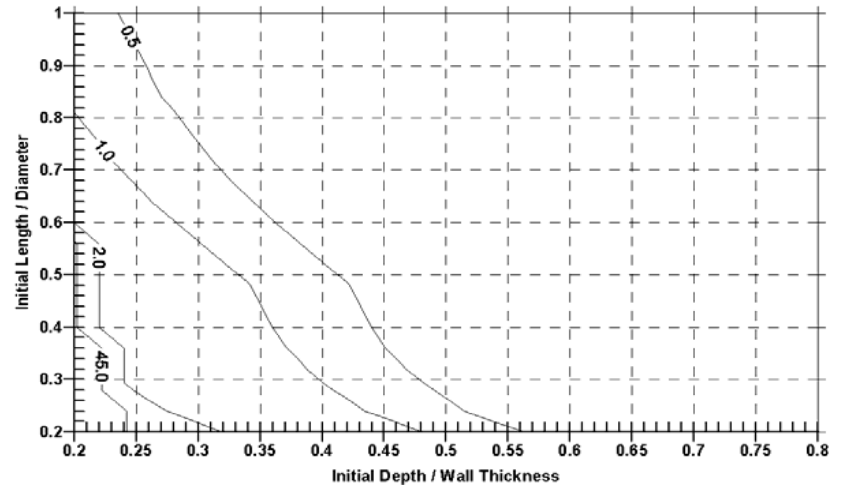
iv) X52, Charpy Full-Size Toughness = 30 ft-lb

a) 24-inch diameter design

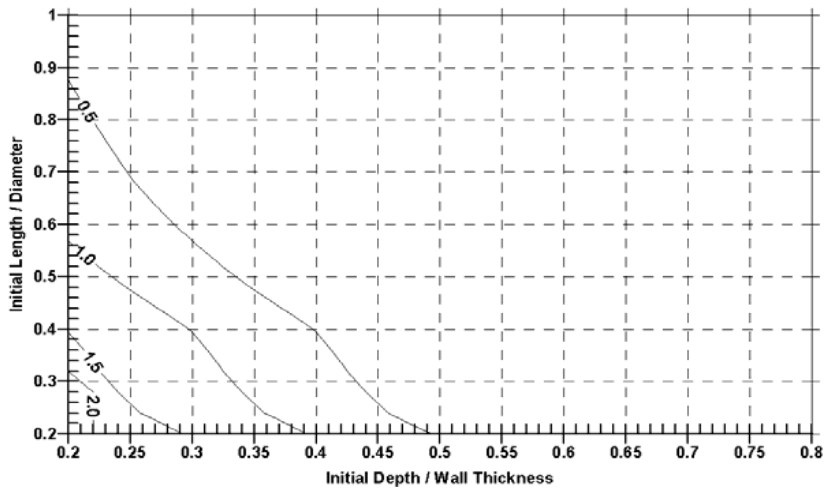
Figure 30. MTBF in years for axial cracking with typical high pH SCC kinetics (continued)



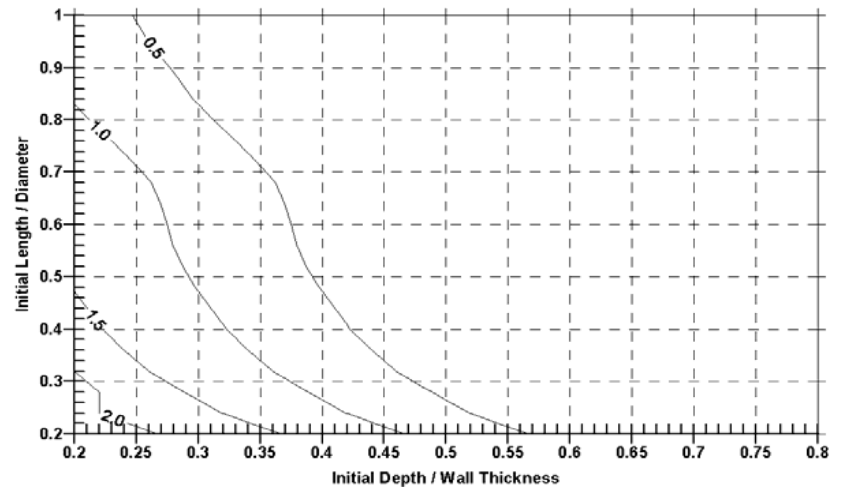
i) Gr B, Charpy Full-Size Toughness = 15 ft-lbs



ii) X42, Charpy Full-Size Toughness = 15 ft-lbs



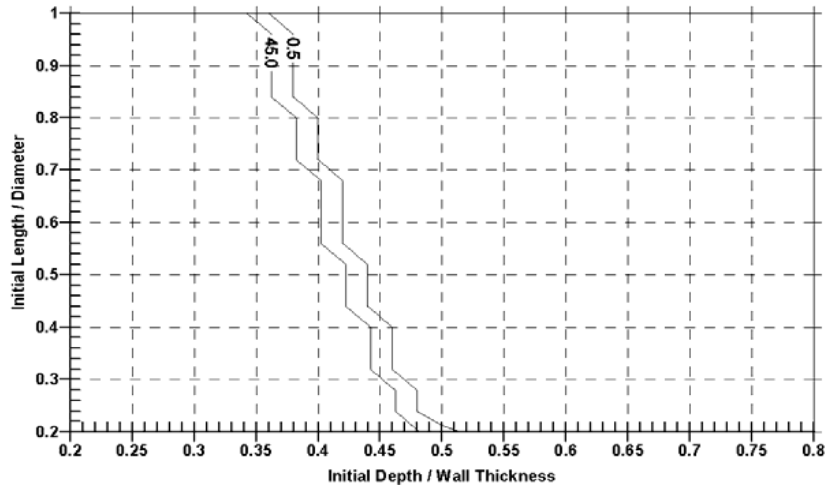
iii) X52, Charpy Full-Size Toughness = 15 ft-lbs



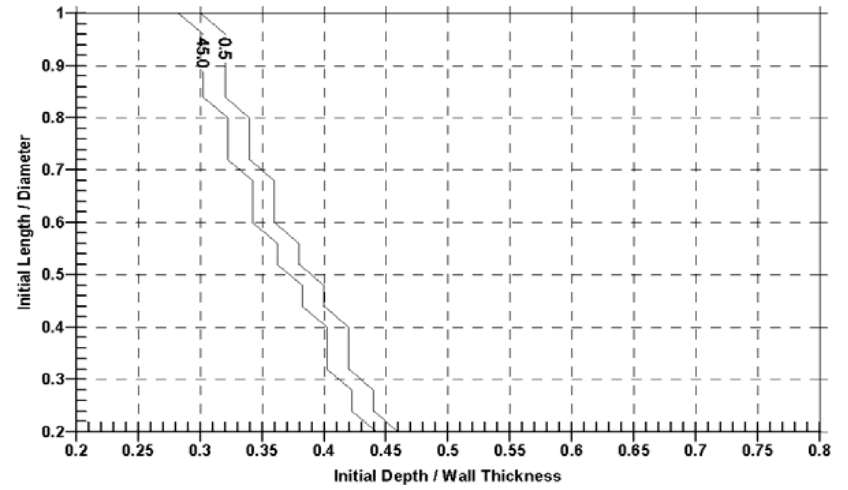
iv) X52, Charpy Full-Size Toughness = 30 ft-lb

b) 12-inch diameter design

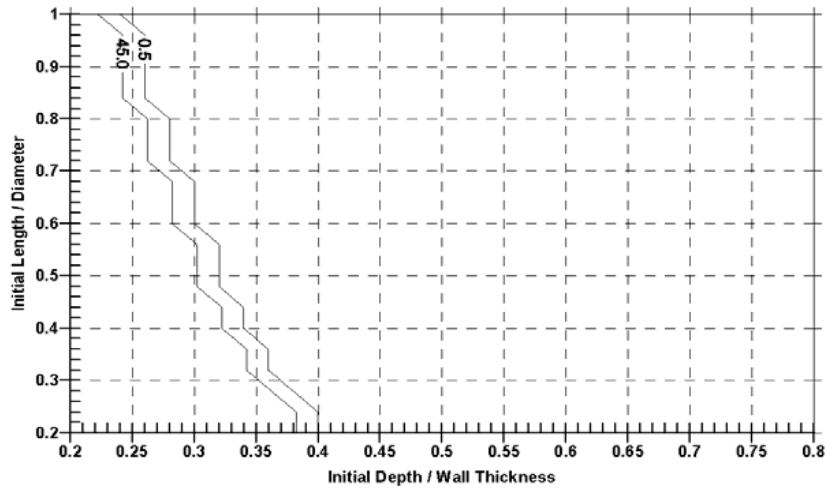
Figure 30. MTBF in years for axial cracking with typical high pH SCC kinetics (continued)



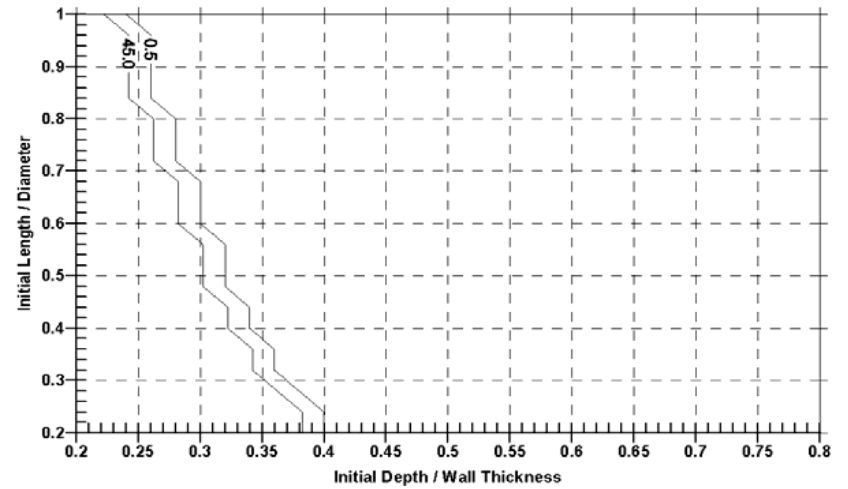
i) Gr B, Charpy Full-Size Toughness = 15 ft-lbs



ii) X42, Charpy Full-Size Toughness = 15 ft-lbs



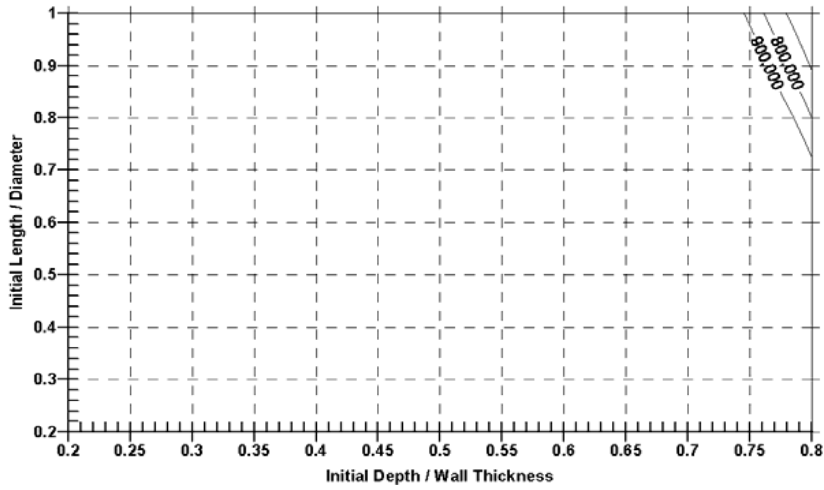
iii) X52, Charpy Full-Size Toughness = 15 ft-lbs



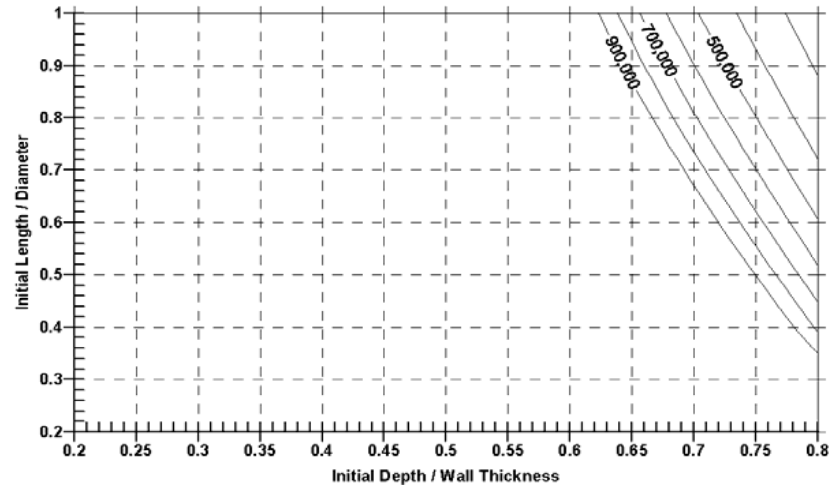
iv) X52, Charpy Full-Size Toughness = 30 ft-lb

c) 4-inch diameter design

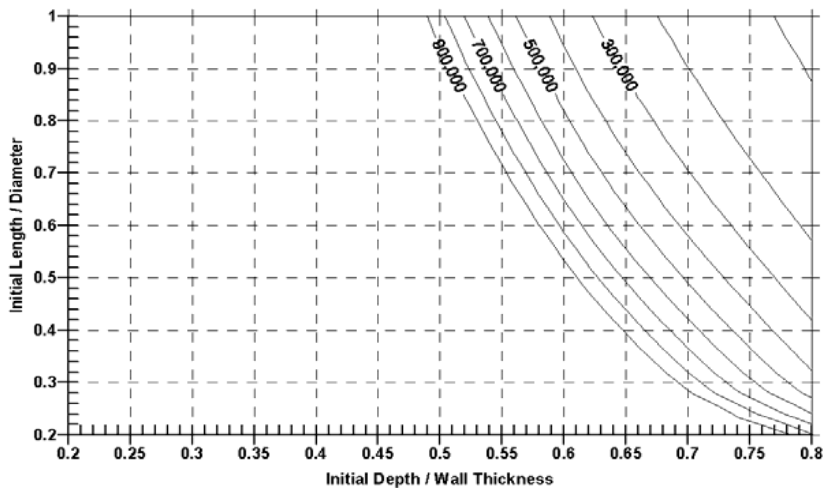
Figure 30. MTBF in years for axial cracking with typical high pH SCC kinetics (concluded)



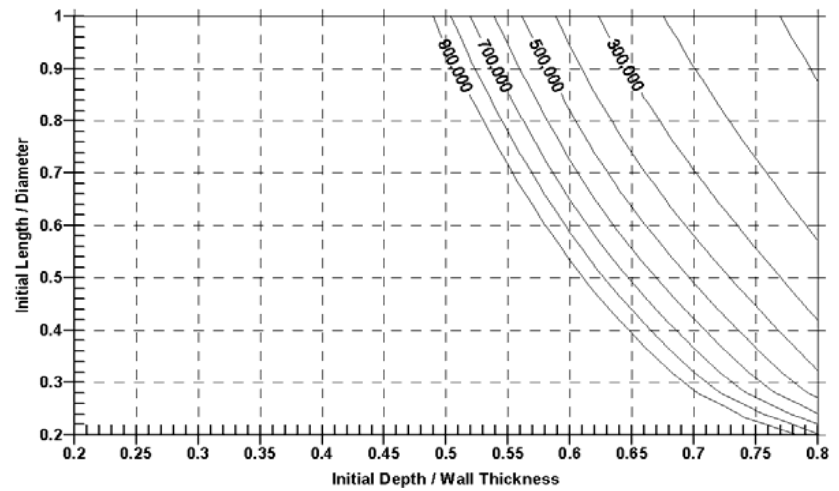
i) Gr B, Charpy Full-Size Toughness = 15 ft-lbs



ii) X42, Charpy Full-Size Toughness = 15 ft-lbs



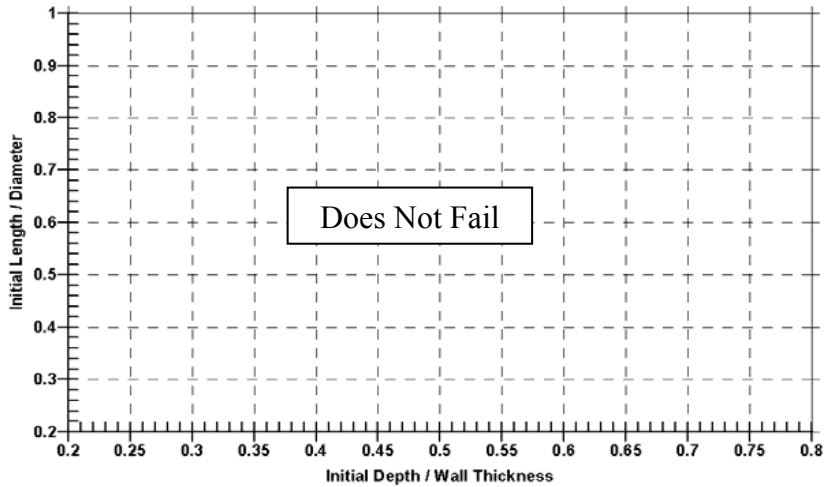
iii) X52, Charpy Full-Size Toughness = 15 ft-lbs



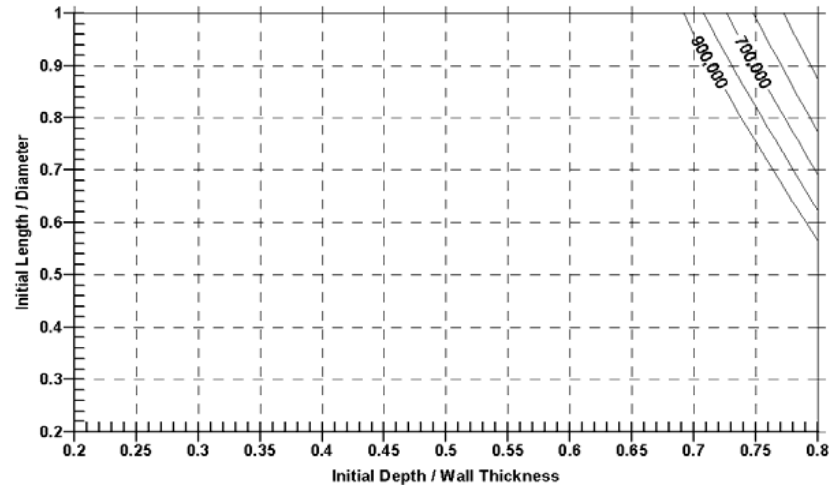
iv) X52, Charpy Full-Size Toughness = 30 ft-lb

a) 24-inch diameter design

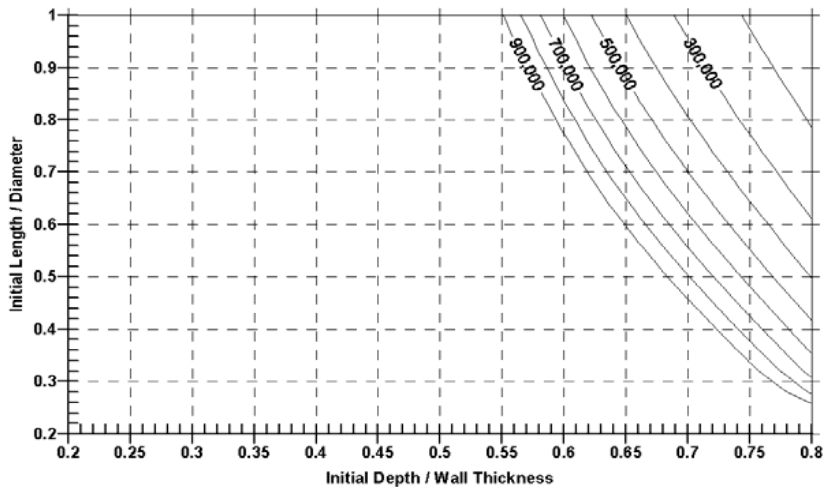
Figure 31. MTBF in cycles for circumferential cracking for Poisson-induced axial stress corresponding to pressure at 72-percent of SMYS (continued)



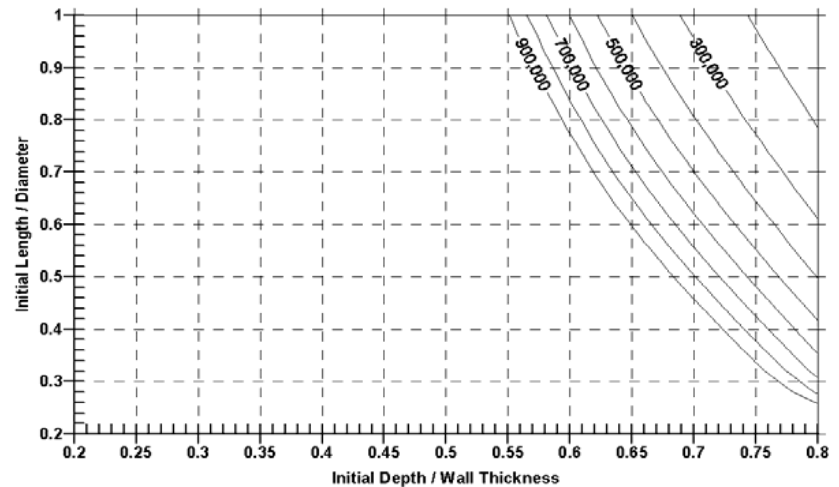
i) Gr B, Charpy Full-Size Toughness = 15 ft-lbs



ii) X42, Charpy Full-Size Toughness = 15 ft-lbs



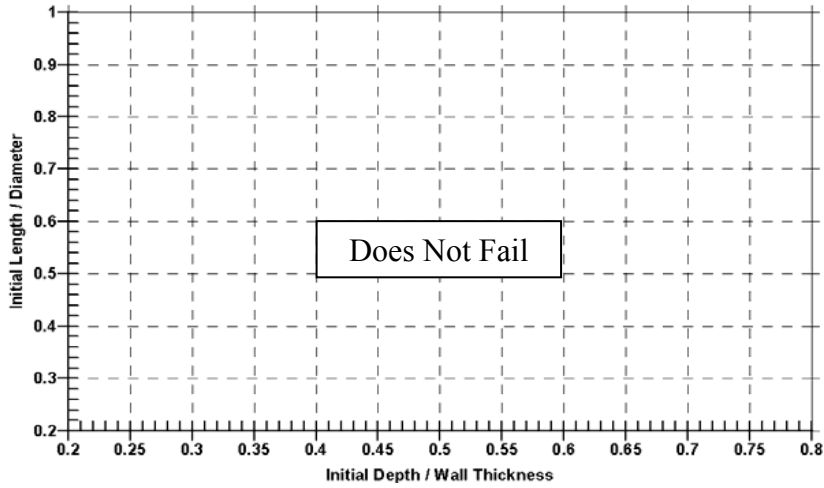
iii) X52, Charpy Full-Size Toughness = 15 ft-lbs



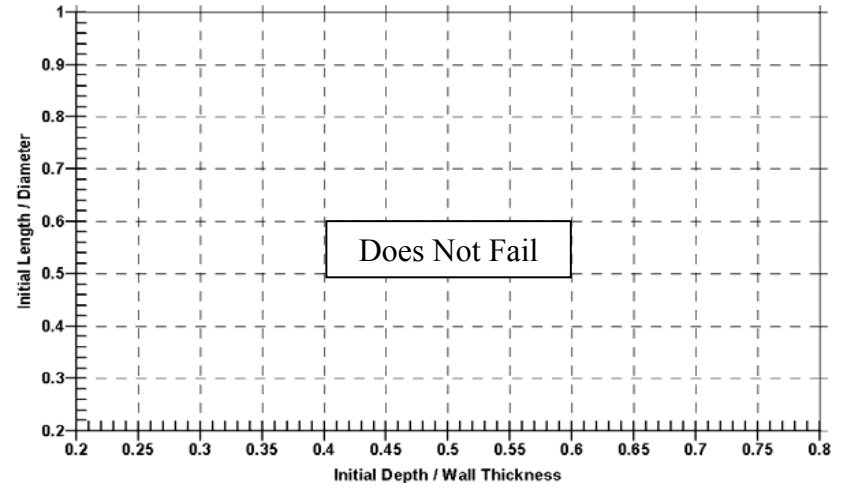
iv) X52, Charpy Full-Size Toughness = 30 ft-lb

b) 12-inch diameter design

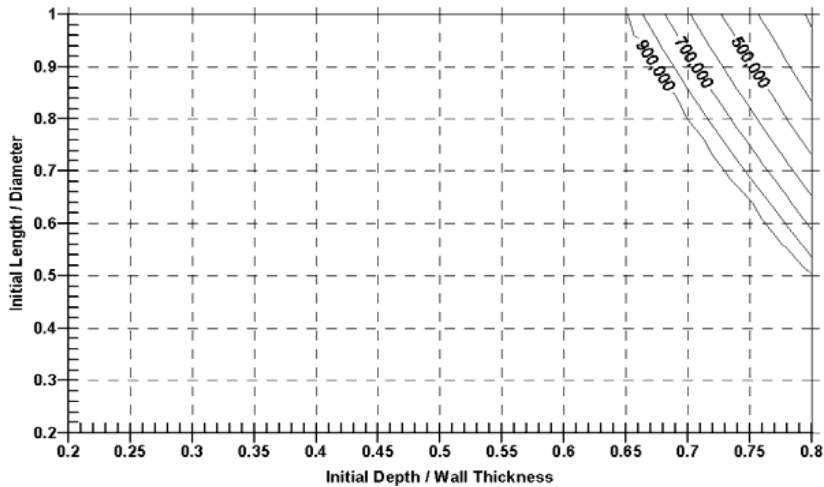
Figure 31. MTBF in cycles for circumferential cracking for Poisson-induced axial stress corresponding to pressure at 72-percent of SMYS (continued)



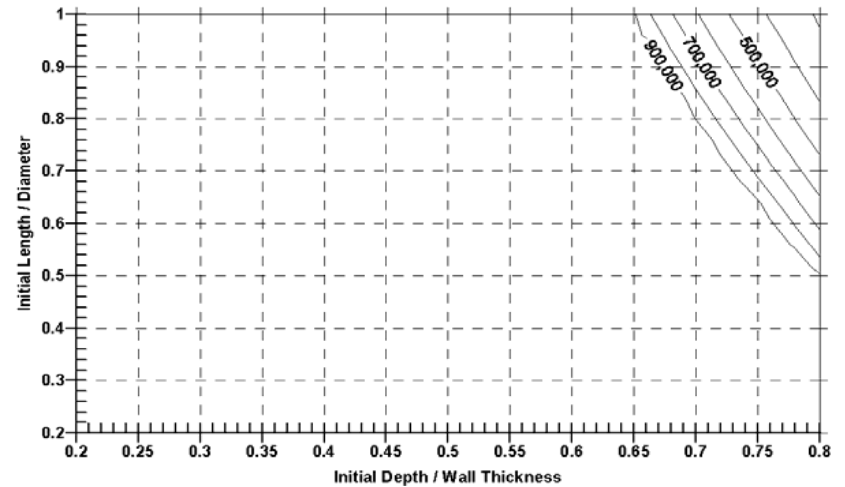
i) Gr B, Charpy Full-Size Toughness = 15 ft-lbs



ii) X42, Charpy Full-Size Toughness = 15 ft-lbs



iii) X52, Charpy Full-Size Toughness = 15 ft-lbs



iv) X52, Charpy Full-Size Toughness = 30 ft-lb

c) 4-inch diameter design

Figure 31. MTBF in cycles for circumferential cracking for Poisson-induced axial stress corresponding to pressure at 72-percent of SMYS (concluded)

Discussion

Effects of Operating Conditions on SCC

Guidance concerning the effects of pipeline operation on SCC kinetics can be developed using predictions from the above-noted field-validated model^(122,124-126), which here is done in reference to its probabilistic reformulation⁽¹²³⁾. This formulation addresses the effects of operation in terms of temperature, maximum pressure, and pressure range. Through repeated analyses that consider variability in line-pipe steel mechanical and fracture properties and other probabilistic inputs, this formulation develops the likelihood of SCC leading to leak or rupture over a pipeline whose length scales analytically to 1,000 miles. Raw data from this model lead to plots in the format of Figure 32, which presents probability of failure on the y-axis and years of service on the x-axis and illustrates the potential value of after-coolers in control of high pH SCC. No provision is included in these results for the time required for the pipeline coating to fail (disbond) or the cracking environment to develop under that disbond, nor do these results include the effects of mitigative action such as hydrostatic retesting. The trends in Figure 32 indicate that potential concerns for such SCC are delayed the order of 15 years if discharge temperatures are reduced by 10°F from 130°F to 120°F, and much more if discharge is reduced to 110°F.

Results in the format of Figure 32 can be analyzed to trend the relative effects of operational factors, typical results for which are shown in Figures 33a, 33b, and 33c. These results reflect parametric analysis or relative trending, and so represent situations where other parameters have been held constant.

Figure 32 shows the well-known influence of temperature on SCC kinetics⁽¹⁰⁶⁾, where higher temperature operation is

indicated to appreciably shorten the period before which cracking has a significant impact, as well as accelerate cracking all else being equal. However, what was not equally apparent then is the fact that MAOP exerts an equally significant effect on the onset of cracking and the kinetics, which affects the SCC process from two perspectives. In reference to the threshold evident in Figure 25c note that higher relative stress motivates the frequency of cracking and also drives increased depth. On this basis, SCC is more likely in more highly

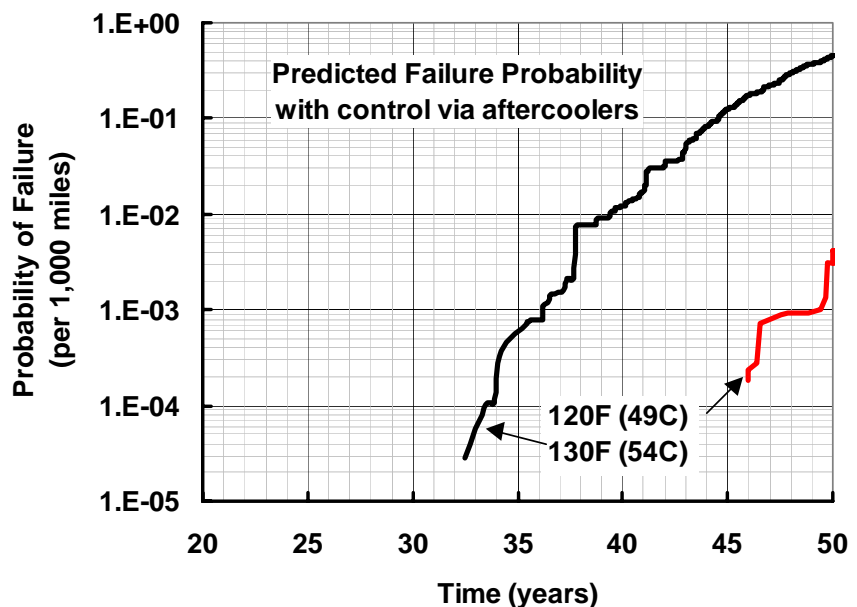
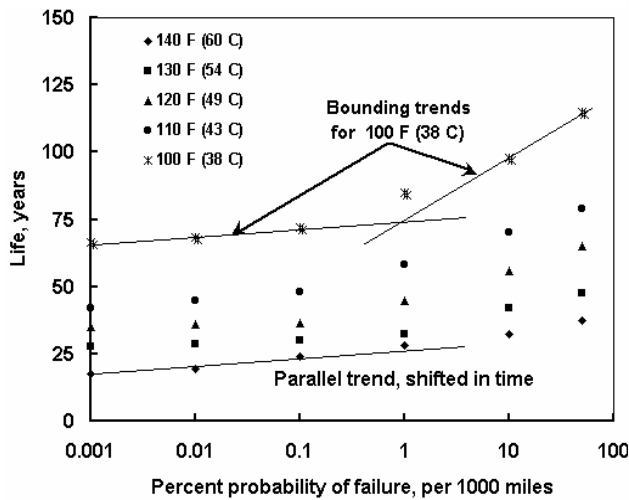


Figure 32. Failure probability for pipelines where SCC is controlled by after-coolers, for mean discharge temperatures at 130°F, 120°F, and 110°F – note that the results for 110°F at these lives fall well below 10⁻⁵

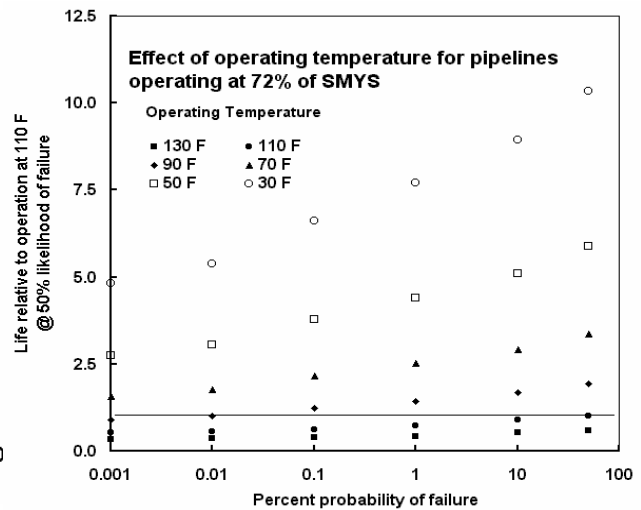
stressed pipelines, suggesting it is more likely in Class 1 Locations than in Class 3 or 4 Locations.

The relative role of temperature is isolated in Figures 33a and 33b with a view to assess its significance in regard to MTBF. Figure 33a presents life in years associated with a given probability of failure, as a function of temperature shown as contours of constant temperature from 100 to 140°F. In contrast to discharge temperatures as high as 170°F on pipelines that experienced the earliest SCC ruptures, temperatures as low as 100°F should defer cracking and result in much longer lives. As Figure 33a indicates such is projected, with a four-fold benefit evident in regard to a decrease from 140 to 100°F at low failure probabilities. However, the trend in benefit changes appreciably at higher likelihood of failure, with higher temperature operation appearing in this format to become more detrimental as the likelihood of failure increases.

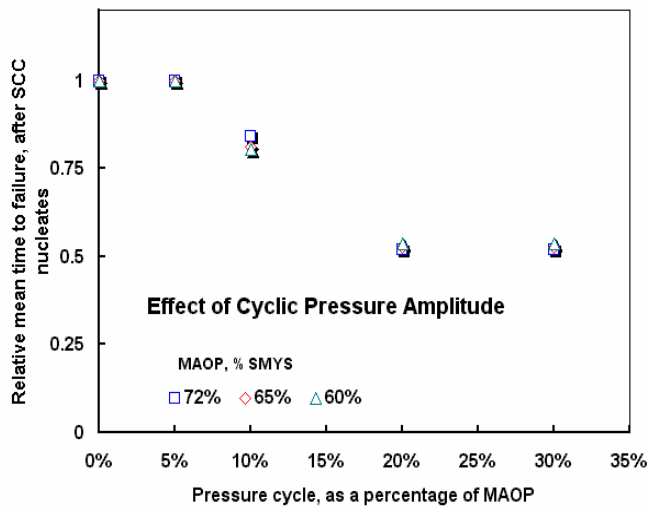
Figure 33b presents the relative dependence of life on gas temperature, under the reasonable assumption that the steady-state temperature of the steel in the pipe wall during operation is very



a) life beyond onset of SCC vs failure probability



b) relative life vs discharge temperature



c) relative life as a function of pressure cycling

Figure 33. Trends in pipeline resistance to SCC involving the temperature and pressure service history

close to this temperature. As can be seen from the labels for the temperature contours, this figure covers a much broader range of temperature, and includes values that reflect liquid natural gas operation as well as operation more typical of liquid petroleum pipelines. All trends shown in this figure have been normalized relative to the behavior for Class 1 gas transmission operation at 110°F at a 50 percent failure probability. This point appears as the solid circle in the lower-right corner of the figure, at the end of the dashed line. This dashed line reflects operation at 110°F. Its value diminishes from unity at 50 percent failure probability to about half that at 10^{-3} . This relative shift in life reflects the changing life with probability alluded to in discussion of Figure 33a. Whereas the format of that figure conveyed the view that higher temperature operation appeared to become increasingly detrimental as the likelihood of failure increased, such is not the case as is evident here. The about 50-percent reduction in life evident for 110°F for 0.5 versus 10^{-3} can be seen here to apply for all data. Thus, regardless of the failure probability, the relative effect of temperature is the same, all else being equal.

In keeping with the well known effect of temperature, the results in Figure 33b indicate the kinetics decrease as temperature decreases. These results show that pipelines experiencing recurrent SCC problems can achieve control of SCC through operating temperature reduction – either through changes in compression ratio, or through use of after-coolers. Field data are consistent with this, the data showing that the incidence of SCC tends to diminish sharply as a function of distance downstream of compressor stations – all else being equal. On this basis, MTBF established by experience for operation close to a given temperature can be scaled to reflect operation of other pipelines as a function of their typical discharge temperature. Significantly, the results in Figure 33b imply that liquid transmission pipelines will eventually experience SCC, with the time delay reflecting the relative effect evident in this figure.

Figure 33c presents the relative mean-life-to-failure on the y-axis as a function of the pressure loading presented in terms of the magnitude of the pressure cycle on the x-axis, the last of the operating parameters. Data are included for three values of the MAOP in the cycle, 72, 65, or 60 percent of SMYS at stress ratios (i.e., R values) from near zero through 0.7. These results present the relative dependence of SCC kinetics referenced to service lives corresponding to operation at MAOP with a near-zero pressure cycle. With this normalized format, the results for each of value of MAOP show similar trends. This does not mean that operation at 72 percent of SMYS leads to the same kinetics as operation at 60 percent of SMYS, as the absolute lives for each of these differs significantly, consistent with the trends of Figure 33 and Figure 25c. In absolute terms, the maximum spread between results at 72 percent and 60 percent of SMYS is on the order of a factor of two. Thus, the near coincidence of these relative trends indicates that the relative effect of pressure cycling on the kinetics is largely independent of the maximum pressure – at least for these finite-life conditions.

Figure 33c shows that little difference in kinetics develops for cycles up to about five percent of MAOP. Thereafter, increasing the range of pressure cycling increases SCC kinetics, through pressure cycling on the order of 20 percent of MAOP. Over this interval, the kinetics show an increase of about a factor of two. For cycling at larger pressure ranges, there is no further effect on SCC kinetics, although there is an increase in corrosion-fatigue kinetics, which is beyond the scope of this project. While these results indicate that a change in operation could affect control of SCC, its effect is less than what could be achieved through temperature control.

Effects of Operating Conditions on Fatigue

As pointed out earlier, the fatigue resistance is a function of the ratio of the minimum to maximum pressure in the pressure cycle, which herein has been denoted R_σ consistent with the usual conventions in the fatigue literature. Figure 29 presented a wide range of results for pressure cycling under near worst-case conditions, for which the value of $R_\sigma = \sim 0.7$. While one cannot simply generalize the effects of R_σ on fatigue in pipelines beyond the earlier discussion involving Equations 7 through 9, one can develop an indication of the dependence of MTBF for pressure cycling by analyzing cases such as those considered in Figure 29 as a function of stress ratio, and thereafter trending MTBF normalized in reference to the life at a given value of R_σ .

Figure 34 presents results typical of analyses for pipelines, which here shows MTBF on the y-axis normalized in reference to $R_\sigma = 0$, as a function of R_σ plotted on the x-axis. It can be seen from Figure 34 that for $R_\sigma < 0.6$, the effect of pressure ratio on fatigue-initiation life is quite modest, however, above this value the life increases sharply. At $R_\sigma = \sim 0.6$ the life is about 10 times longer than for $R_\sigma = 0$, whereas at $R_\sigma = \sim 0.83$ the life is about 100 times that for $R_\sigma = 0$.

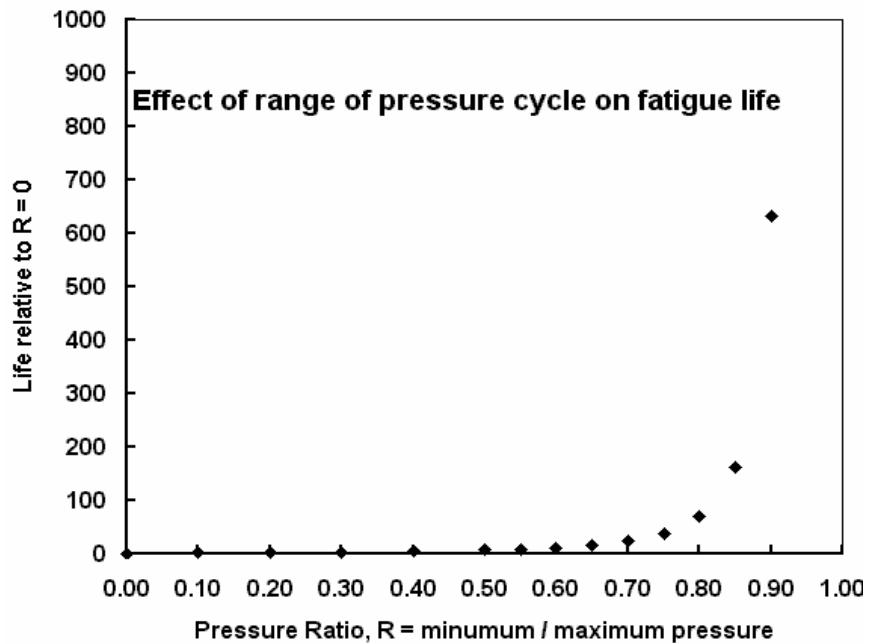


Figure 34. Illustrating the nonlinear dependence of MTBF on pressure cycling and the value of R_σ

As the pressure range continues to decrease, the life becomes about 600 times longer at $R_\sigma = 0.9$ as compared to $R_\sigma = 0$, tending to infinity at $R_\sigma = 1.0$. It is apparent from Figure 34 that for operations involving pressure cycling much below $R_\sigma = 0.7$, fatigue becomes an increasingly important consideration. Whether or not it becomes problematic depends on design details and operational factors beyond the present scope. Data such as that in Figure 23 provide the basis for such analyses, details and examples of which can be found in References 19, and 138 - 140.

The calculations that underlie Figure 34 reflect “finite lives,” which means that eventually fatigue-induced failure occurs because the cycles are large or frequent enough. Thus, where cycling is frequent, design to avoid fatigue must rely on reducing the range of the stress cycles. The literature indicates that the fatigue mechanism exhibits a threshold stress level below which the kinetics slow to the point they no longer are a practically significant concern.^(e.g., see 15-17) As is evident in Figure 23, such thresholds are evident for smooth-bar data for line-pipe steels, which reflect the fatigue resistance to crack initiation^(e.g., see 19), as well as for pre-cracked

specimens that reflect fatigue crack propagation behavior^(e.g., see 15-17). Care must be taken to ensure that periodic large cycles do not occur, as such occurrences can eliminate or reduce these thresholds. Readers interested in details on practices to avoid fatigue should consult the references cited above.

Validation

Throughout, the results presented to evaluate MTBF as a function of defect size and shape and the service conditions are based on models that simulate the mechanics and physics of these failure processes. Such simulations have been made for decades now in applications such as airframes, ground vehicles, and structures such as offshore platforms. For pipelines such simulations have been validated in direct reference to the technologies used in this report in reference to full-scale testing for the fatigue and fracture models^(e.g., see 82). Validation of the models used herein for corrosion assessment and its failure by plastic collapse likewise have validation in reference to full-scale testing as well as coupon testing, which data are consistent with observed field failures^(65,104) and field trends⁽⁷⁾. Finally, models used to simulate SCC have extensive validation in reference to failure criteria, which includes successful blind predictions⁽¹⁰⁴⁾ as well as consistent prediction of trends observed in field failures, full-scale tests, and related failure analyses^(e.g., 82). Consequently, while the MTBF results reflect simulations, the basis for all elements of the underlying models have been directly validated, which in some cases involve blind predictions. As such, these trends can be considered viable indicators of field performance or trends.

Flow Chart for Integrity Assessment

Figure 35 presents a flow chart that can be used to guide integrity assessment when the sequence

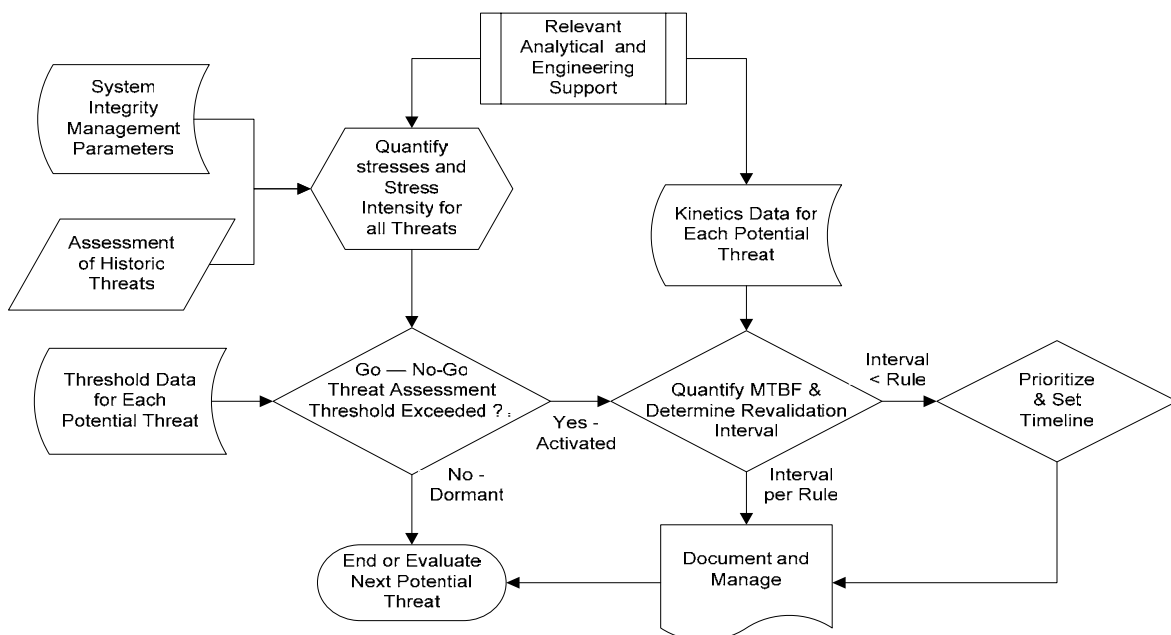


Figure 35. Flow chart to guide integrity management of corrosion, fatigue, and SCC

of steps in Figure 2a indicates that Step Three must be taken. Figure 35 is developed in light of the slightly higher-level version presented earlier as Figure 2b. The essential difference is that Figure 35 incorporates the analysis and threshold / kinetics results presented herein to quantify the decision points.

Summary and Conclusions

Recent changes in the US Department of Transportation Office of Pipeline Safety regulatory requirements mandate transmission pipeline operators develop formal integrity management plans for portions of their system that run through high consequence areas. Pipeline operators must establish and demonstrate the safe condition of their pipeline system passing through high-consequence areas, with the requirement to periodically revalidate that safe condition. One aspect of demonstrating the safe condition of a pipeline is evaluating the many factors that affect pipeline degradation over time, potentially leading to incidents and/or affecting their consequences. As the vintage pipeline system reflects the oldest of the systems in operation in the US, it is logically the focus of concern for such time-dependent degradation. The objective was to develop a quantitative basis for evaluating the significance of specific time-dependent threats on steel pipelines, which could guide evaluating the effectiveness of mitigative measures proposed in integrity management plans. By virtue of its gas-transmission-based cost-share, the scope embraced onshore gas transmission pipelines.

This report first establishes the characteristics of the vintage pipeline system in reference to historical data and recent work that serves as the cost-share for this project that has evaluated the integrity characteristics of this system. For the purposes of this report, pipe making and construction practices that are no longer used, including some early variations of current practices, were considered “historic,” with “vintage” pipelines defined as lines built using historic steel and pipe making pipe technology and related construction practices. On this basis, previous work as part of the cost-share for this project indicated the vintage pipeline system comprises lines constructed prior to about 1970⁽¹¹⁾. Pipeline designs considered typical of the vintage system in terms of diameters, wall thickness, service conditions, grade, and toughness were then identified for subsequent evaluation.

Thereafter, this report formulated an analytical approach to quantify the effects of factors that contribute to the time-dependent degradation of pipelines. Results developed were used to analyze causes of pipeline failure and their consequences, which can change along a pipeline’s right-of-way. Such results were presented in terms of the mean-time-between-failure (MTBF) as a function of the sizes of defects that have caused incidents in pipeline systems. Causes of time-dependent degradation and possible failure that have been quantified in terms of MTBF include corrosion, fatigue, and stress corrosion cracking (SCC). Hydrogen embrittlement also has been considered, although not in regard to mean-time-between-failure.

This report develops tools and technology that were used to generate results and trends useful in assessing the severity of threats due to anomalies introduced by historic steel-making, pipe-making, construction, and fabrication. Such information can provide guidance in developing and implementing an integrity management plan, as an aid to managing the integrity of the vintage pipeline system. Pipeline designs considered typical of vintage pipeline system were evaluated subject to typical gas-transmission operating conditions to determine case-specific mean-time-between-failure data, which were then trended. Such results reflect degradation due to corrosion,

fatigue, and SCC. This report uses technology to trend the time-dependent growth of defects to help operators develop rational integrity management plans in reference to the potential for defect growth and the revalidation of lines that might involve such defects.

Important conclusions regarding re-inspection intervals that can be derived from this work and the MTBF results generated include:

- Re-inspection intervals for corrosion targeted at the order of seven to ten years appear to be viable based on the present results.
- Re-inspection intervals involving fatigue will depend on the pipeline's operating pressure history. For the high-stress ratio, $R_\sigma = \text{minimum stress}/\text{maximum stress}$, infrequent cycling that is typical of most gas-transmission pipeline service fatigue is an unlikely cause of failure, such that fatigue is not a viable threat for such gas-transmission pipelines. However, where the stress ratio falls below about 0.7 fatigue does become a concern. Re-inspection intervals for such pipelines should be evaluated as a function of the current condition of the pipeline and its operating pressure history.
- Re-inspection intervals involving high pH SCC will depend on the pipeline's current condition, past experience with SCC, the pipeline's right-of-way, and its operating pressure history in reference to pressure as it affects temperature and pressure cycles. For Class 1 scenarios the wall stress at MAOP is above typical high pH SCC thresholds such that this threat should be evaluated, whereas where the pressure or right-of-way-induced stresses are well below apparent thresholds this threat is diminished. Typical laboratory test conditions used to study high pH SCC under accelerated conditions produce growth rates orders of magnitude faster than often observed in the field. While acceleration is useful and essential to evaluate factors controlling SCC, care must be used where such data are considered to guide integrity management decisions. Right-of-way and operational factors have a first-order effect on SCC kinetics and must be addressed when making integrity management decisions. Where growth rates are high, in-line inspection will have diminished value, while hydrotesting remains effective with the added benefit of blunting deeper cracks and diminishing the microplastic strain essential for SCC nucleation.
- Re-validation intervals where there is significant potential for circumferential defects, due for example to the presence of vintage girth-welds or SCC activated by axial loading, and there is a continued threat of axial stresses in the pipe wall, due for example to Poisson pressure induced axial tension, are dependent on the magnitude of the stresses and the size and shape of the defect(s). Pressure cycling does aggravate the situation in areas adjacent to where the pipeline is earth-anchored, but the effect is small in the absence of externally applied axial loading.

Recommendations

Because the degradation processes leading to pipeline failure are complex, which makes results developed for MTBF and related implications for re-inspection specific to the pipeline design and its mechanical and toughness properties, as well as the operational conditions for the line. As such, validated models have been used to simulate MTBF – in a process that involves feeding results from pressure history analysis models and numerical failure criteria that determine critical defect sizes into models of failure kinetics all of which are complex and so presently exist as

“specialists” tools. Yet, with the advent of powerful personal computers and user-friendly graphical user interfaces such tools could be integrated into a single processor and provided, along with essential training, to the industry to develop pipeline-specific integrity management.

Consideration should be given to the integration of such tools and their delivery along with appropriate training. For those not prone to use computer-based tools, a compendium of results covering a broad yet practical range of pipeline scenarios could be developed. Finally, while comprehensive in many ways, the present work has focused on only a portion of the important threats to pipeline safety, and done so in reference to gas pipelines by virtue of its cost-share basis. Consideration should be given to the remaining threats, and potentially important differences between liquids/products pipelines and gas transmission pipelines in reference to product properties and operational histories.

References

1. Anon., United States Department of Transportation, Research and Special Projects Agency web site, <http://primis.rspa.dot.gov/comm>; see also <http://primis.rspa.dot.gov/iim>; see also related legislative action.
2. Anon., United States Department of Transportation, Transmission Pipeline Incident Databases, Office of Pipeline Safety web site, <http://ops.dot.gov>.
3. Anon., Code of Federal Regulations, Title 49-Transportation, Part 192 and Part 195.
4. Kiefner, J. F., Mesloh, R. E., and Kiefner, B. A.; "Analysis of DOT Reportable Incidents For Gas Transmission and Gathering System Pipelines, 1985-1997", PRCI, PR-218-9801, 1999.
5. Anon., ASME Code Supplement on Integrity Management for Pressure Piping, B31.8S, Revision 1, 2002, ASME.
6. Anon., United States Department of Transportation, Transmission Pipeline Incident Reporting, <http://ops.dot.gov/forms.htm#7000-1/2>.
7. Leis, B. N., and Bubenik, T. A., "Periodic Re-Verification Intervals for High-Consequence Areas," GRI Report-00/0230, January 2001.
8. Leis, B. N. and Bubenik, T. A., "Implementation Plan for Periodic Re-Verification Intervals for High-Consequence Areas," Battelle Report to GTI, GRI Report-00/0246, January 2001.
9. Kiefner, J. F. and Clark, E. B., "History of Line Pipe Manufacturing in North America," ASME Research Report CRTD-Vol.43, 1996.
10. Kiefner, J. F. and Trench, C. J., "Oil Pipeline Characteristics and Risk Factors: Illustrations from the Decade of Construction," American Petroleum Institute, December 2001.
11. Clark, E. B., Leis, B. N., and Eiber, R. J., "Integrity Characteristics of Vintage Pipelines," Battelle Report to the INGAA Foundation, October, 2004.
12. Leis, B. N., Chang, O. C., and Bubenik, T. A., "Leak versus Rupture Considerations for Steel Low-Stress Pipelines," GRI Report-00/0232, Gas Research Institute, January 2001.
13. Anon., "Specification for Line Pipe," API Specification 5L, American Petroleum Institute, Dallas, 2004.
14. Eiber, R. J. and Leis, B. N., "Fracture Control Technology for Natural Gas Pipelines – Circa 2000", PRCI Catalog No. L51846, Pipeline Research Council International, 2002.
15. Broek, D., "Engineering Fracture Mechanics," Nordhoff, 1974.
16. Rolfe, S. T. and Barsom, J. M., "Fracture and Fatigue Control in Structures," Prentice-Hall, 1977.
17. Hertzberg, R. W., "Deformation and Fracture Mechanics of Engineering Materials," John Wiley and Sons, 1976.
18. Tada, H., Paris, P. C., and Irwin, G. R., "The Stress Analysis of Cracks Handbook," Del Research Corp., 1977: see also Anon., "Stress Intensity Factors Handbook," Vol 1, Pergamon Press, New York, 1987.
19. Rice, R. C., Leis, B. N., and Nelson, D. V. editors, "Fatigue Design Handbook," Second Edition, Society of Automotive Engineers, \Volume AE 10, 1989.

20. Manning, S. D. and Yang, J. N., "USAF Durability Design Handbook: Guidelines for the Design of Durable Structures", AFWAL-TR-83-3027, 1984: see also Manning, S. D. and Yang, J. N., "Advanced Durability Analysis, Volume I – Analytical Methods", AFWAL-TR-86-3017, and Volume II – Analytical Predictions, Test Results and Analytical Correlations", AFWAL-TR-86-3027, 1987: precursor company proprietary handbooks existed as for example Rawe, R. E., "Fracture Mechanics and Safe Life Design", Douglas Aircraft Corporation, Report DAC 59591, August, 1970.
21. Yukawa, S., "ASME Nuclear Code Applications of Structural Integrity and Flaw Evaluation Methodology," in "Structural Integrity Technology," ASME, 1979, pp. 29-38.
22. Marshall, P. W., "Strategy for Monitoring, Inspection and Repair for Fixed Offshore Platforms," in "Structural Integrity Technology," ASME, 1979, pp. 97-110: see also Pelleni, W. S., "Principles of Structural Integrity," Office of Naval Research, 1976.
23. Maxey, W. A., Kiefner, J. F., Eiber, R. J., and Duffy, A. R., "Ductile Fracture Initiation, Propagation and Arrest in Cylindrical Vessels," ASTM STP 514, American Society for Testing and Materials, Philadelphia, 1972, pp. 70-81: see also Kiefner, J. F., Maxey, W. A., Eiber, R. J., and Duffy, A. R., "The Failure Stress Levels of Flaws in Pressurized Cylinders," ASTM STP 536, 1973, pp 461-481.
24. Leis, B. N. and Brust, F. W., "Ductile Flaw Growth Model," Seventh Biennial Joint Technical Meeting on Line Pipe Research, Pipeline Research Council International, Volume One, pp. 18.1-20.
25. Leis, B. N., Brust, F. W., and Scott, P. M., "Development and Validation of a Ductile Flaw Growth Analysis for Gas Transmission Line Pipe," PRCI Catalog No. L51543, Pipeline Research Council International, June 1991.
26. Leis, B. N., Appendix B to "Hydrostatic Testing Of Transmission Pipelines: When It Is Beneficial and Alternatives When It Is Not", PRCI Catalog No. L51844, 2001.
27. Broek, D. and Leis, B. N., "Fatigue Crack Initiation and Growth Analysis for Structures", in Fatigue Resistance Testing and Forecasting. Society of Automotive Engineers, SAE SP-448, September, 1978, pp. 1-12: see also Leis, B. N., "Predicting Crack Initiation Fatigue Life in Structural Components", in Methods of Predicting Fatigue Life, ASME, 1979, pp. 57-76.
28. Leis, B. N. and Parkins, R. N., "Mechanics and Material Aspects in Predicting Serviceability Limited by Stress-Corrosion Cracking", *Fatigue and Fracture of Engineering Materials & Structures* 1998; Vol. 21: pp 583-601.
29. Leis, B. N., Zhu, X. K., and Clark, E. B., "Criteria to Assess Wrinklebend Severity for Use in Pipeline Integrity Management," PRCI Catalog No. L52190, August 2004.
30. Groeneveld, T. P., "Hydrogen-Stress Cracking", Paper X, 6th Symposium on Line Pipe Research, PRCI Catalog No. L30174, October, 1979: see also Groeneveld, T. P., Wenk, R. L., and Elsea, A. R., "Investigation of the Susceptibility of High-Strength Steels to Hydrogen-Stress Cracking", NG-18 Report No. 37, 1972 (PRCI Proprietary).
31. Leis, B. N., "Characterization of Axial Flaws in Pipelines, With a Focus on Stress-Corrosion Cracking", NG-18 Report No. 212, PRCI Catalog No. L51807, 1997.
32. Anon., Federal Power Commission Incident Database, 1950-1965.
33. Jones, D. J., Kramer, G. S., Gideon, D. N., and Eiber, R. J., "An Analysis of Reportable Incidents for Natural Gas Transmission and Gathering Lines 1970 through 1984," PRCI Catalog No. L51499, March 1986.

34. Petersen, C. W., et al., "Improving Long Distance Gas Transmission Economics: X120 Development Overview," Pipeline Technology Conference, Oostende, May 2004, Volume I, pp 3-30.
35. Leis, B. N. and Bubenik, T. A., "Primer on Design to Avoid Failure in Steel Transmission Pipelines", GRI 00/0229, January 2001.
36. Timoshenko, S. P. and Woinowsky-Krieger, S., Theory of Plates and Shells, McGraw-Hill, 1959: see also Timoshenko, S. P. and Goodier, J. N., Theory of Elasticity, McGraw-Hill, Third Edition, 1970.
37. Anon., "American Tentative Standard Code for Pressure Piping," American Engineering Standards Committee, Sectional Committee B31, 1935.
38. <http://www.proceq-usa.com/products/equotip2.php> for general in situ hardness tools, and frontics@frontics.com or <http://exm.sagepub.com/cgi/content/refs/44/1/55> for illustration of its use to infer properties.
39. Francini, R. B., Burgoon, D. A., Chang, O. C., Leis, B. N., Rust, S. W., and Clark, E. B. "An Alternative to 49 CFR 192, Appendix B To Determine Unknown Yield Strength", OGPT 10256, ASME, February 2000, pp. 1-11.
40. Hart, B. O., Brongers, M. P. H., Bubenik, T. A., and Vieth, P. H., "Unique Properties of Seams in Early-Generation Pipelines," PRCI Catalog No. L52064, July 2004.
41. Leis, B. N., Flamberg, S., and Clark, E. B., "Battelle Data Mining", PRCI Catalog No. L52062, in progress.
42. West, T., "Web Database: Pipeline & Weld Properties," PRCI Catalog No. L52033, in progress.
43. Rogers, G., Rapp, S. C., and Matocha, G., "Integrity Evaluation of an Older Vintage Pipeline," IPC2002-27052, October 2002.
44. Leis, B. N., Galliher, R. D., Sutherby, R. L., and Sahney, R., "Hydrotest Protocol for Applications Involving Lower-Toughness Steels," International Pipeline Congress, Calgary, October 2004, ASME, IPC04-0665, 12 pages.
45. Anon., Pipelines and Public Safety, Special Report 219, Transportation Research Board, United States National Research Council, 1988.
46. Keifner & Associates, Inc., "GRI Guide for Locating and Using Pipeline Industry Research", Gas Research Institute, May 2000.
47. Hereth, M., Zurcher, J., and Selig, B., "Prevention Detection and Mitigation of Natural Gas Transmission Pipeline Failures," GRI-00/0193, December 2000.
48. Cosham, A. and Hopkins, P., "The Pipeline Defect Assessment Manual", Proceedings of IPC 2002: International Pipeline Conference, Calgary, IPC02-27067, October 2002.
49. anon., ASTM Standard E23-98, Notched Bar Impact Testing of Metallic Materials, ASTM Vol. 03.01.
50. anon., "Fracture Toughness Testing," and "Drop-Weight Tear Testing," Supplemental Requirements Five and Six in Reference 13, pp 121-123.
51. Leis, B. N., "Evolution of Line-Pipe Steel and its Implications for Transmission Pipeline Design," International Pipeline Congress, Calgary, October 2002, ASME, IPC04-0665.
52. Leis, B. N. and Kilinski, T. J., "Mechanical and Fracture Properties Essential in Integrity Management of Steel Transmission Pipelines", Draft Final Report, PRCI Report PR-3-9606/9737, December, 2000.

53. Boulger F. W. and Hansen, W. R., "A Study of the Effect of Manufacturing Variables on the Properties of Line-Pipe Steels," AGA NG-18 Report 16, January 1966.
54. Roovers, P., Denys, R., Leis, B. N., and van Dyck, J., "Assessment of Older Pipelines – Part 1: Proposed Methodology and Statistical Approach", and Part 2: Validation of Initiation and Propagation Models," Pipeline Technology Conference, Oostende, May 2004, Volume II, pp 565-579 and 581-592.
55. Janzen, T. S. and Horner, W. N., "The Alliance Pipeline," 1998 International Pipeline Conference, ASME, Volume 1, pp. 83-88, 1998.
56. Eiber, R. J., Carlson, L. E., and Leis, B. N., "Fracture Control for the Alliance Pipeline", International Pipeline Conference - 2000, ASME, Calgary, October, 2000, pp. 267-277.
57. Kiefner, J. F., Maxey, W. A., Eiber, R. J., "A Study of the Causes of Failures of Defects that have Survived a Prior Hydrostatic Test", NG-18 Report No. 111, November, 1980.
58. B31G American National Standards Institute (ANSI)/American Society of Mechanical Engineers (ASME) B31G "Manual for Determining the Remaining Strength of Corroded Pipelines," 1984.
59. Kiefner, J.F. and Vieth, P.H., "A Modified Criterion for Evaluating the Remaining Strength of Corroded Pipe," Final Report on Project PR 3-805, Pipeline Research Council International, PRCI Catalog No. L51688, December 1989.
60. Kiefner, J. F., Vieth, P. H., and Roytman, I., "Continuing Validation of RSTRENG," Pipeline Research Council International, PRCI Catalog No. L51689, 1996.
61. Kanninen, M. F. et al., "Instability Predictions for Circumferentially Cracked Type 304 Stainless Steel Pipes under Dynamic Loading," EPRI NP-2347, 1982: see also Wang, Y.-Y., Wilkowski, G.M., and Horsley, D.J., "Plastic Collapse Analysis of Pipelines Containing Surface-Breaking Circumferential Defects," Pipeline Technology, Volume I, Third International Pipeline Technology Conference, Brugge, R. Denys, Ed., Elsevier Science, 2000, pp. 195-209.
62. Rosenfeld, M. J., "Serviceability of Corroded Pipeline Girth Welds," Final Report to PRCI Contract No. PR 218-9434, May 1996.
63. Miller, A. G., "Review of Limit Loads of Structures Containing Defects," I J Pressure Vessels & Piping, Vol. 32, No. 1-4, 1988.
64. Cronin, D. "Prediction of Corrosion Defect Failure Pressure for Finite Length Defects," Fifth International Pipeline Conference (IPC 2004), Calgary, ASME, October 2004, IPC04-0692.
65. Leis, B. N. and Stephens, D. R., "An Alternative Approach to Assess the Integrity of Corroded Line Pipe – Part One: Current Status and Part Two: Alternative Criterion", 7th International Conference on Offshore Pipelines and Polar Engineering, Vol. 3, pp 624 – 634 and pp 635 – 641, 1997.
66. Zhu, X. K. and Leis, B. N., "Strength Criteria and Analytic Predictions of Failure Pressure in Corroded Line Pipes", *International Journal of Offshore and Polar Engineering*, Vol.14, June, 2004, pp 125-131: see also Zhu, X.-K. and Leis, B. N., "Influence of the Yield-to-Tensile Strength Ratio on the Failure Assessment of Corroded Pipelines", Proceedings of ASME-PVP 2003, Cleveland, July 2003, to appear in J. P.V. P, ASME.

67. Stonesifer, R. B., Brust, F. W., and Leis, B. N., "Stress-Intensity Factors for Long Axial Exterior Surface Cracks in Large R/t Pipes", ASTM STP 1131, American Society for Testing and Materials, Philadelphia, pp 29-45, 1992.
68. Stonesifer, R. B., Brust, F. W., and Leis, B. N., "Mixed Mode Stress Intensity Factors for Interacting Semi-Elliptical Surface Cracks in a Plate", *Engineering Fracture Mechanics*, Vol. 45, No. 3, pp. 357-380, 1993.
69. Brust, F. W. and Leis, B. N., "A New Model for Predicting Primary Creep Damage in Axially-Cracked Cylinders: Part I – Theory ", *Engineering Fracture Mechanics*, Vol. 43, pp 615-627, 1992: see also "A New Model for Predicting Primary Creep Damage in Axially-Cracked Cylinders: Part II – Application ", *ibid*, pp 629-639, 1992.
70. Shih, C. F., German, M. D., and Kumar, V., "An Engineering Approach for Examining Crack Growth and Stability in Flawed Structures", G. E. Report No. 80CRD205 (August 1980); see also, Kumar, V., et al., "An Engineering Approach for Elastic-Plastic Fracture Analysis", EPRI NP-1931 (July 1981).
71. Rice, J. R. and Rosengren, G. F., "Plane Strain Deformations Near a Crack Tip in a Power-Law Hardening Material," *J. Mech. Phys. Solids*, Vol. 16, pp 1-12, 1968.
72. Hutchinson, J. W., "Singular Behavior at the End of a Tensile Crack in a Hardening Material," *J. Mech. Phys. Solids*, Vol. 16, pp 13-31, 1968: see also Hutchinson, J. W., "Fundamentals of the Phenomenological Theory of Nonlinear Fracture Mechanics", *J. of App. Mech.*, Vol. 50, pp 1042-1051, 1983.
73. Ernst, H. A. and Paris, P. C., "Technique of Analysis of Load-Displacement Records by J Integral Method", U.S. Nuclear Regulatory Commission, NUREG/CR-122: see also, Ernst, H. A., Paris, P.C., and Landes, J. D., "Estimation of the J-Integral and Tearing Modulus T from Single Specimen Test Records", Fracture Mechanics - 13th Conference, ASTM STP 743, ASTM, pp 476-502 (1981).
74. Paris, P. C., Tada, H., Zahoor, A., and Ernst, H., "The Theory of Instability of the Tearing Mode of Elastic-Plastic Crack Growth", Elastic-Plastic Fracture, ASTM STP 668, pp 5-36 (1979): see also Hutchinson, J. W.; and Paris, P. C.: Stability of Analysis of J Controlled Crack Growth, ASTM STP 668, pp. 37-64, 1979.
75. Anon., ASTM Standard E399-99, Measurement of Plane-Strain Fracture Toughness, ASTM Vol. 03.01.
76. Anon., ASTM Standard E1820-99, Measurement of Fracture Toughness, ASTM Vol. 03.01.
77. Nishioka, T. and Atluri, S. N., "Analytical Solution For Embedded Elliptical Cracks, And Finite Element Alternating Method For Elliptical Surface Cracks, Subjected To Arbitrary Loadings," *Eng. Fract. Mech.*, Vol.17(3), pp. 247-268, 1983: see also Vijayakumar, K. and Atluri, S. N., "An Embedded Elliptical Flaw In An Infinite Solid, Subject To Arbitrary Crack-face Traction," *J. Appl.Mech.*, Vol. 48, pp. 88-96, 1981.
78. Iida, K., Kiyoshi, A., and Hirata, T., "An Evaluation Technique for Fatigue Life of Multiple Surface Cracks", *Japanese Society of Naval Architects*, Vol. 153, pp 177-199, June, 1983.
79. Newman Jr., J. C. and Raju, I. S., "Stress-Intensity Factor Equations for Cracks in Three-Dimensional Finite Bodies Subjected to Tension and Bending Loads", Mechanics and Mathematical Methods - First Series: Computational Methods in Mechanics, Vol 2, Chapter 9, pp 312-334, Ed. S. N. Atluri, 1986.

80. Yang, Y. Y., "Elastic T-Stress Solutions for Semi-Elliptical Surface Cracks in Finite Thickness Plates," *Engineering Fracture Mechanics*, Vol. 70, 2003, pp. 731-756.
81. O'Dowd, N.P. and Shih, C.F., 1992, "Family of Crack-Tip Fields Characterized by a Triaxiality Parameter – II. Fracture Applications," *Journal of the Mechanics and Physics of Solids*. **40**, pp.939-963.
82. Olson, R. J., Narendran, V. K., Leis, B. N., Kilinski, T. J., Scott, P. M., and Gertler, R. C., "Full-Scale Testing to Validate PAFFC and Develop Data to Assist Evaluating the Benefits of Hydrotesting", Appendix 7 of Reference 83.
83. Leis, B. N., "Hydrostatic Testing of Transmission Pipelines: When It Is Beneficial and Alternatives When It Is Not," PRCI Catalog No. L51844, Pipeline Research Council International, 2001.
84. Brooks, L. E., "Hydrostatic Testing of Pipe Lines", *Journal of the Pipeline Division*, ASCE, Vol. 83, No. PL3, September 1957: see also Heineman, W. P., "Testing of Pipe and Pipelines", ASCE Transportation Engineering Conference, Minneapolis, MN, Preprint No. 211, May 1965.
85. Duffy, A. R., McClure, G. M., Maxey, W. A., and Atterbury, T. J., "Study of the Feasibility of Basing Natural Gas Pipeline Operating Pressure on Hydrostatic Test Pressure," Pipeline Research Council International, PRCI Catalog No. L30050, 1968.
86. Leis, B. N., Zhu, X.-K., Forte, T. P. and Glenn, B. C., "Design Basis for Fracture Arrestors in Gas Transmission Pipelines", in Volume II -Pipeline Technology, Science Surveys Ltd., 2004, pp 515 - 533.
87. Jones, D. A., "Principles and Prevention of Corrosion," Macmillian, 1991.
88. Rebinder, P. A. and Shchukin, E. D., "Effects of Chemisorbed Hydrogen," *Uspekhi Fizicheskikh Nauk*, Vol 108, No 3, 1972.
89. Birnbaum, H. K. and Sofronis, P., "Hydrogen-Dislocation Interactions", Proceedings 5th Conference on Hydrogen Effects in Materials, TMS, 1994, pp 15-34.
90. Helle, H. P. E., "An Investigation of Ship Propeller Fatigue," Ph.D. Thesis, T. U. Delft, 1981.
91. McAllister, E. W., editor, "Pipeline Rules of Thumb Handbook", 5th edition, NACE, 2002
92. Romanoff, M., "Underground Corrosion", NBS Circular 579, 1957.
93. Flitt, H. J., Spero, C., and Ferris, P.M., "Prediction of Mild Steel Corrosion Rate in Clay Soil", Proceedings of Life Prediction of Corrodible Structures, Hawaii, Vol. 1, pp 320-333, 1991.
94. Klesnil, M. and Lukas, P., "Fatigue of Metallic Materials", Elsevier, 1980.
95. Leis, B. N., "A Nonlinear History Dependent Damage Model for Low Cycle Fatigue", Low Cycle Fatigue: Directions for the Future, ASTM STP 942, 1988, pp 143-159.
96. Leis, B. N., "An Energy-Based Fatigue and Creep-Fatigue Damage Parameter", *Journal of Pressure Vessel Technology*, Trans. ASME, Vol. 99, No. 4, 1977, pp. 524-533.
97. Morrow, J. D., Wetzell, R. M., and Topper, T. H., "Laboratory Simulation of Structural Fatigue Behavior," ASTM STP 462, 1970, pp. 74-91: see also Skeleton, R. P., "Application of Small Specimen Crack Growth Data to Engineering Components at High Temperature: A Review", ASTM STP 942: Low-Cycle Fatigue, H D Solomon, G R Halford, L R Kaisand, and B N Leis, editors, 1988, pp. 209-235.

98. Anon., "American Welding Society Structural Welding Code, AWS D1.1", American Welding Society, 1998.
99. Leis, B. N. and Forte, T. P., "Fatigue Damage Analysis Under Variable Amplitude Loading", Random Fatigue Life Prediction, PVP/ASME, PVP Vol. 72, 1983, pp. 89-105.
100. Gurney, T. R., "Fatigue of Welded Structures," Cambridge University Press (UK), 1979.
101. Leis, B. N., Kanninen, M. F., Hopper, A. T., Ahmad, J., and Broek, D., "Critical Review of the Fatigue Growth of Short Cracks", *Engineering Fracture Mechanics*, Vol. 23, No. 5, 1986, pp. 883-896.
102. Suresh, S. "Fatigue of Materials," Cambridge University Press, 1998.
103. Broek, D., and Leis, B. N., "Similitude and Anamolies in Crack Growth Rates", Materials, Experimentation, and Design in Fatigue, Westbury House, UK, March, 1981, pp. 129-148.
104. Anon., Report of the Public Inquiry Concerning Stress Corrosion Cracking on Canadian Oil and Gas Pipelines, Proceeding MH-2-95: National Energy Board (Canada), 1996.
105. Parkins, R. N., and Fessler, R. R., "Line Pipe Stress-Corrosion Cracking -- Mechanisms and Remedies," Paper 320, *Corrosion '86*, NACE, 1986.
106. Parkins, R. N., "The Controlling Parameters in Stress-Corrosion Cracking", 5th Symposium on Line Pipe Research, Pipeline Research Committee, A.G.A., Paper U, pp. U.1- 39, 1974: see also R. N. Parkins and B. S. Greenwell, "The Interface Between Corrosion Fatigue and Stress-Corrosion Cracking", *Metal Science* **11**, pp. 405-407: see also R. N. Parkins, "Factors Influencing Stress-Corrosion Crack Growth Kinetics", *Corrosion* **43**, p. 130, 1987.
107. Parkins, R. N., "Environment Sensitive Cracking (Low pH Stress-Corrosion Cracking) of High-Pressure Pipelines" AGA NG-18 Report No. 191, AGA Catalog No. 51623, 1990: see also Parkins, R. N., "An Overview of Stress-Corrosion Cracking Research Activities for High-Pressure Pipelines", AGA NG-18 Report No. 215, 1994.
108. Fessler, R. R., "Stress Corrosion Cracking Gap Analysis," Report No. GRI-8293, Pipeline Research Council International, Sept. 2002.
109. Logan, H. L., "Film Rupture", *J. National Bureau of Standards*, Vol. 48, pp 99, 1952.
110. Scully, J. C., "Slip Dissolution", *Corrosion Science*, Vol. 7, pp 197, 1967.
111. Colwell, J. A., Leis, B. N., and Singh, P. M., "Crack Initiation of Line Pipe Steels in Near-Neutral pH Environments", 2nd International Conference on Environmentally Initiated Cracking in Materials, NACE, September, 2004.
112. Leis, B. N., Colwell, J. A., and Singh, P. M., "Crack Initiation Mechanisms for Line Pipe Steels in Near-Neutral pH Environments", PRCI Project Report PR-03-0320, 2005 (in preparation).
113. Leis, B. N., "Stress-Corrosion Cracking in Gas Transmission Pipelines – The Interplay Between Serviceability and Inspection," Proceedings 9th Line Pipe Symposium, Pipeline Research Committee International, American Gas Association Catalog No. L51746, September 1996, pp. 23.1 – 29.
114. Ugiansky, G. M. and Payer, J. H., editors, "Stress-Corrosion Cracking -- The Strain-Rate-Rate Technique", ASTM STP 665, 1979.
115. Tandon, K. N. and Tangri, K., "Slip Sources in the Surface Layers of Polycrystalline Fe-3 Pct Si in the Early Stages of Deformation", *Metallurgical Trans A* **6A**, pp. 809-813, 1975.
116. McGregor-Tegart, W. J., "Elements of Mechanical Metallurgy," Macmillan, 1966.

117. Fessler, R. R. and Barlo, T. J. "Threshold-Stress Determination Using Tapered Specimens and Cyclic Stresses," ASTM STP 821, 1984, pp. 368-382.
118. Leis, B. N. and Colwell, J. A., "Initiation of Stress-Corrosion Cracking on Gas Transmission Piping," Effects of the Environment on the Initiation of Crack Growth, ASTM STP 1298, W. A. Van Der Sluys, R. S. Piascik, and R. Zawierucha, Eds., American Society for Testing and Materials, pp 34-58, 1997.
119. Leis, B. N., "Analysis Methods for Stress-Corrosion Cracking", Proceedings Pipeline Technology Conference, Part B, Oostende, pp. 18.1-11, 1990.
120. Beavers, J. A., Parkins, R. N., Koch, G. H., and Berry, W. E., "Test Method for Defining Susceptibility of Pipeline Steels to Stress-Corrosion Cracking," A.G.A. NG-18 Report No. 146, PRCI Catalog No. 51484, 1985.
121. B. N. Leis and W. J. Walsh, "Mechanics-Based Analysis of Stress-Corrosion Cracking of Line-Pipe Steel in a Carbonate-Bicarbonate Environment", ASTM STP 1049, Edited by B. W. Lisagor, T. W. Crooker, B. N. Leis, pp. 243-265, 1990.
122. Leis, B. N., Forte, T. and Ghadiali, N. D., "Stress-Corrosion Cracking Life Prediction Model -- SCCLPM: Users Manual and Software, Version 1.0", NG-18 Report No. 217, 1995.
123. Kurth, R. E. and Leis, B. N., "Probabilistic Modeling of Stress-Corrosion Cracking: Part One – Model Development", ASME PVP-Volume 386, August 1999, pp. 3-12: see also Leis, B. N., and Kurth, R. E., "Probabilistic Modeling of Stress-Corrosion Cracking: Part Two –Validation and Implications for Control", ASME PVP-Volume 386, August 1999, pp. 13-23.
124. Leis, B. N., "Validation of a High pH Stress-Corrosion Cracking Life Prediction Model (SCCLPM) for Gas-Transmission Pipelines", Final Report: Validation Task, PR 3-9531, November 1997.
125. Leis, B. N., "Field Data and Observations to Validate Models of High pH Stress-Corrosion Cracking Life Prediction on Gas-Transmission Pipelines", Final Report: Data Gathering Task, PR 3-9531, November 1997.
126. Anon., NACE RP0472-2000, "Standard Recommended Practice - Methods and Controls to Prevent In-Service Environmental Cracking of Carbon Steel Weldments in Corrosive Petroleum Refining Environments", National Association of Corrosion Engineers, September 2000.
127. Gerberich, W. W., Chen, Y. T., and St. John, C., "A Short-Time Diffusion Correlation for Hydrogen-Induced Crack Growth Kinetics," *Met. Trans.*, 1975, A6 (8), pp. 1485-1498.
128. Graville, B. A., "Effect of Hydrogen Concentration on Hydrogen Embrittlement," *British Welding Journal*, Vol. 15, No. 4, pp 191-195.
129. Leis, B. N. and Eiber, R. J., "SCC Service History Evaluation", 9th PRC/EPRG Biennial Joint Technical Meeting on Line Pipe Research, Houston, 1993: see also Leis, B. N., "Recurrent SCC in Gas Transmission Pipelines: Service History and Material Property Considerations", NG-18 Report No. 210, 1994.
130. van Dyjk, G. M., "Statistical Load Data Processing," 6th ICAF Symposium, May 1971.
131. Matsuishi, M. and Endo, T., "Fatigue of Metals Subjected to Varying Stress", *Bull. JSME*, 1968.

132. Anon., "Standard Practices for Cycle Counting," ASTM Standard E 1049, American Society for Testing and Materials Vol. 03.01.
133. Stephens, D.R., Leis, B.N., Kurre, J.D., and Rudland, D.L., "Development of an Alternative Failure Criterion for Residual Strength of Corrosion Defects in Moderate- to High-Toughness Pipe," PRCI Cat. No. L51794, January 1999.
134. Leis, B. N. and Parkins, R. N., "Modeling Stress-Corrosion Cracking of High-Pressure Gas Pipelines", 8th Symposium on Line Pipe Research. PRCI Catalog No. L51680, 19.1-21, 1993.
135. Leis, B. N., "Mechanics Based Analysis of Environmentally Assisted Crack Nucleation in Systems Controlled by Dissolution", Modeling Environmental Effects on Crack Growth Processes, AIME, pp. 301-319, 1986.
136. Leis, B. N., Rungta, R., and Jentge, R. L., "Stress-Corrosion Cracking and Fatigue -- A Mechanics-Based Step to an Interactive Model", Embrittlement by the Localized Crack Environment, Edited by R. P. Gangloff, pp. 211-227, 1984.
137. Leis, B. N., "Coalescence Conditions for Stress-Corrosion Cracking Based on Interacting Crack-Pairs", Pipeline Technology, R. Denys, Ed., Elsevier Science B V, 1995, Volume I, pp 614 – 622.
138. Klesnil, M. and Lukas, P., "Fatigue of Metallic Materials", Elsevier, 1980.
139. Anon., "Fatigue and Fracture", ASM Handbooks, Volume 19, ASM International, 1996.
140. Kiefner, J. F. and Rosenfeld, M. J. "Effects of Pressure Cycles on Gas Pipelines," GRI-04/718, September 2004.
141. Anon./Battelle, "Summary of Field Failure Investigations," PRCI NG-18 Report 131, March 1982.
142. Anon., National Transportation Safety Board:
 - "High Pressure Natural Gas Pipeline, near Houston, Texas, September 9, 1969," Report PAR-71-01;
 - "Southern Union Gas Company, El Paso, Texas, April 22, 1973", PAR-74-02;
 - "Washington Gas Light Company, Bowie, Maryland, June 23, 1973", PAR-74-05;
 - "Michigan Wisconsin Pipeline Company, Monroe, Louisiana, March 2, 1974", PAR-75-01;
 - "Southern Union Gas Company, Transmission Pipeline Failure, near Farmington, New Mexico, March 15, 1974", PAR-75-03;
 - "Transcontinental Gas Pipeline Corp., 30 inch Transmission Line Failure, near Bealeton, Virginia, June 9, 1974", PAR-75-02;
 - "Pennsylvania Gas and Water Company, Natural Gas Explosions, Williamsport, Pennsylvania, January 25, 1977", PAR-77-04;
 - "Mid-America Pipeline System Liquefied Petroleum Gas Pipeline Rupture and Fire, Donnellson, Iowa, August 4, 1978", PAR-79-01;
 - "Colonial Pipeline Company, Petroleum Products Pipeline Failures, Manassas and Locust Grove, Virginia, March 6, 1980", PAR-81-02;
 - "Texas Eastern, Jackson, Louisiana -- November 25, 1984", PAR-86-01*;
 - "Continental Pipe Line Company Pipeline Rupture and Fire Kaycee, Wyoming, July 23, 1985," PAR-86-01;

- “Northeast Utilities Service Co. Explosion and Fire Derby, Connecticut December 6, 1985”, PAR-86-02;
- “Williams Pipe Line Company Liquid Pipeline Rupture and Fire Mounds Views, Minnesota July 8, 1986”, PAR-87-02;
- “Continental Pipe Line, Kaycee, WY, July 23, 1985”, “Buckeye, Freeport, PA, March 30, 1990”, SIR-96-02;
- “Hazardous Liquid Pipe Failure and Leak, Marathon Ashland Pipe Line, LLC Winchester, Kentucky, January 27, 2000”, PAR-01-02;
- “Hazardous Liquid Pipe Failure and Leak, Explorer Pipeline Company, Greenville, Texas, March 9, 2000”, PAR-01-03;
- “Pipeline Accident Report: Rupture of Piney Point Oil Pipeline and Release of Fuel Oil near Chalk Point, Maryland”, PAR-02-01.

Appendix A: Experience with Historic Line Pipe

The following sections present incident data, pipe manufacturing processes, and pipe manufacturers for line pipe built into vintage pipelines. Incidents attributed to a defect in the pipe body and those due to a problem in the seam weld are included in each section. Note that only one of the datasets (the Office of Pipeline Safety data from 1970 through mid 1984) includes incidents that occurred during pre-service and subsequent pressure testing. Neither of the other two datasets includes detailed test data. The data on pre-service testing and retesting are included because, while not directly related to service failures, they provide an indication of time periods during which line pipe with anomalies were made.

The data are grouped by year for each manufacturer when the incidents occurred in periods separated by one year or less. The data should be taken as an indication of the time periods when anomalies were periodically introduced into production. Other relevant data can be found in the several appendices of Reference 11.

Butt-Welded Pipe

Butt-welded pipe is prone to anomalies related to weld strength and reliability. When anomalies are present, the weld seam may be weaker than the pipe body. 49CFR192 includes a longitudinal joint factor (described earlier) of 0.6 for butt-welded pipe to account for the potential that defective welds can be weaker than the body of the pipe. Very little, if any, butt-welded pipe has been used for high pressure transmission lines since about 1940.

Reference 9 lists 19 manufacturers of furnace or continuous butt-welded pipe from 1911 through present.¹⁷ These 19 manufacturers operated 40 mills, producing pipe diameters from ¼ inch to 4.5 inches. Of these, the incident data identify five manufacturers for which incidents are attributed to anomalies in the pipe body or seam weld.

Reference 9 summarizes reported pipe-body and seam-weld incidents. A total of seven pipe body incidents have been reported for butt-welded pipe, six of which occurred in service. A much larger number of seam-weld incidents were reported, but none of these occurred in service.¹⁸

Reference 9 shows that relatively few pipe-body incidents have occurred in butt-welded pipe. There is no apparent trend in terms of year of production. Pipe produced by Youngstown Sheet & Tube may be somewhat more prone to pipe-body problems, but the data are too sparse to make a definitive conclusion. The small number of service incidents attributed to defects in the body of butt-welded pipe may reflect the amount of pipe in service: butt-welded pipe is produced in small diameters, which is not widely used in transmission pipelines. The number may also reflect that most incidents may have occurred well before the dates for which incident reporting began (1950) and that much of the potentially defective pipe has since been replaced or retired.

¹⁷ Reference 9 lists manufacturers of API-stamped pipe. These lists are necessarily incomplete, especially for earlier pipe-making processes. Butt-welded pipe was available well before 1911.

¹⁸ The occurrence of failures in-service is distinguished from those when not in service because the latter occur during pressure testing that are done at much higher pressure, or under other circumstances designed to expose potentially deleterious anomalies prior to their causing problems during operations.

A much larger number of seam-weld incidents have been reported. Both Armco and Republic Steel show many retest failures due to seam-weld anomalies. In each case, the incidents are on a single pipeline and from pipe made during a single year, suggesting a lapse in quality assurance. The relatively large number of incidents raises questions about the effectiveness of quality assurance programs for these suppliers. Armco (in 1949) and Republic Steel (in 1931) account for over 90 percent of the reported incidents on vintage natural-gas pipelines based on the data assembled in this appendix, which are summarized in Table A-1.

Table A-1. Incidents attributed to butt welded pipe

Pipe Manufacturer	Year Made	Pipe Body			Seam Weld		
		Pre-Service	Retest	Service	Pre-Service	Retest	Service
A. O. Smith ¹⁹	'50		1				
Armco	'49					49	
Bethlehem	'42			1			
Republic	'31					11	
	'52					1	
	'57					1	
	'81 ²⁰			1			
Youngstown Sheet & Tube	'28-30			2			
	'53			1			
	'58			1			
Totals		0	1	6	0	62	0

Lap- and Hammer-Welded Pipe

Lap- and hammer-welded pipe were prone to weld defects resulting from slag or oxides present on the welding surfaces or because the weld was “burnt” (overheated). Proper welding temperatures and weld quality depend on the process controls used during welding. Like butt-welded pipe, 49CFR192 accounts for lap- and hammer-weld defects with a longitudinal joint factor or through the use of an effective yield stress determined by full-scale burst tests.

Reference 9 lists 12 manufacturers of lap- or hammer-welded pipe from around 1920 through 1969. These 12 manufacturers operated 23 mills, producing pipe from 1-¼ to 36 inches in diameter. Of these, the incident data identify two manufacturers for which incidents are attributed to anomalies in the pipe body or seam weld.

Table A-2 summarizes reported pipe-body and seam-weld incidents. A total of 26 pipe-body incidents have been reported for lap- and hammer-welded pipe, four of which occurred in

¹⁹ There are a number of apparent errors in the published incident datasets used in this study. For example, A. O. Smith is listed as the manufacturer of butt-welded pipe that failed during a retest, but Reference 9 does not include A. O. Smith as a producer of butt-welded pipe. The data in the tables in this appendix include the pipe manufacturers identified in the incident datasets, regardless of whether the manufacturers are listed in Reference 9.

²⁰ Reference 9 states that Republic Steel stopped producing butt-welded pipe in 1964.

service. A total of 58 seam-weld incidents were reported, of which 17 occurred in service. Only two manufacturers are included in the list, with U. S. Steel accounting for the vast majority of the reported incidents. The predominance of U. S. Steel in Table A-2 suggests recurrent quality control problems with that mill.

Table A-2. Incidents attributed to lap and hammer welded pipe

Pipe Manufacturer	Year Made	Pipe Body			Seam Weld		
		Pre-Service	Retest	Service	Pre-Service	Retest	Service
U. S. Steel (National Tube, National Supply)	'29-31		17	4		27	14
	'35						1
	'43		3			12	
	'55		2				1
Youngstown Sheet & Tube		0				2	1
Totals			22	4		41	17

Electric Resistance and Flash Welded Pipe

Regardless of when or how electric resistance weld (ERW) pipe was (is) made, good quality welds can be (are) made with proper process controls. Nonetheless, historic ERW welds can be more prone to the following types of anomalies:

1. Lack of fusion and presence of oxides along the bond line, generally due to poor process controls,
2. Stitched welds (alternating complete and incompletely fused or partially fused areas) due to uneven heating (generally associated with low-frequency ERW processes),
3. Hook-cracks near the bond line caused by inclusions in the plane of the wall thickness at the edge of the skelp that are upset or turned toward the pipe surface in the forging process,
4. Excessive trim or grooving (wall thickness reduction), and
5. Arc burns resulting from poor or intermittent welding electrode contact adjacent to the weld.

As the ERW process evolved in conjunction with mill inspections and quality controls, the likelihood of ERW seam defects decreased. For example, ERW pipe manufacturers began converting from low to high frequency (alternating current) welding in the early 1960s. This modification essentially eliminated “stitched welds” as a quality concern. During this same period, pipe steel quality also improved, reducing the incidence of hook cracks. The anomalies in flash welded seam are the same as found in low frequency ERW seams.

Reference 9 lists 72 manufacturers of ERW pipe from 1929 through present. Of these, 25 continue to produce ERW pipe. These manufacturers operated 86 mills (per Reference 9, 42 are currently in operation), producing pipe from 1/2 to 36 inches in diameter (per Reference 9, the current range is 1/2 to 24 inches). Of these, the incident data identify 12 manufacturers – one out

of six manufacturers – for which incidents are attributed to anomalies in the pipe body or seam weld.

Table A-3 summarizes the reported low frequency ERW pipe-body and seam-weld incidents, while Table A-4 summarizes the comparable results for high frequency ERW pipe. The incident datasets did not identify low versus high frequency pipe. Consequently, data separated in these tables reflects the use of Reference 9 and personal experience to cull data from the incident databases. Nine out of the 12 manufacturers have incidents reported for both low frequency and high frequency ERW pipe; two have reports for low frequency only, and one has reports for high frequency only.

Table A-3. Incidents attributed to low frequency ERW pipe

Pipe Manufacturer	Year(s) Made	Pipe Body			Seam Weld		
		Pre-Service	Retest	Service	Pre-Service	Retest	Service
Acero Del Pacifica	'51-52					17	8
American Steel Pipe	'37 ²¹			1			
Bethlehem	'57-58 '69			1		3	1
Cal Metal	'57					2	
Jones & Laughlin	'57-64		1	1		17	2
Kaiser	'51-56 '60-63	1	1		2	13 3	1 2
Lone Star	'59-65			7		17	2
Republic	'31-32 '38-62			1			2
		3		5		118	8
Stupp	'40			1			
U. S. Steel	'31 '61 '65				1		1 1 1
Youngstown Sheet & Tube	'19 '31 '40-59 '66-67 '71					20 92	3 54
		1	6	20			
		1	1	1			
Totals		6	9	39	3	302	86

The number of incidents listed for low frequency ERW pipe is significantly larger than that for high frequency ERW pipe²². Given the amount of ERW produced, the numbers of pipe-body

²¹ According to Reference 9, ACIPCO did not begin producing ERW pipe until 1963.

incidents are reasonably consistent with those for the other pipe manufacturing methods discussed above and with improvements in steel-making practices and in American Petroleum Institute (API) inspection specifications.

Both low and high frequency ERW show test and retest incidents. The retest data are typically from programs aimed at removing potentially weak ERW seams from service. The low frequency pipe shows significantly more in-service seam-weld incidents, which is expected.

Several pipe manufacturers dominate the number of reported incidents for both low and high frequency pipe. For low frequency pipe, Republic and Youngstown Sheet & Tube account for 70 percent of the reported incidents, while Acero del Pacifica, Jones & Laughlin, Kaiser, and Lone Star account for over 20 percent more.

Table A-4. Incidents attributed to high frequency ERW pipe

Pipe Manufacturer	Year Made	Pipe Body			Seam Weld		
		Pre-Service	Retest	Service	Pre-Service	Retest	Service
American Steel Pipe	'70-78	6		2		28	
Bethlehem	'73			1		3	
Cal Metal	'70					1	1
	'77					1	
Jones & Laughlin	'70-73	6			8		
	'79-80						2
Kaiser	'71-75		1		6		
	'83				1		
Lone Star	'70-76			1	11		
Republic	'70	1					
	'81			1			
Stupp	'70-77	3	3		30		1
	'81-82	1			3		2
Tex Tube	'70				1		
	'74				1		
	'78				1		
	'82						8
U. S. Steel	'68-82	13		4	52		11
Totals		30	4	9	114	33	25

For the high frequency pipe, American Steel Pipe, Stupp, and U. S. Steel dominate, accounting for nearly 75 percent of the total. Nearly all of the incidents attributed to Stupp pipe occurred

²² Production practices in high-frequency ERW have evolved since this process was first introduced, as have mill inspection practices, which has led to much improved pipe quality. Nevertheless, pre-service hydrotesting periodically expose seam defects in this product, even from so-called quality mills.

during a relatively short period – from 1970 to 1977. Kaiser (~4 percent), Jones & Laughlin (~7 percent), and Lone Star (~6 percent) are also notable.

Table A-5 summarizes reported pipe-body and seam-weld incidents for flash-welded pipe. Only one manufacturer, A. O. Smith, produced flash-welded pipe. A total of 276 incidents are evident in this table, with most being attributed to the weld. Problematic pipe appears to have been made in nearly every year for which flash-welded pipe was produced. One of the problems with flash-welded pipe is that the weld seam was not heat treated.

A number of retest failures in A. O. Smith flash-welded pipe have occurred after 1984, as the pipeline industry instituted programs to excise defective flash-welded pipe from their systems. Pressure testing above the maximum allowable operating pressure is an effective way of removing defective flash-welded (and ERW) pipe. However, in mid 1984, OPS stopped collected data on pre-service and retest failures such that this retest data is generally unavailable.

Table A-5. Incidents attributed to flash welded pipe

Pipe Manufacturer	Year Made	Pipe Body			Seam Weld		
		Pre-Service	Retest	Service	Pre-Service	Retest	Service
A.O Smith	'28-31		5			3	2
	'37			1			
	'40-43					29	4
	'46-65		8	18		162	37
	'67						2
	'69-71	2				2	1
Totals		2	13	19	0	196	46

Single-Sided Arc and Double Submerged-Arc Welded Pipe

Single arc and double submerged-arc welds are not particularly prone to anomalies. There have been isolated occurrences of the following anomalies:

- 1) weld metal cracks,
- 2) toe cracks at the edge of the weld reinforcement,
- 3) lack of sidewall or inter-run fusion,
- 4) inclusions,
- 5) weld metal porosity,
- 6) offset welds, and
- 7) undercut.

These anomalies are much more prevalent in vintage single arc and double submerged-arc welded pipe than they are in modern production.

Reference 9 lists 22 manufacturers of arc welded or double submerged-arc welded pipe from 1940 through present. Of these, eight manufacturers continue to produce double submerged-arc

welded pipe. These manufacturers operated 30 mills, 11 of which are still in operation, currently producing pipe from 16 to 120 inches in diameter. Of these, the incident data identify eight manufacturers – roughly one out of three manufacturers – for which incidents are attributed to anomalies in the pipe body or seam weld.

Table A-6 summarizes the reported arc welded and double submerged-arc welded pipe-body and seam-weld incidents. Again, several manufacturers dominate the reported incidents, with Kaiser accounting for nearly half and U. S. Steel accounting for nearly 20 percent of the total.

Table A-6. Incidents attributed to arc welded and double submerged-arc welded pipe

Pipe Manufacturer	Year Made	Pipe Body			Seam Weld		
		Pre-Service	Retest	Service	Pre-Service	Retest	Service
Acero Del Paci	'52-53						8
ARMCO	'52 '73-74 '79	5		1	4 1		
Bethlehem	'52 '57-62 '71-72 '75		1 2	1		1 5	4 1
Claymont	'51					5	2
Consolidated Western	'47 '50 '54-56		8	2 2		2 6	3 3
Kaiser	'49-56 '60 '70-73 '76 '79-81	1	51	2 1		3 2 1	6 1
Republic	'48-50 '67 '73		4 1 5	1 1			
US Steel	'31 '49-51 '54-62 '65-66 '69-71 '77-82		3 5	7 2 2 1		3 6 4	1 1 9 3
Totals		8	80	24	11	89	42

A more detailed examination of the incident data for double submerged-arc welded pipe shows a strong dependence on age. Over 44 percent of the incidents are attributed to pipe produced in 1950, with another 17 percent in 1949, 1951, or 1952. These years represent the time period in which double submerged-arc welded pipe was gaining widespread acceptance in the United States.

Spiral-Welded Pipe

There are two basic processes by which spiral-welded pipe can be made. Small amounts of vintage spiral-welded pipe were made by hammer welding and ERW processes, mostly for the water industry. Later, several foreign manufacturers produced spiral-welded pipe using double submerged-arc welding. None of the incident records examined by the authors identify spiral-welded pipe as the type of pipe that led to incidents.

Seamless Pipe

Irregularities that have occurred in seamless pipe include scabs, blisters, slivers, seams, laps, laminations, pits, roll-ins, hot tears, and plug scores. Surface imperfections, such as blisters, slivers, seams, pits, plug scores and laps, arise from the twisting, upsetting, and abrading of the surface during pipe formation. Hot tears result from the working of the metal with an insufficient temperature for rewelding of torn material. Laminations typically result from imperfections and insufficient ingot cropping.

Reference 9 lists 18 manufacturers of seamless pipe operating 30 pipe mills from 1895 through present. These manufacturers produced pipe in diameters from 1/4 to 26 inches. Of these, the incident data identify only one manufacturer – U. S. Steel – for which incidents are attributed. Table A-7 summarizes the data.

Table A-7. Incidents attributed to seamless pipe

Pipe Manufacturer	Year Made	Pre-Service	Retest	Service
US Steel	'30			2
	'33		1	
	'38		2	
	'43-53		15	7
	'56			1
	'59			4
	'64-65		1	1
	'70-74	9		
	'77-78		3	
Totals		9	22	15

Upsets in Pipe Making and Pipeline Construction

This section considers the occurrence of problems that occurred during the process of pipe making or pipeline construction that created anomalies prevalent across a range of product types

or suppliers. There are two generic categories of such anomalies – arc burns and hard-spots that are a potential source for hydrogen stress cracking, and transportation-induced fatigue cracking.

Hydrogen Stress Cracking - Arc Burns and Hard Spots

Hydrogen stress cracking (HSC) on gas transmission pipelines transporting sweet dry gas is nearly always associated with arc burns, hard spots, with such cracking also possible in high-hardness ERW seams.

The presence of arc burns and hard spots is not, by itself, sufficient to indicate cracking will occur. In order for cracking to occur several other conditions must co-exist. First, the hard spot or arc burn must be exposed to the environment where diffusion of atomic hydrogen into steel can occur. On pipelines, such conditions can be created in the presence of higher than normal cathodic protection potentials that liberate hydrogen at the exposed metal surfaces. A second condition for HSC requires that the hard spot be exposed, typically as a result of coating degradation. While coating degradation is not uncommon, the amount of bare steel in a poorly coated line is typically small. Last, the hard spot must be sufficiently hard. Hydrogen stress cracking occurs at hardness at or above about Rockwell C22^(43,44), with lower hardness levels being associated with strong sources of hydrogen, such as can occur with sour service.²³

Table A-8. Hard spot incident summary

Pipe Seam Type	Pipe Manufacturer	Pipe Production Year	No. Of Incidents
Flash weld	A.O. Smith	1952	17
		1954	1
		1955	1
		1957	1
DSAW	Bethlehem	1957	2
	Kaiser	1955	1
	Republic	1949	2
		1957	1
ERW	Youngstown Sheet & Tube (YS&T)	1947	1
		1950	1
		1960	1

Transportation Damage

Line pipe with weld seam reinforcement that protrudes above the pipe surface (i.e., FW, DSAW) has experienced shipping fatigue cracks due to the seams contacting rail car bottoms or other pipes, with cracks forming at the edge of the weld reinforcement bead^(e.g., see 70). Fatigue cracks

²³ It is also possible for the stress fields due to pipe forming and service pressure to nucleate and grow cracks in hard spots. While this is plausible, such cracking would either be severe enough to be exposed early in service, or otherwise exposed in pressure testing. Remaining cracks would lie dormant unless changes in service due to pressure increase activated them.

have also formed in all types of line pipe due to rivet heads, projections in rail cars contacting the pipe body or pipe ends, foreign objects in a rail car, bearing strip misalignment, or insufficient support^(e.g., see 70). In these cases, the conditions necessary to promote fatigue cracking result from vibration during shipment.

Transportation fatigue often occurred in pipe with high diameter/thickness ratios in the period prior to 1970. Between 1957 and 1962, 32 field failures were recorded. This included pipe with diameter/thickness (D/t) ratios that ranged from 54 to 91. Full-scale tests to measure actual pipe stress (D/t range: 88-128) were conducted during this same period. Field failures and test data prompted development of a pipe loading Recommended Practice for rail transportation by the API first issued in 1965 as API RP 5L. This was followed by similar recommended practices for pipe shipment in vessels (API RP 5L5, 1975) and inland waterways (API RP 5L6, 1979). The requirements contained in these documents have reduced the frequency of transportation related damage.

Requirements for pipe transportation by rail have been included 49CFR192 since 1973. Any pipe with a D/t ratio of 70 or higher to be operated at a hoop stress of 20 percent SMYS or greater must be transported in accordance with API 5L1. For pipe transported prior to November, 1970, a proof test commensurate with the class location must be conducted.

Quality Requirements

A number of specifications were developed to establish minimum requirements for pipe used in transmission pipelines. Commonly used pipe specifications are API Specifications 5L and 5LX. These specifications provide requirements on composition, mechanical properties, pressure testing, dimensions, weights, end preparation, inspection, and other quality components with toughness recently being included. The requirements on pressure (hydrostatic) testing and inspection have the largest effects on pipeline integrity.

It should be noted that not all pipelines were constructed from pipe manufactured in accordance with API specifications. Prior to the introduction of API specifications, quality requirements were established by each purchaser. Methods included company pipe specifications, manufacturing inspections by company personnel, and third party inspections by contractors, individually or in combination. Additional measures included defined pipe production procedures established by a pipe manufacturer, as amended and/or agreed to by the purchaser to suit particular requirements.

The API specifications provided an industry-wide basis for pipe specifications and standardized many of the pipe making practices. In time, they largely replaced the requirements developed by individual purchasers. Nonetheless, many pipeline operators chose (and continue to choose) to add requirements in proprietary specifications. These additions are typically predicated on the intended pipeline service environment and/or the fluids to be transported.

The evolution of pipe quality control requirements contained in the API specifications provides useful insight into pipe characteristics and quality. From their first editions through the present, yield and tensile strength requirements have increased on a regular basis, reflecting improvements in steel- and pipe-making processes. For example, one of the original pipe grades (Grade A) has a minimum yield strength of 25 ksi, while the most recently added grade (X80) calls for a yield strength of 80 ksi. In addition, requirements for 100 ksi (X100) and 120 ksi

(X120) steels are actively being developed for future API Specifications. In addition, mechanical testing requirements have been added. Typical destructive testing requirements include bend and strength tests of production welds to ensure they are at least as strong as the pipe body.

Pressure testing and inspections are important quality assurance methods used in the API specifications. In the earliest versions of API 5L, pressure tests were largely used to ensure leak tightness, not strength, with minimum hydrostatic pressures of 40 to 50 percent SMYS. By 1970, the API 5L pressure requirements had increased to 60 to 75 percent SMYS – comparable to the maximum stress levels in Class 1 and 2 locations.

The API 5LX pressure requirements are generally higher (60 to 75 percent pipe diameters below 8 inches and 85 to 90 percent for larger diameters). For pipe diameters greater than 8 inches, the mill hydrostatic tests produce stresses well above operating stress levels.

From the earliest API specifications, destructive tests were required on pipe and weld samples (typically one set of tests per 100 or 200 pipe joints). Typically tests were used to demonstrate the pipe body met the strength and elongation requirements while bending tests were used to demonstrate the weld seam could withstand high strain levels without cracking. Early workmanship requirements stated that the pipe should be free of “injurious defects”, including defective welds, pits, blisters, slivers, and laminations. Injurious defects were further defined as those defects greater than 12.5 percent of the wall thickness. Additional visual inspections to identify injurious defects were at the discretion of the purchaser.

By the early 1960s, more destructive tests were required, including weld tensile and ductility tests. Fracture toughness testing was at the discretion of the purchaser. The list of workmanship defects had been expanded to address a wide variety of conditions, including dents, offset of plate edges, out-of-line weld beads, excessive weld reinforcement, improper trimming of flash, and hard spots. Other defect types were identified, including all cracks and leaks, surface breaking laminations and inclusions, arc burns, weld undercut, arc burns, and any other imperfection having a depth greater than 12.5 percent of the wall thickness.

Non-destructive inspections of welds were also added in the 1960s. Depending on the weld type, the entire weld was required to be inspected using radiological, ultrasonic, or electromagnetic techniques. In addition, magnetic particle inspection of each pipe end was required to locate open welds, partial or incomplete welds, intermittent welds, cracks, seams, and slivers.

In summary, since 1928, API specifications have evolved to ensure minimum pipe quality, with their evolution reflecting changes in steel- and pipe-making practices, and the expanding capabilities of real-time nondestructive inspection. By the early 1960s, the specifications began to significantly reduce the historic pipe body and weld seam anomalies discussed above. Because of this impact, quality control and quality assurance have become central to the pipe production and supply specifications in use throughout the industry.

Relative Significance of Anomalies

Tables A-9 and A-10 summarize these process and production anomalies and their characteristics, while the ensuing paragraphs consider their potential impact on integrity. These tables and the following discussion rely on the author's personal experience and/or published data to identify the most significant anomalies, where possible. This approach is necessary for two reasons. First, as compared to other incident causes, pipe body and seam weld anomalies are a much less frequent cause, as was evident in the introduction to this report. Thus, the potential database available for trending or statistical analysis is limited. Second, the reporting requirements for OPS data did not motivate reporting details of the type of pipe-body or weld-seam defect that led to an incident, which precludes conclusively determining anomalies of

Table A-9. Weld-seam anomalies

Pipe-Making Process	Defect or Characteristic	Comments
Furnace Butt Welded, Continuous Butt Welded Pipe, Lap Welded and Hammer Welded Pipe	Oxides trapped between weld surfaces; inconsistent quality welds	Addressed in 49CFR192 with longitudinal joint factor, or by use of an effective yield stress
Electric Resistance Welded (ERW) and Flash Welded Pipe	Oxides trapped in weld, inconsistent quality welds	Welding controls and inspection practices have largely eliminated these types of anomalies
	Stitched welds	More common in low-frequency ERW pipe
	Hook cracks	More common in earlier steels with higher levels of impurities and inclusions
	Excessive trim	Rare in modern line pipe
	Arc burns and hard weld zones	Like hard spots (see Table A-8)
Single Arc Welded and Double Submerged-Arc Welded Pipe	Weld metal cracks, toe cracks, lack of sidewall or inter-run fusion, undercut inclusions, porosity, offset welds,.	Rare

greatest concern. The same was true for the FPC database. In spite of this, there is significant literature that can be used to better understand the cause – effect relationship between defects and incidents.

Important information sources include the five-page tabulation and analysis of historical defects causing pre-service and hydrostatic retest failures that comprises Table A1-3 in Appendix A of Reference 83. Those tables reflect input from Europe via Mr. Peter Peters, then retired but recently manager of Mannesmann Mulheim Works, and the U.S. and elsewhere via Dr. Malcolm Gray, a principal of MicroAlloying International. This information was supplemented by results in archived Battelle failure reports developed to assess and characterize defects that caused failures in hydrotesting during the era such failures were reported but not as in-service incidents. Another key source was the quite extensive evaluation of failure causes documented on behalf of the PRCI as Reference 141. Finally, the extensive literature selected in regard to historic pipelines and organized here as Reference 142 was useful, although somewhat more topical than is typically needed to meet the needs here.

When the process of assembling the data and evaluating causes was completed, the data from failure analyses, the authors' experience, and the literature indicate that incidents originating at a defect in the weld seam are most commonly due to cracks in or around the weld, inconsistent quality welds, or preferential corrosion in or near the weld. Other causes are much less important as compared to this to this one.

Table A-10. Summary of pipe-body and weld-seam anomalies

Evaluation Criteria	Years	Most Frequently Reported Manufacturer(s)	Comments
Pipe Specific			
Butt/Lap weld	Pre 1960	Armco, Republic	Use of a longitudinal joint factor reduces loading on weld
DSAW, SSAW, and other welded seams	Pre 1960	Kaiser, U. S. Steel	
Low frequency ERW	Pre 1971	Republic, Youngstown Sheet & Tube	Acero del Pacifica, Jones & Laughlin, Kaiser, and Lone Star also have higher incident rates than others manufacturers
High Frequency ERW	Pre 1980	Stupp	Kaiser, Jones & Laughlin, and Lone State also have higher incident rates than others manufacturers
Flash weld		A. O. Smith	All
Seamless	1940s and early 50s; 1970s	U. S. Steel	
Defect Specific			
Cracking in Hard Spots or Arc Burns	1950s	A. O. Smith	
Transportation Fatigue	Pre 1970		Double submerged-arc and flash welded pipe are more susceptible than other types of pipe; High diameter-to-thickness ratios are more prone to damage
Mechanical Damage	Vintage pipe is more likely to have experienced mechanical damage due to handling than later pipe		Thin walled pipe and pipe with high diameter-to-thickness ratios are more prone to some forms of cracking in mechanical damage

Cracking

The most common form of cracking in seam welds is hook cracks associated with ERW or flash-welded pipe. Hook cracks are most likely in pipe made from earlier steels. Hook cracks are generally stable up to the maximum pressure to which the pipe has been exposed, unless the pipe is exposed to large pressure cycles.

Inconsistent Quality Seam Welds

Inconsistent quality seam welds are potential anomalies for all of the earlier pipe-making processes. While most pipe manufacturers succeeded in making pipe of consistent quality, there are several notable exceptions:

- Acero del Pacifica (low frequency ERW pipe),
- American Steel Pipe (high-frequency ERW pipe),
- A. O. Smith (flash-welded pipe),
- Armco (butt-welded pipe),
- Jones & Laughlin (low- and high-frequency ERW pipe),
- Kaiser (low- and high- frequency ERW pipe, arc or double submerged-arc welded pipe),
- Lone Star (low- and high- frequency ERW pipe),
- Republic (butt-welded pipe, low-frequency ERW pipe),
- Stupp (high-frequency ERW pipe),
- U. S. Steel (lap welded pipe, high-frequency ERW pipe, arc or double submerged-arc welded pipe, seamless pipe), and
- Youngstown Sheet & Tube (low-frequency ERW pipe).

Inconsistent quality welds are considered stable up to the maximum pressure to which the pipe has been exposed in prior service. Pressure testing of pipelines with seam defects opens the door to pressure reversals.